Charge Carrier Dynamics in Polymer Solar Cells(Dissertation_全文)

AUTHOR(S):

Yamamoto, Shunsuke

Charge Carrier Dynamics

in Polymer Solar Cells

Shunsuke YAMAMOTO

2012

Contents

Chapter 1. General Introduction

1.1. Background and Motivation 1

1.1.1. Organic Semiconductors 1

1.1.2. Organic Solar Cells 4

1.1.3. Methodologies Used in This Thesis 10

1.2. Outline of This Thesis 13

1.3. References 15

Part I

Chapter 2. Formation of Methanofullerene Cation in Bulk Heterojunction Polymer Solar Cells

2.1. Introduction 23

2.2. Results 25

2.2.1. Transient Absorption Spectra 25

2.2.2. Assignment of Charge Carriers 28

2.3. Discussion 33

2.3.1. Charge Carriers Formed in MDMO-PPV/PCBM Blends 33

2.3.2. Mechanisms of PCBM Radical Cation Generation 37

2.4. Conclusions 39

2.5. Experimental 40

2.6. References and Notes 42

Chapter 3. Formation Mechanism of Fullerene Cation in Bulk Heterojunction

Polymer Solar Cells

3.1. Introduction 45

3.2. Results 48

3.2.1. Transient Absorption 48

3.2.2. Monte Carlo Simulation 54

3.3. Discussion 57

3.3.1. Formation Mechanism of PCBM Cation 57

3.3.2. Energetic Conditions 58

3.4. Conclusions 60

3.5. Experimental 62

3.6. Appendix 64

3.7. References 68

Part II

Chapter 4. Molecular Understanding of the Open-Circuit Voltage of Polymer:Fullerene Solar Cells

4.1. Introduction 75

4.2. Results 79

4.2.1. *J*–*V* Characteristics 79

4.2.2. Temperature Dependence of J_0 83

4.3. Discussion 86

4.3.1. Recombination Current 86

4.3.2. Origin of Open-Circuit Voltage 87

4.4. Conclusion 91

4.5. Experimental 93

4.6. Appendix 96
4.7. References and Notes 99
Chapter 5. Charge Dissociation and Recombination through Interfacial Charge Transfer State in Low-Bandgap Polymer Solar Cells
5.1. Introduction 104
5.2. Results 106
5.3. Discussion 112
5.4. Conclusions 117
5.5. Experimental 118
5.6. Appendix 120
5.7. References and Notes 122
Chapter 6. Charge Generation and Recombination in Fluorene-based Polymer Solar Cells
6.1. Introduction 125
6.2. Results 126
6.2.1 Photovoltaic Properties 126
6.2.2 Transient Absorption 129
6.3. Discussion 135
6.4. Conclusion 140
6.5. Experimental 142
6.6. Appendix 143
6.7. References and Notes 144
Summary 147
List of Publications 151
Acknowledgment 153

Chapter 1

General Introduction

1.1. Background and Motivation

1.1.1. Organic Semiconductors

The electronic properties of organic materials have attracted much interest in the scientific and engineering fields. Pioneer studies on photo- and dark conductivity of anthracene and its related compounds were reported in the early 20th century.[1–5] In 1948, Eley reported the conductivity of phthalocyanines.[6] On the other hand, Inokuchi investigated the charge transport mechanism in polynuclear aromatic compounds and demonstrated that these materials are semiconductors.[7,8] On the other hand, Shirakawa *et al.* reported in 1977 the conductivity of iodine-doped poly(acetylene).[9,10] Since this discovery of the conductive polymers marked developments have been made both in scientific research and engineering applications. Meanwhile, Kroto *et al.* discovered C_{60} fullerene in 1985.[11,12] Since the discovery of fullerene, the electron transport property,[13,14] the molecular magneticity,[15] and the superconductivity of this material and its derivatives were intensively studied.[16,17]

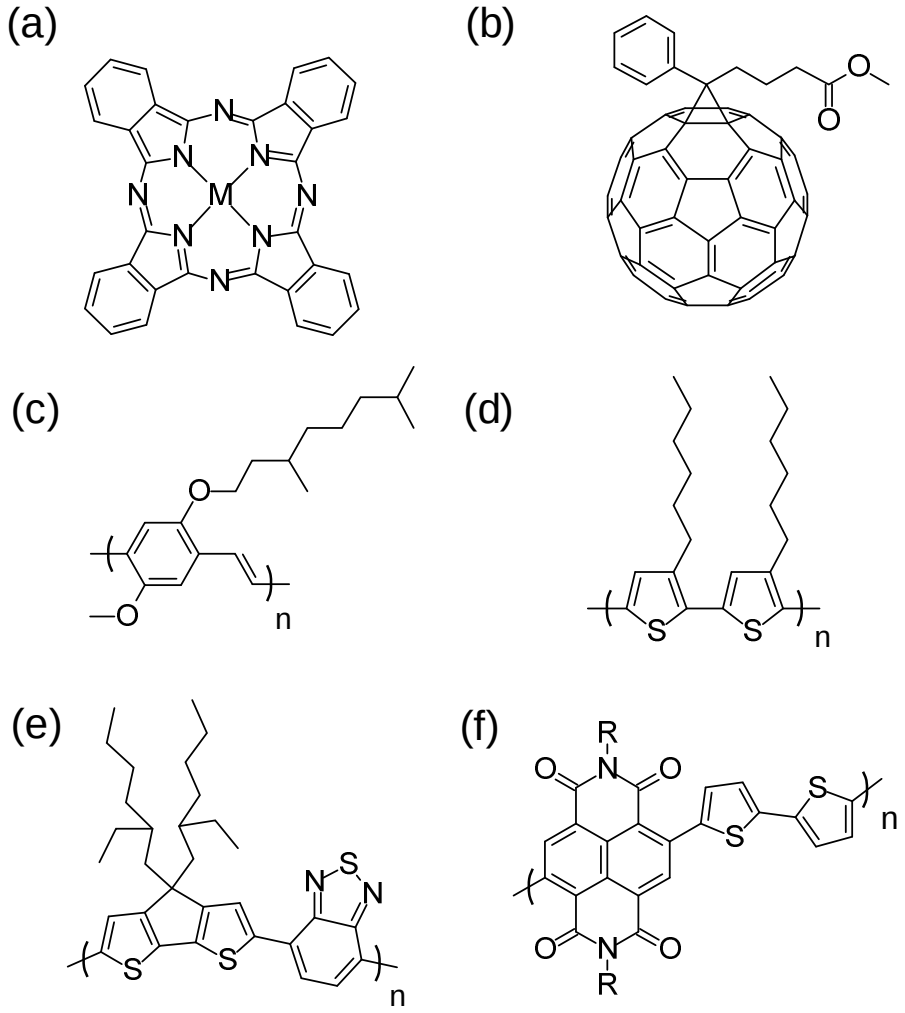

Figure 1-1. Chemical structures of representative organic semiconductors: (a) phthalocyanine (M = metal), (b) a fullerene derivative: [6,6]-phenyl-C_{61}-butyric acid methyl ester (PCBM), (c) a poly(*p*-phenylenevinylene) derivative: poly[2-methoxy-5-(3,7-dimethyloctyloxy)-1,4-phenylenevinylene] (MDMO-PPV), (d) regioregular poly(3-hexylthiophene) (RR-P3HT), (e) a low-bandgap polymer poly[2,6-(4,4-bis-(2-ethylhexyl)-4*H*-cyclopenta[2,1-b;3,4-b']dithiophene)-*alt*-4,7-(2,1,3-benzothiadiazole)] (PCPDTBT) (f) a naphthalenediimide-based acceptor polymer poly{[*N*,*N*'-bis(2-octyldodecyl)-naphthalene-1,4,5,8-bis(dicarboximide)-2,6-diyl]-*alt*-5,5'-(2,2'-bithiophene)} (P(NDI-2OD-T2)) (R = alkyl chain)

In the past two decades, many organic semiconducting materials have been developed and are being applied to various optoelectronic devices. Historically, Tang *et al.* reported the organic light-emitting diode (OLED) and organic photovoltaic (OPV) device in the late 1980s.[18,19] They developed bilayered devices with semiconducting small molecules: *N,N*-di(naphthalene-1-yl)-*N,N*-diphenyl-benzidene) (NPB) and tris(8-hydroxyquinolinato)aluminum (Alq3) in OLED, copper phthalocyanine and a perylene derivative in OPV. In the early 1990s, Friend *et al.* reported a polymer OLED device[20] and Sariciftci *et al.* reported a polymer/fullerene OPV device.[21] Both of these two devices are based on PPV-based polymers. In the field of OPV, Hiramoto *et al.* reported that a mixed-layer architecture fabricated by the co-deposition technique can improve the photocurrent.[22] In 1995, Yu *et al.* applied such a mixed layer to a polymer solar cell based on a blend of conjugated polymer and fullerene, which is called bulk heterojunction.[23] This bulk heterojunction promoted the research on polymer solar cells. For instance, regioregular poly(3-alkylthiophene)s (RR-P3ATs) and a methanofullerene derivative have been intensively investigated because RR-P3ATs have a good balance between solubility and crystallinity.[24–26] In particular, poly(3-hexylthiophene) (P3HT) and [6,6]-phenyl-C_{61}-butyric acid methyl ester (PCBM) have been widely used for OPV devices during the past 5 years.[26] On the other hand, low-bandgap polymers are attractive due to their good near-IR (NIR) light absorption property. For instance, poly[2,6-(4,4-bis-(2-ethylhexyl)-4*H*-cyclopenta[2,1-b;3,4-b']dithiophene)-*alt*-4,7-(2,1,3-benzothiadiazole)] (PCPDTBT) is a typical low-bandgap polymer, which was firstly reported in 2006.[27] This polymer consists of the cyclopentadithiophene donor unit and the benzothiadiazole acceptor unit in the main chain as shown in Figure 1-1. Because of the donor–acceptor interaction, this polymer has absorption red-shifted up to ~800 nm. The use of a high boiling point additive in the spin-coating solvent of the PCPDTBT-based

polymer solar cell improves short-circuit current J_{SC} over 15 mA cm^{-2}.[28] As briefly mentioned above, organic semiconductors advanced along the development of the device study. Next, the details of organic photovoltaics (organic solar cells) will be described.

1.1.2. Organic Solar Cells

Organic solar cells are made of electron donor and electron acceptor materials in the active layer, which is sandwiched between two electrodes. Electron donor and electron acceptor materials are characterized by their relative energy alignment of the highest occupied molecular orbital (HOMO) and the lowest unoccupied molecular orbital (LUMO): a material with a relatively shallow HOMO level is an electron donor and a material with a relatively deep LUMO level is an electron acceptor.[29,30] For instance, phthalocyanines,[31] acenes,[32] and most of the conjugated polymers are used as electron donor materials. On the other hand, perylenes,[33] fullerenes,[21] and perylenediimide-based or naphthalenediimide-based copolymers such as poly{[*N*,*N*'-bis(2-octyldodecyl)- naphthalene-1,4,5,8-bis(dicarboximide)-2,6-diyl]-*alt*-5,5'-(2,2'-bithiophene)} (P(NDI-2OD-T2)) are used as electron acceptor materials.[34,35] The photovoltaic conversion in organic solar cells is divided into five processes: i) photon absorption, ii) exciton diffusion, iii) charge transfer, iv) charge dissociation, and v) charge transport. The schematic diagram is shown in Figure 1-2. The device performance is given by the product of the efficiency of each process. Therefore, even one inefficient process limits the overall photovoltaic conversion performance. Details of each photovoltaic conversion process will be surveyed.

Upon excitation of an organic material, singlet excitons are formed first. This is different from inorganic semiconductors in which charge carriers are directly formed by

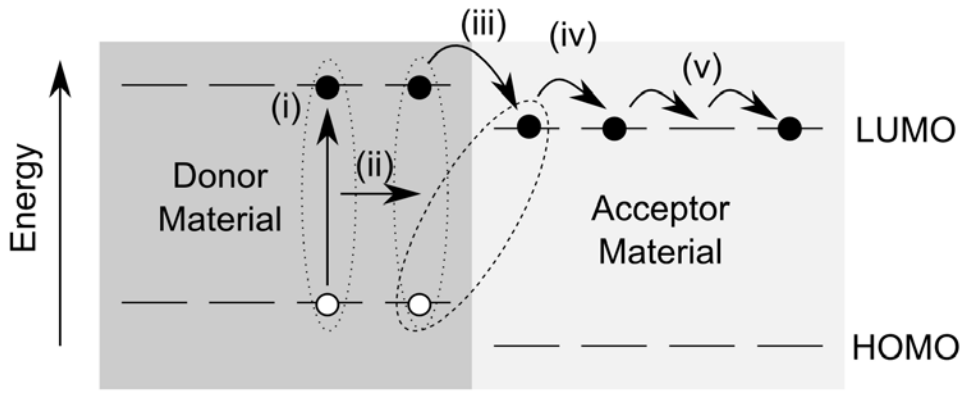

Figure 1-2. Schematic diagram of photovoltaic conversion processes in an organic solar cell: i) photon absorption, ii) exciton diffusion, iii) charge transfer, iv) charge dissociation, and v) charge transport The open and closed circles indicate holes and electrons, respectively. The dotted and broken ellipses indicate excitons and an interfacial charge pair, respectively. Note that this diagram shows a situation of donor excitation.

photon absorption.[36] This is ascribed to two reasons: (i) the strong Coulomb binding due to low permittivity of organic material and (ii) the weak non-covalent electronic interaction between organic molecules.[37–39] The exciton binding energy for organic materials is estimated to be 0.2 – 0.4 eV.[40,41] If the energy offset at the heterojunction is sufficient to overcome this binding energy, excitons dissociate to an interfacial charge pair by charge transfer reaction. In the case of donor excitation, the difference in LUMO level ΔE_{LUMO} is responsible for the charge transfer reaction. Thus, the energy gap at the heterojunction should be arranged by employing an appropriate combination of electron donor and acceptor materials. On the other hand, this charge transfer reaction occurs only at the heterojunction. Thus the phase-separated domain size should be as small as the exciton diffusion length for excitons to reach the interface. The diffusion length of a singlet exciton is as short as ~10 nm in a typical organic material.[42–46] In other words, the domain size should be as small as ~10 nm for efficient photovoltaic conversion.

Therefore the relative alignment of two materials both in energy level and at an spatial distribution is important for efficient conversion from exciton to interfacial charge pair.

The dissociation of the interfacial charge pair is the next process for photovoltaic conversion. Such interfacial charge pairs are also called interfacial charge transfer (CT) states.[47–49] The schematic diagram of dissociation and recombination of interfacial CT states are shown in Figure 1-3. The dissociation with a rate constant of k_{dis} competes with geminate recombination of interfacial CT states with a rate constant k_{rec}. In the Onsager–Braun theory, the rate constant of the interfacial CT state dissociation k_{dis} is formulated by Equation 1-1[50,51]

$$\begin{aligned} k_{dis} &= \gamma K \\ &= \frac{q\langle\mu\rangle}{\langle\varepsilon_r\rangle\varepsilon_0} \times \frac{3}{4\pi a^3} \exp\left(-\frac{E_b}{k_B T}\right) \end{aligned} \tag{1-1}$$

where γ and K are the bimolecular recombination rate constant and the equilibrium constant of dissociation of the interfacial CT states, q is the elementary charge, $<\mu>$, $<\varepsilon_r>$, and ε_0 are the spatial averaged charge mobility, the relative permittivity, and the vacuum permittivity, respectively, a is the thermalization radius, E_b is the Coulomb binding energy of the interfacial CT state, k_B is the Boltzmann constant, and T is the temperature. Note that this formula is valid for zero field. The second term K comes from the ratio between recombination and dissociation of interfacial CT states. Braun established his model on the comparison to equilibrium constant of ion pair dissociation in solution.[51,52] Another formulation is proposed by Tachiya *et al.* This includes not only the finite intrinsic recombination rate but also the nonzero reaction radius.[53] Nevertheless, the charge dissociation process in bulk heterojunction device requires further study.

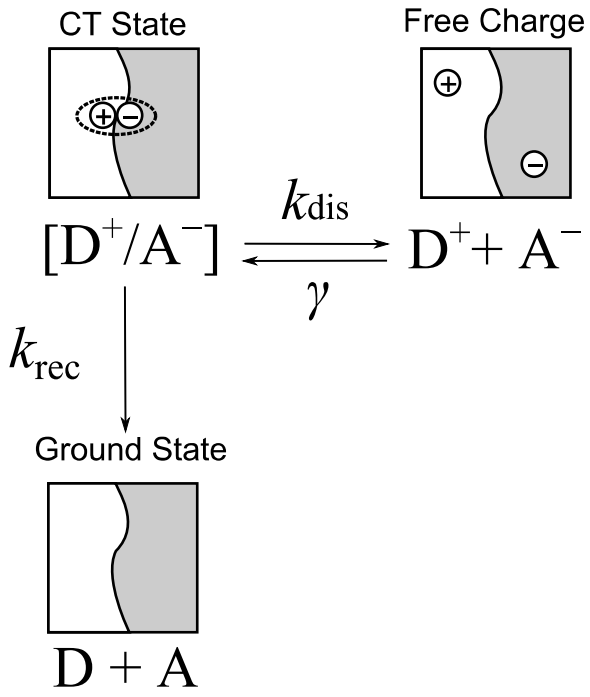

Figure 1-3. Schematic diagram of interfacial CT state dissociation and recombination processes: γ bimolecular recombination rate constant of free charge, k_{dis} dissociation rate constant of CT state, and k_{rec} recombination rate constant of CT state.

On the other hand, CT state emissions are detected by photoluminescence or electroluminescence techniques in some polymer/fullerene blend films. Inganäs *et al.* reported a series of studies on CT emissions of MDMO-PPV/PCBM, P3HT/PCBM, and fluorene-based copolymer/PCBM blend films by electroluminescence.[54] On the other hand, Loi *et al.* reported photoluminescence of CT state in PCPDTBT/PCBM blend films.[55] These emissions are red-shifted away from the singlet exciton emission band. For example, in the PCPDTBT/PCBM blend, CT state emission is observed at 1100 nm whereas emission of the PCPDTBT singlet exciton is observed at 900 nm, and that of PCBM is observed at 750 nm.[56] From the CT state emission, the lifetime of the CT state can be estimated. On the other hand, a recent transient absorption study showed that the charge dissociation efficiency is high in RR-P3HT/PCBM but low in blend films of

regiorandom P3HT and PCBM.[57] However, the origin of the difference in the dissociation yield is not fully understood.

The free charge carriers are transported within the device and collected by the electrodes. It is generally considered that holes and electrons are transported in conjugated polymers and fullerene derivatives, respectively.[29,30] Indeed, organic semiconductors with a shallow ionization potential tend to be *p*-type semiconductors and organic semiconductors with a deep ionization potential tend to be *n*-type semiconductors. On the other hand, ambipolar transport properties have been recently reported for not a few materials including fullerenes, pentacene, and conjugated polymers in the field effect transistor (FET) devices with appropriate electrodes and gate dielectrics.[58–64] These reports indicate that organic semiconducting materials are inherently capable of being ambipolar. On the other hand, recent studies have shown that the hole mobility of the MDMO-PPV/PCBM blend is larger than that of pristine MDMO-PPV by more than two orders of magnitude at 80 wt% PCBM.[65,66] This suggests that the charge transport in the blend is much more balanced. This finding seems contradictory to the prevailing view that conjugated polymers such as MDMO-PPV act as a hole-transporting material and that fullerene derivatives such as PCBM act as an electron-transporting material. Blom *et al.* proposed that the ring-like molecular conformation of MDMO-PPV might be the origin of the poor transport properties in the pristine film, which would be hindered in the blend to improve the hole mobility.[65] On the other hand, Nelson *et al.* demonstrated that adding PCBM to the blend increases the mobility of both the electron and hole compared to that of pristine MDMO-PPV.[66] They also found that electron and hole mobilities are of similar magnitude for PCBM dispersed in a polystyrene (PS) matrix. Indeed, the ambipolar charge transport has already been reported for fullerene-based FET including PCBM.[61,62] However, it is still not clear whether holes are transported in PCBM or not. On the other

hand, the charge transport process competes with bimolecular recombination. If the charge lifetime is shorter than the charge collection time, a limited short-circuit current J_{SC} would be observed because most of the charge carrier should decay before the collection. Therefore, the charge transport process has a critical impact on the J_{SC} of the device.

Meanwhile, the charge recombination is responsible for the open-circuit voltage (V_{OC}) of the polymer/fullerene device. This is because the recombination flux is equal to the charge generation flux at the open-circuit condition.[67,68] On the other hand, the maximum photovoltage is considered to be limited by the energy gap between the highest occupied molecular orbital (HOMO) level of a donor polymer and the lowest unoccupied molecular orbital (LUMO) level of an acceptor fullerene (ΔE_{DA}). Indeed, V_{OC} has been reported to increase with lowering the HOMO level of polymers and raising the LUMO level of fullerenes.[49,69–71] Although there have been several studies showing a linear relationship between qV_{OC} and ΔE_{DA} experimentally, V_{OC} is generally 0.2 – 0.5 eV smaller than ΔE_{DA}.[49,69–71] Recently, the difference between qV_{OC} and ΔE_{DA} has been discussed. For example, Koster *et al.* reported that the difference is related to the dissociation probability of bound electron–hole pair and the Langevin recombination of free carriers.[72,73] On the other hand, Inganäs *et al.* reported a linear relationship between qV_{OC} and the CT emission energy E_{CT} for blend films based on various conjugated polymers and PCBM. In this relationship, qV_{OC} is reduced by 0.5 – 0.6 eV compared to E_{CT}[56,74,75], which is similar to the difference between qV_{OC} and ΔE_{DA}. They ascribed ~0.25 eV of the reduction to radiative losses that are related to the formation of CT complex, and the rest (~0.35 eV) to nonradiative losses.[75] As described above, the difference between V_{OC} and ΔE_{DA} has been discussed in terms of the bimolecular recombination dynamics in which CT states are involved. However, the origin of V_{OC} in polymer solar cells is not fully understood.

As surveyed above, (i) spatial and (ii) energetic alignments of heterojunction are crucial for photovoltaic conversion. On the spatial alignment, the bulk heterojunction leads to a relatively high charge dissociation probability; however the charge collection efficiency is not always high because the charge transport paths are not always percolated to each electrode. Rather, the phase separation in the active layer significantly affects the photovoltaic conversion efficiency. For instance, a finely mixed structure leads to an efficient charge separation; however inefficient charge collection is expected because of the lack of charge transport paths, and vice versa. Indeed, many studies have been devoted to the control of the phase separation to improve the photovoltaic conversion efficiency by various technique such as thermal annealing,[76–78] solvent vapor treatment,[77,79] or usage of additives.[28,80,81] For example, the overall power conversion efficiency (PCE) of PCPDTBT/PCBM device is enhanced by a factor of ~1.5 by using 1,8-diiodooctane as an additive for spin-coating solution.[81] On the other hand, energetic alignment of materials, the charge transfer reaction at the interface is dependent on the energy gap as mentioned above. Similarly, the V_{OC} is considered to be limited by the energy gap between the HOMO level of a donor polymer and the LUMO level of an acceptor fullerene. Moreover, the relative energy alignment is thought to be the determinant of polarity of charge carrier in the material. In this thesis, each photovoltaic conversion process will be discussed at the sight of these two alignments of two materials.

1.1.3. Methodologies Used in This Thesis

A. Transient Absorption Spectroscopy

Time-resolved spectroscopy such as time-correlated single photon counting (TCSPC) and transient absorption spectroscopy (TAS) is a powerful tool for investigating chemical reactions directly. Among them, transient absorption spectroscopy can detect

even a non-fluorescent species such as charge carriers formed in OPV devices. Therefore, this is suitable for observation of charge carriers formed in polymer/fullerene solar cells. This kind of technique was first proposed by Porter and Norrish in 1949 and 1950 as flash photolysis.[82,83] At this time, a flash lamp was used for the excitation. Therefore, its time resolution was limited to a microsecond time regime. This technique has been developed along the evolution of laser techniques. In 1967, Novak and Windsor reported nanosecond laser photolysis and spectroscopy using a Q-switched ruby laser.[84] After that, in the late 1980s mode-locked titan-doped sapphire (Ti:Sapphire) laser provides ultrashort pulse (~100 fs).[85] The pump and probe technique with ultrashort pulse lasers allows researchers to directly observe ultrashort phenomena such as elemental processes in chemical reactions.

The transient measurements of solution samples have been actively performed by transient absorption or time-resolved fluorescence measurements. However, transient absorption measurement of thin films is a challenging issue because of the small signal due to short optical length of the sample. This is difficult especially after sub-microsecond time domain at which the signal amplitude is extremely low. In this study, signal amplifier with band pass filters are employed to gain a high signal-to-noise (S/N) ratio in a sub-micro- to millisecond time regime. The band pass filter limits the observation window typically to 3 orders of magnitude in the time domain. Furthermore, the signals are accumulated more than 1000 times to improve the S/N ratio. As a result, the system can detect signal as weak as $\Delta OD \approx 10^{-6}$. This level is sufficient to detect transient species formed in a thin film sample. In this thesis, this high-sensitive microsecond transient absorption spectrometer and a femtosecond transient absorption spectrometer are employed to quantitatively detect charge carriers over the whole time range from photon excitation to charge transport processes.

B. Equivalent Circuit Model

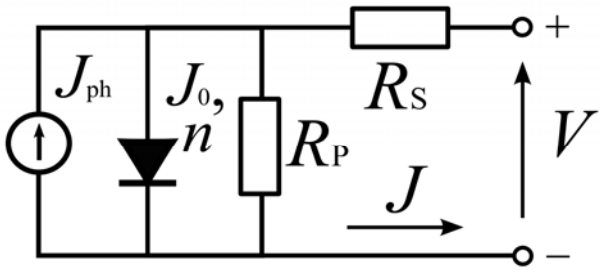

Figure 1-4. Equivalent circuit model of polymer solar cells used in this thesis. A diode with series resistor R_s, and a parallel resistor R_p are assumed. J_0 and n are the diode parameters of saturation current and ideal factor, respectively.

The current–voltage characteristics of solar cell devices are analyzed using the equivalent circuit model based on one diode a series resistor R_s, and a parallel resistor R_p as shown in Figure 1-4. Herein, the Sah–Noyce–Shockley (SNS) diode model is employed. This SNS diode model is submitted by Sah and Noyce as a modification of the original Shockley model. The SNS model concerns the recombination process[86,87] whereas Shockley model is based on diffusion of the minority carrier under a forward bias without recombination.[88] This SNS diode model explained the current–voltage properties of Si (E_g = 1.12 eV) or GaAs (E_g = 1.42 eV) inorganic *p*–*n* junction diodes in early times where charge generation–recombination processes are not negligible.[86] In this model, current flow across the diode is described as $J_0[\exp(qV/nk_BT) - 1]$. Therefore, *J*–*V* characteristics of the device can be derived by Equation 1-2.

$$J = J_0\left\{\exp\left[\frac{q(V - JR_sA)}{nk_BT}\right] - 1\right\} + \frac{(V - JR_sA)}{R_pA} - J_{ph} \qquad (1\text{-}2)$$

where J_0 is the saturation current density, n is the ideality factor, R_s is the series resistance,

R_p is the parallel resistance, A is the active area of the device, and J_{ph} is the photocurrent density. Recent studies have shown that this model can explain the J–V characteristics not only of inorganic solar cells but also of organic solar cells.[89–96] Assuming that J_{ph} is equal to J_{SC}, Equation 1-2 can be simplified into Equation 1-3 under the open-circuit condition because of $V_{OC} << J_{SC}R_pA$ and $J_0 << J_{SC}$.

$$V_{OC} = \frac{nk_BT}{q}\ln\left[1+\frac{J_{SC}}{J_0}\left(1-\frac{V_{OC}}{J_{SC}R_pA}\right)\right] \approx \frac{nk_BT}{q}\ln\left(\frac{J_{SC}}{J_0}\right) \quad (1\text{-}3)$$

On the other hand, V_{OC} is dependent on the saturation current density J_0 in terms of the diode-based equivalent circuit model. Recently, it is reported that the molecular structures affect V_{OC} in small molecule-based organic solar cells.[94–97] This suggests that V_{OC} is dependent on the electron transfer at the interface because of the difference in the electronic coupling between donor and acceptor molecules. This thesis discusses the origin of the open-circuit voltage by analysis on a diode parameters J_0 estimated from the J–V characteristics of devices.

1.2. Outline of This Thesis

The main topic of this thesis is to clarify the photovoltaic conversion mechanism in polymer/fullerene solar cells. In photophysical and device physical studies, the photovoltaic conversion processes are discussed at the sight of each elemental process.

This thesis consists of six chapters. The first chapter describes the motivation, background and methodology of this thesis. The following chapters are divided into two parts.

In Part I (Chapters 2 and 3), the PCBM cation formation in polymer/fullerene solar cells is discussed. In Chapter 2, the formation of PCBM cation is investigated for

MDMO-PPV/PCBM blend films by high-sensitive microsecond transient absorption measurements. As a result, it is shown that PCBM cation is formed in this blend film. In Chapter 3, the formation of PCBM cation is systematically studied in blend films of PCBM and conjugated polymers with different ionization potentials in order to address the formation mechanism of PCBM cation in polymer/fullerene blends. Computational simulations are also employed to discuss the formation mechanism and the energetic condition of the PCBM cation formation in polymer/PCBM blend films.

In Part II (Chapters 4 to 6), the recombination of charge carriers in polymer/fullerene solar cells are discussed. In Chapter 4, the open-circuit voltage of P3HT/fullerenes devices is discussed in terms of CT state recombination. The equivalent circuit analysis is performed for the current–voltage properties of devices with seven different fullerene derivative(s). In Chapter 5, such CT state recombination and dissociation are discussed on the basis of the transient absorption measurements of low-bandgap polymer solar cells. In Chapter 6, all the photovoltaic conversion processes are comprehensively discussed for a fluorene-based copolymer solar cell to explain the device performance.

1.3. References

[1] H. Inokuchi, H. Akamatu, *Sol. Stat. Phys.* **1961**, *12*, 93–148.

[2] W. Brutting, *Physics of Organic Semiconductors*, **2005**, Wiley, NewYork.

[3] A. Pocchettino, *Accad. Lincei, Rend.* **1906**, *15*, 355.

[4] J. Koenigsberger, K. Schilling, *Ann. Physik* **1910**, *32*, 179–230.

[5] M. Volmer, *Ann. Physik* **1913**, *40*, 775–796.

[6] D. Eley, *Nature* **1948**, *162*, 819.

[7] H. Akamatu, H. Inokuchi, *J. Chem. Phys.* **1950**, *18*, 810–811.

[8] H. Inokuchi, *Bull. Chem. Soc. Jpn.* **1954**, *27*, 22–27.

[9] H. Shirakawa, E. J. Louis, A. G. MacDiarmid, C. K. Chiang, A. J. Heeger, *J. Chem. Soc., Chem.Commun.* **1977**, 578–580.

[10] K. Chiang, C. R. Fincher, Jr., Y. W. Park, A. J. Heeger, H. Shirakawa, E. J. Louis, S. C. Gau, A. C. MacDiarmid, *Phys. Rev. Lett.* **1977**, *39*, 1098–1101.

[11] H. W. Kroto, J. R. Heath, S. C. O'Brien, R. F. Curl, R. E. Smalley, *Nature* **1985**, *318*, 162–163.

[12] H. W. Kroto, A. W. Allaf, S. P. Balm, *Chem. Rev.* **1991**, *91*, 1213–1235.

[13] J. Paloheimo, H. Isotalo, J. Kastner, H. Kuzmany, *Synth. Met.*, **1993**, *55–57*, 3185–3190.

[14] R. C. Haddon, A. F. Hebard, M. J. Rosseinsky, D. W. Murphy, S. J. Duclos, K. B. Lyons, B. Miller, J. M. Rosamilia, R. M. Fleming, A. R. Kortan, S. H. Glarum, A. V. Makhija, A. J. Muller, R. H. Eick, S, M. Zahurak, R. Tycko, G. Dabbagh, F. A. Thiel, *Nature* **1991**, *350*, 320–322.

[15] T.Kambe, K. Kajiyoshi, M. Fujiwara, K. Oshima, *Phys. Rev. Lett.* **2007**, *99*, 177205.

[16] Y. Ganin, Y. Takabayashi, Y. Z. Khimyak, S. Margadonna, A. Tamai, M. J. Rosseinsky, K. Prassides, *Nat. Mater.* **2008**, *7*, 367–371.

[17] Y. Takabayashi, A. Y. Ganin, P. Jeglič, D. Arčon, T. Takano, Y. Iwasa, Y. Ohishi, M. Takata, N. Takeshita, K. Prassides, M. J. Rosseinsky, *Science* **2009**, *323*, 1585–1590.

[18] W. Tang, S. A. VanSlyke, *Appl. Phys. Lett.* **1987**, *51*, 913–915.

[19] W. Tang, *Appl. Phys. Lett.* **1986**, *48*, 183–185.

[20] J. H. Burroughes, D. D. C. Bradley, A. R. Brown, R. N. Marks, K. Mackey, R. H. Friend, P. L. Burns, A. B. Holmes, *Nature* **1990**, *347*, 539–541.

[21] N. S. Sariciftci, L. Smilowitz, A. J. Heeger, F. Wudl, *Science* **1992**, *258*, 1474–1476.

[22] M. Hiramoto, H. Fujiwara, M. Yokoyama, *Appl. Phys. Lett.* **1991**, *58*, 1062–1064.

[23] G. Yu, J. Gao, J. C. Hummelen, F. Wudi, A. J. Heeger, *Science* **1995**, *270*, 1789–1791.

[24] N. Camaioni, G. Ridolfi, G. Casalbore-Miceli, G. Possamai, M. Maggini, *Adv. Mater.* **2002**, *14*, 1735–1738.

[25] P. Schilinsky, C. Waldauf, C. Brabec, *J. Appl. Phys.* **2002**, *81*, 3885–3887.

[26] M. T. Dang, L. Hirsch, G. Wantz, *Adv. Mater.* **2011**, *23*, 3597–3602.

[27] Mühlbacher, M. Scharber, M. Morana, Z. Zhu, D. Waller, R. Gaudiana, C, Brabec, *Adv. Mater.* **2006**, *18*, 2884–2889.

[28] J. Peet, J. Y. Kim, N. E. Coates, W. L. Ma, D. Moses, A. J. Heeger, G. C. Bazan, *Nat. Mater.* **2007**, *6*, 497–500.

[29] P. Heremans, D. Cheyns, B. P. Rand, *Acc. Chem. Res.* **2009**, *42*, 1740–1747.

[30] B. Kippelen, J. L. Brédas, *Energy Environ. Sci.* **2009**, *2*, 251–261.

[31] M. Hiramoto, K. Sakai, *Proc. SPIE 7052* **2008**, 70520H–1–6.

[32] I. Salzmann, S. Duhm, R. Optiz, R. L. Johnson, J. P. Rabe, N. Koch, *Appl. Phys. Lett.* **2008**, *104*, 114518.

[33] V. Kamm, G. Battagliarin, I. A. Howard, W. Pisula, A. Mavrinskiy, C. Li, K. Müllen, F. Laquai, *Adv. Energy Mater.* **2011**, *1*, 297–302.

[34] E. Zhou, K. Tajima, C. Yang, K. Hashimoto,. *J. Mater. Chem.* **2010**, *20*, 2362–2368.

[35] H. Yan, B. A. Collins, E. Gann, C. Wang, H. Ade, C. R. McNeill, *ACS Nano in press*, DOI:10.1021/nn204150.

[36] C. Kittel, *Introduction to Solid State Physics* 8th ed. **2005**, Wiley, New York.

[37] B. A. Gregg, M. C. Hanna, *J. Appl. Phys.* **2003**, *93*, 3605–3614.

[38] S. E. Gledhill, B. Scott, B. A. Gregg, *J. Mater. Res.* **2005**, *20*, 3167–3179.

[39] G. Malliaras, R. Friend, *Phys. Today* **2005**, *58*, 53–58.

[40] J. L. Brédas, J. Cornil, A. J. Heeger, *Adv. Mater.* **1996**, *8*, 447–451.

[41] M. Pope, C. E. Swenberg, *Electronic Processes in Organic Crystals and Polymers* 2nd ed. **1999**, Oxford Science Publications, New York.

[42] J. J. M. Halls, K. Pichler, R. H. Friend, S. C. Moratti, A. B. Holmes, *Appl. Phys. Lett.* **1996**, *68*, 3120–3122.

[43] T. Stübinger, W. Brütting, *J. Appl. Phys.* **2001**, *90*, 3632–3641.

[44] E. Markov, E. Amsterdam, P. W. M. Blom, A. B. Sieval, J. C. Hummelen, *J. Phys. Chem. A* **2005**, *109*, 5266–5274.

[45] S. R. Scully, M. D. McGehee, *J. Appl. Phys.* **2006**, *100*, 034907.

[46] Y. Terao, H. Sasabe, C. Adachi, *Appl. Phys. Lett.* **2007**, *90*, 103515.

[47] C. Deibel, V. Dyakonov, *Rep. Prog. Phys.* **2010**, *73*, 096401.

[48] H. Ohkita, S. Cook, Y. Astuti, W. Duffy, S. Tierney, W. Zhang, M. Heeney, I. McCulloch, J. Nelson, D. D. C Bradley, J. R. Durrant, *J. Am. Chem. Soc.* **2008**, *130*, 3030–3042.

[49] C. Veldman, S. C. J. Meskers, R. A. J. Janssen, *Adv. Funct. Mater.* **2009**, *19*, 1939–1948.

[50] L. Onsager, *Phys. Rev.* **1938**, *54*, 554–557.

[51] C. L. J. Braun, *Chem. Phys.* **1984**, *80*, 4157–4161.

[52] M. Fuoss, F. Accascina, *Electrolytic Conductance*, **1959**, Interscience, New York.

[53] M. Wojcik, M. Tachiya, *J. Chem. Phys.* **2009**, *130*, 104107.

[54] K. Tvingstedt, K. Vandewal, A. Gadisa, F. Zhang, J. Manca, O. Inganäs, *J. Am. Chem. Soc.* **2009**, *131*,11819–11824.

[55] D. Jarzab, F. Cordella, J. Gao, M. Scharber, H.-J. Egelhaaf, M. A. Loi, *Adv. Energy Mater.* **2011**, *1*, 604–609.

[56] S. Cook, H. Ohkita, Y. Kim, J. J. Benson-Smith, D. D. C. Bradley, J. R. Durrant, *Chem. Phys. Lett.* **2007**, *445*, 276–280.

[57] J. Guo, H. Ohkita, H. Benten, S. Ito, *J. Am. Chem. Soc.* **2010**, *132*, 6154–6164.

[58] J. Zaumseil, H. Sirringhaus, *Chem. Rev.* **2007**, *107*, 1296–1323.

[59] E. J. Meijer, D. M. de Leeuw, S. Setayesh, E. van Veenendaal, B. H. Huisman, P. W. M. Blom, J. C. Hummelen, U. Scherf, T. M. Klapwijk, *Nat. Mater.* **2003**, *2*, 678–682.

[60] T. Yasuda, T. Goto, K. Fujita, T. Tsutsui, *Appl. Phys. Lett.* **2004**, *85*, 2098–2100.

[61] T. D. Anthopoulos, C. Tanase, S. Setayesh, E. J. Meijer, J. C. Hummelen, P. W. M. Blom, D. M. de Leeuw, *Adv. Mater.* **2004**, *16*, 2174–2179.

[62] T. Nishikawa, S. Kobayashi, T. Nakanowatari, T. Mitani, T. Shimoda, Y. Kubozono, G. Yamamoto, H. Ishii, M. Niwano, Y. Iwasa, *J. Appl. Phys.* **2005**, *97*, 104509.

[63] L. L. Chua, J. Zaumseil, J. F. Chang, E. C W. Ou, P. K. H. Ho, H. Sirringhaus, R. H. Friend, *Nature* **2005**, *434*, 194–199.

[64] E. C. P. Smits, T. D. Anthopoulos, S. Setayesh, E. Van Veenendaal, R. Coehoorn, P. W. M. Blom, B. De Boer, D. M. De Leeuw, *Phys. Rev. B* **2006**, *73*, 205316.

[65] C. Melzer, E. J. Koop, V. D. Mihailetchi, P. W. M. Blom, *Adv. Funct. Mater.* **2004**, *14*, 865–870.

[66] S. M. Tuladhar, D. Poplavskyy, S. A. Choulis, J. R. Durrant, D. D. C. Bradley, J. Nelson, *Adv. Funct. Mater.* **2005**, *15*, 1171–1182.

[67] T. Kirchartz, B. E. Pieters, K. Taretto, U. Rau, *J. Appl. Phys.* **2008**, *104*, 094513.

[68] T. Kirchartz, K. Taretto, U. Rau, *J. Phys. Chem. C* **2009**, *113*, 17958–17966.

[69] C. J. Brabec, A. Cravino, D. Meissner, N. S. Sariciftci, T. Fromherz, M. T. Rispens, L. Sanchez, J. C. Hummelen, *Adv. Funct. Mater.* **2001**, *11*, 374–380.

[70] M. C. Scharber, D. Mühlbacher, M. Koppe, P. Denk, C. Waldauf, A. J. Heeger, C. J. Brabec, *Adv. Mater.* **2006**, *18*, 789–794.

[71] K. Vandewal, A. Gadisa, W. D. Oosterbaan, S. Bertho, F. Banishoeib, I. V. Severen, L. Lutsen, T. J. Cleij, D. Vanderzande, J. V. Manca, *Adv. Funct. Mater.* **2008**, *18*, 2064–2070.

[72] L. J. A. Koster, V. D. Mihailetchi, R. Ramaker, P. W. M. Blom, *Appl. Phys. Lett.* **2005**, *86*, 123509.

[73] L. J. A. Koster, E. C. P. Smits, V. D. Mihailetchi, P. W. M. Blom, *Phys. Rev. B* **2005**, *72*, 085205.

[74] K. Vandewal, K. Tvingstedt, A. Gadisa, O. Inganäs, J. V. Manca, *Nat. Mater.* **2009**, *8*, 904–909.

[75] K. Vandewal, K. Tvingstedt, A. Gadisa, O. Inganäs, J. V. Manca, *Phys. Rev. B* **2010**, *81*, 125204.

[76] W. Ma, C. Yang, X. Gong, K. Lee, A. J. Heeger, *Adv. Funct. Mater.* **2005**, *15*, 1617–1622.

[77] G. Li, V. Shrotriya, J. Huang, Y. Yao, T. Moriarty, K. Emery, Y. Yang, *Nat. Mater.* **2005**, *4*, 864–868.

[78] Y. Kim, S. Cook, S. M. Tuladhar, S. A. Choulis, J. Nelson, J. R. Durrant, D. D. C. Bradley, M. Giles, I. McCulloch, C. S. Ha, M. Ree, *Nat. Mater.* **2006**, *5*, 197–203.

[79] J. H. Park, J. S. Kim, J. H. Lee, W. H. Lee, K. Cho, *J. Phys. Chem. C* **2009**, *113*, 17579–17584.

[80] Y. Yao, J. Hou, Z. Xu, G. Li, Y. Yang, *Adv. Funct. Mater.* **2008**, *18*, 1783–1789.

[81] J. K. Lee, W. L. Ma, C. J. Brabec, J. Yuen, J. S. Moon, J. Y. Kim, K. Lee, G. C. Bazan, A. J. Heeger, *Appl. Phys. Lett.* **2008**, *92*, 243308.

[82] R. G. W. Norrish, G. Porter, *Nature*, **1949**, *164*, 658.

[83] G. Porter, *Proc. Roy. Soc. A* **1950**, *200*, 284–300.

[84] J. R. Novak, M. W. Windsor, *Proc. Roy. Soc. A* **1968**, *308*, 95–110.

[85] J. D. Kafka, M. L. Watts, J. W. J. Pieterse, *IEEE J. Quant. Electron.* **1992**, *28*, 2151–2162.

[86] S. M. Sze, *Physics of Semiconductor Devices* 2nd ed. **1981**, Wiley, New York.

[87] C. T. Sah, R. N. Noyce, W. Shockley, *Proc. IRE* **1957**, *45*, 1228–1243.

[88] W. Shockley, *Bell Sys. Tech. J.* **1949**, *28*, 435–489.

[89] A. Orimo, K. Masuda, S. Honda, H. Benten, S. Ito, H. Ohkita, H. Tsuji, *Appl. Phys. Lett.* **2010**, *96*, 043305.

[90] C. J. Brabec, S. E. Shaheen, C. Winder, N. S. Sariciftci, P. Denk, *Appl. Phys. Lett.* **2002**, *80*, 1288.

[91] T. Aernouts, W. Geens, J. Poortmans, P. Heremans, S. Borghs, R. Mertens, *Thin Solid Films* **2002**, *403–404*, 297–301.

[92] S. Yoo, B. Domercq, B. Kippelen, *J. Appl. Phys.* **2005**, *97*, 103706.

[93] C. Waldauf, M. C. Scharber, P. Schilinsky, J. A. Hauch, C. J. Brabec, *J. Appl. Phys.* **2006**, *99*, 104503.

[94] W. J. Potscavage, Jr., S. Yoo, B. Kippelen, *Appl. Phys. Lett.* **2008**, *93*, 193308.

[95] W. J. Potscavage, Jr., A. Sharma, B. Kippelen, *Acc. Chem. Res.* **2009**, *42*, 1758–1767.

[96] M. D. Perez, C. Borek, S. R. Forrest, M. E. Thompson, *J. Am. Chem. Soc.* **2009**, *131*,

9281–9286.

[97] P. Erwin, M. E. Thompson, *Appl. Phys. Lett.* **2011**, *98*, 223305.

Part I

Chapter 2

Formation of Methanofullerene Cation in Bulk Heterojunction Polymer Solar Cells

2.1. Introduction

Since the discovery of efficient electron transfer in blend films of conjugated polymer with fullerene,[1,2] such blend systems have attracted increasing interest in photophysical studies and application to organic devices. For blend films of poly[2-methoxy-5-(3,7-dimethyloctyloxy)-1,4-phenylenevinylene] (MDMO-PPV) with [6,6]-phenyl-C_{61}-butyric acid methyl ester (PCBM), ultrafast charge separation has been reported.[3] Furthermore, the intermixing of the polymer electron donor and the fullerene electron acceptor can provide a significantly enlarged interfacial area of donor and acceptor "bulk heterojunction", resulting in a high charge separation efficiency. This blend system is one of the most thoroughly studied donor–acceptor pairs for bulk heterojunction organic solar cells, exhibiting power conversion efficiencies of about 3% with a 1 : 4 weight ratio of polymer to fullerene.[4–6] In other words, the most efficient solar cells based on MDMO-PPV and PCBM require a high content of PCBM (80 wt %). This is however unfavorable for light absorption, because fullerene derivatives such as PCBM have small absorption in the visible region compared with conjugated polymers such as MDMO-PPV. Moreover, this biased ratio seems to have a disadvantage for charge transport, because charge-carrier mobility for electrons in PCBM (2×10^{-3} cm^2 V^{-1} s^{-1})[7] is more than three orders of magnitude larger than that for holes in MDMO-PPV pristine film (3×10^{-7} cm^2 V^{-1} s^{-1}).[8]

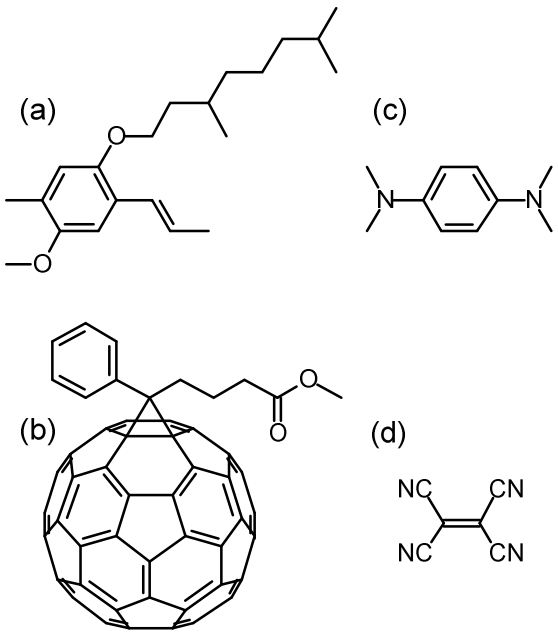

Figure 2-1. Chemical structures used in this study: (a) MDMO-PPV, (b) PCBM, (c) TMPD, and (d) TCNE.

Recent studies have shown that the hole mobility of the MDMO-PPV/PCBM blend is larger than that of pristine MDMO-PPV by more than two orders of magnitude at 80 wt% PCBM,[8,9] suggesting that the charge transport in the blend is much more balanced than previously assumed. This finding seems contradictory to the prevailing view that conjugated polymers such as MDMO-PPV act as a hole-transporting material and that fullerene derivatives such as PCBM act as an electron-transporting material. Blom ***et al.*** proposed that ring-like molecular conformation of MDMO-PPV might be the origin of the poor transport properties in the pristine film, which would be hindered in the blend to improve the hole mobility.[8] On the other hand, Nelson and her coworkers have demonstrated that adding PCBM to the blend increases the mobility of both electron and hole compared to the pristine MDMO-PPV.[9] They also found that electron and hole mobilities are of similar magnitude for PCBM dispersed in a polystyrene (PS) matrix.

Indeed, ambipolar charge transport has already been reported for fullerene-based field-effect transistors (FET) including PCBM.[10,11] However, it is still not clear whether PCBM radical cation is formed as a hole carrier in the blend films or not.

Herein, a detailed spectroscopic study of charged carriers formed in MDMO-PPV/PCBM blend films at a PCBM concentration ranging from 0 to 80 wt% by transient absorption spectroscopy was reported. For identification of charge carriers formed in the blend, the absorption spectrum and the molar absorption coefficient of each charge carrier, MDMO-PPV hole polaron, PCBM radical anion, and PCBM radical cation, were measured by using various combinations of electron donor and acceptor materials shown in Figure 2-1. The transient absorption spectra of the blend (<10 wt% PCBM) were reproduced by a simple summation of that of MDMO-PPV hole polaron and PCBM radical anion. On the other hand, the transient spectra (>30 wt% PCBM) were not reproduced by the simple summation but well reconstructed by a summation of that of MDMO-PPV hole polaron, PCBM radical anion, and PCBM radical cation. This finding provides spectroscopic evidence of formation of PCBM radical cation in the blend at higher PCBM concentrations, suggesting that PCBM serves as not only an electron-transporting material but also a hole-transporting material in bulk heterojunction solar cells with high PCBM fractions.

2.2. Results

2.2.1. Transient Absorption Spectra

Figure 2-2 shows the transient absorption spectra of MDMO-PPV/PCBM blend films with various concentrations of PCBM ranging from 5 to 80 wt%. The blend films with PCBM at low concentration (<10 wt%) exhibited broad absorption bands from 900

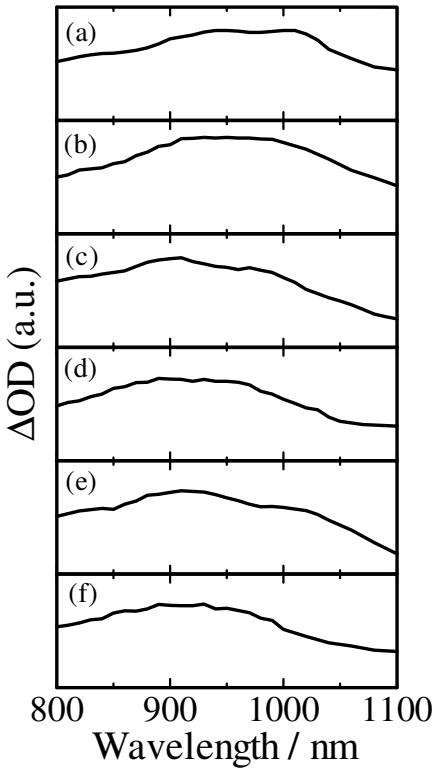

Figure 2-2. Transient absorption spectra of MDMO-PPV/PCBM blend films at 1 μs after the laser excitation at 500 nm with a fluence of 30 μJ cm^{-2}. The PCBM concentration is as follows: (a) 5, (b) 10, (c) 30, (d) 50, (e) 68, and (f) 80 wt %.

to 1000 nm. The absorption peak at ~1000 nm is characteristic of fullerene radical anions.[12] The remaining broad absorption around 950 nm is indicative of formation of MDMO-PPV hole polarons as reported previously.[13] Therefore, the broad absorption from 900 to 1000 nm is tentatively assigned to the formation of MDMO-PPV hole polaron and PCBM radical anion as charge carriers in the blend films at the low PCBM concentrations. On the other hand, the transient absorption spectra changed at higher PCBM concentrations (>30 wt%) where a new absorption band appeared at ~900 nm. One possible explanation for this spectral change is that another charge carrier is newly

formed in the blend films with PCBM at high concentration as mentioned below. Another explanation is that the absorption spectra of charge carriers vary with the PCBM concentration. Fullerene anions in film state have essentially the same absorption spectra as in solutions.[14] More probably, therefore, the absorption spectrum of MDMO-PPV polarons may be dependent upon the PCBM concentration. Note that Blom et al. propose the conformational change of MDMO-PPV due to interactions between MDMO-PPV and PCBM to explain the high hole mobility in the blend films with PCBM at a concentration.[7] The conformational change would cause a spectral change in transient absorption of the blend films heavily doped with PCBM.

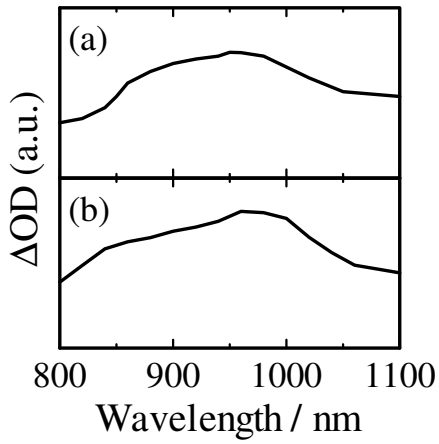

Figure 2-3. Transient absorption spectra of MDMO-PPV/TCNE blend films at 10 μs after the laser excitation at 500 nm with a fluence of 30 μJ cm^{-2}. The TCNE concentration is: (a) 5 and (b) 50 wt%.

To examine the dependence of absorption spectrum of MDMO-PPV polarons on dopant concentrations, blend films with tetracyanoethylene (TCNE) were fabricated instead of PCBM because TCNE radical anion has no absorption band from 900 to 1000

nm. Furthermore, TCNE is a strong electron acceptor ($E_{1/2}(TCNE^-/TCNE)$ = 0.24 V vs SCE)[15] compared with C_{60} ($E_{1/2}(C_{60}^-/C_{60})$ = −0.3 – 0.4 V vs SCE).[12] Figure 2-3 shows the transient absorption spectra of MDMO-PPV/TCNE blend films with 5 and 50 wt% TCNE. For the blend film with 5 wt% TCNE, a broad absorption was observed at ~950 nm. A similar absorption was observed at ~960 nm for the blend film with 50 wt% TCNE. As mentioned before, both spectra can be safely assigned to MDMO-PPV hole polaron. It should be noted that there is no distinct absorption peak at ~900 nm where a new absorption band was observed for MDMO-PPV/PCBM blend films with high PCBM concentrations (> 30 wt%). Therefore, these results suggest that the new absorption band at ~900 nm cannot be ascribed to the spectral change of MDMO-PPV hole polaron due to the heavy doping of electron-accepting molecules. Rather the 900-nm band is more probably due to the formation of charge carriers related with PCBM. To study charge carriers formed in the blend films, the absorption spectrum for possible charge carriers will be assigned in the following section.

2.2.2. Assignment of Charge Carriers

For the quantitative discussion, the author will not only assign the absorption spectrum but also evaluate the molar absorption coefficient of each charge carrier by using various combinations of electron donor and acceptor materials.

First, transient absorption spectra of an MDMO-PPV pristine film were measured to confirm the absorption of MDMO-PPV hole polaron. The solid lines in Figure 2-4a show transient absorption spectra of the MDMO-PPV pristine film from 2 to 10 μs after the laser excitation. The absorption peak shifted from 860 nm at <2 μs to ~950 nm for time delay >5 μs, demonstrating the formation of two independent transient species in the pristine film. Figure 2-4b shows the time evolution of the transient signals at 850 nm

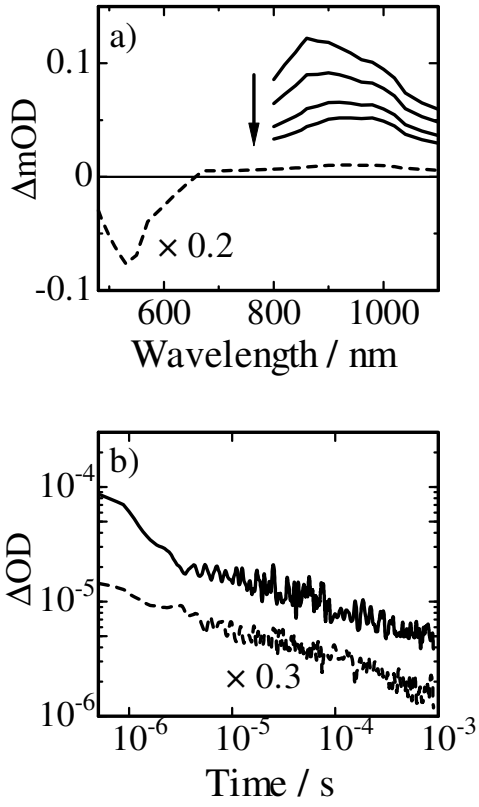

Figure 2-4. (a) Transient absorption spectra of an MDMO-PPV pristine film (solid lines) at 1, 2, 5, and 10 μs after the laser excitation at 500 nm with a fluence of 30 μJ cm^{-2}. The broken line represents the transient spectrum at 10 μs multiplied by a factor of 0.2. (b) The transient decay at 850 nm (solid line) and 940 nm (broken line). The decay at 940 nm is multiplied by a factor of 0.3.

(solid line) and 940 nm (broken line). The decay at 850 nm was fitted with a sum of a single-exponential function and a power equation, $\Delta OD = A \exp(-t/\tau) + B\, t^{-\alpha}$, while the decay at 940 nm was well fitted with only a power equation. The monoexponential phase decayed with a lifetime of $\tau \sim 0.5$ μs under Ar atmosphere and disappeared under O_2 atmosphere. The absorption peak and the lifetime in the earlier time domain were in agreement with those reported for triplet–triplet (T–T) absorption of PPV derivatives.[16,17]

This fast decay is therefore assigned to MDMO-PPV triplet excitons. For the time delays >5 μs, on the other hand, the decay at both 850 and 940 nm were well fitted by the power equation with the same exponent $\alpha = 0.27$, suggesting that there is one decay pathway. The power-law decay is characteristic of the bimolecular recombination of charged species in the presence of energetic disorder.[18] Furthermore, the transient absorption spectra at >5 μs of the MDMO-PPV pristine film were similar to that assigned to MDMO-PPV hole polaron in MDMO-PPV/TCNE blend films shown in Figure 2-3, suggesting that there is little contribution of MDMO-PPV electron polaron to the absorption band. Thus, the absorption band at ~950 nm is safely attributable to MDMO-PPV hole polaron. The molar absorption coefficient will be evaluated later by using the absorption spectrum at 10 μs as MDMO-PPV hole polaron.

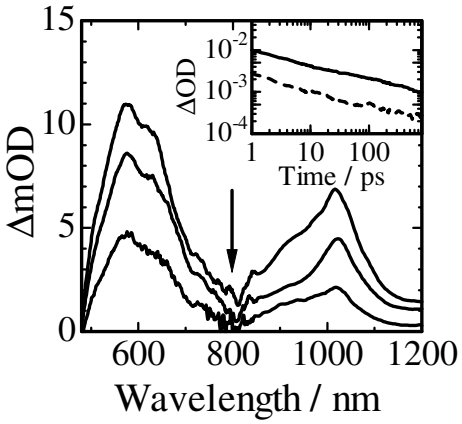

Figure 2-5. Transient absorption spectra of PS/TMPD/PCBM/ (5 : 2 : 3 w/w) blend films at 1, 2, and 10 ps after the laser excitation at 400 nm with a fluence of 65 μJ cm^{-2}. The inset shows the transient decay at 600 nm (solid line) and 1050 nm (broken line).

Next, transient absorption spectra of PS films doped with *N,N,N',N'*-tetramethyl-*p*-phenylenediamine (TMPD) as an electron donor and PCBM as an

electron acceptor were measured to assign the absorption of PCBM radical anion. The weight ratio of each component in the film was PS : TMPD : PCBM = 5 : 2 : 3. As shown in Figure 2-5, two absorption bands were observed at 570 and 1020 nm. The absorption band at 570 nm is in good agreement with that reported for the oxidation product of TMPD called Wurster's Blue,[19] and therefore was assigned to TMPD radical cation. The absorption band at 1020 nm is assigned to PCBM radical anion because, as mentioned before, various radical anions of fullerene derivatives have a characteristic absorption band around 1000 nm: a fullerene radical anion (1080 nm), a methanofullerene radical anion (1040 nm), and a fulleropyrrolidine radical anion (1010 nm).[12] In a time domain longer than 10 ps, as shown in the inset to Figure 2-5, both bands obeyed the power-law decay dynamics with the same exponent $\alpha \approx 0.25$. Thus, the same decay dynamics observed at 570 and 1020 nm is ascribable to the bimolecular recombination of TMPD radical cation and PCBM radical anion without other decay pathways, suggesting that no other transient species such as singlet and triplet excitons contribute to the transient absorption spectra on the longer time scales (>10 ps). Therefore, the molar absorption coefficient of PCBM radical anion can be evaluated from the transient absorption spectra at 10 ps. On the basis of the molar absorption coefficient of TMPD radical cation (ε = 12000 M^{-1} cm^{-1}),[19,20] that of PCBM radical anion was evaluated to be ε = 6000 M^{-1} cm^{-1} at 1020 nm. This value is smaller than that reported for the C_{60} radical anion (ε = 15000 M^{-1} cm^{-1}) but rather comparable to that of fullerene derivatives, a fulleropyrrolidine radical anion (ε = 8000 M^{-1} cm^{-1}) and a methanofullerene radical anion (ε = 10000 M^{-1} cm^{-1}).[12] Note that essentially the same transient absorption spectra were obtained for PS/TMPD/PCBM (2 : 2 : 6 w/w) blend films (data not shown). In other words, the PCBM radical anion has a characteristic absorption around 1020 nm independently of the PCBM concentration. This trend is consistent with the previous report for C_{60}.[14]

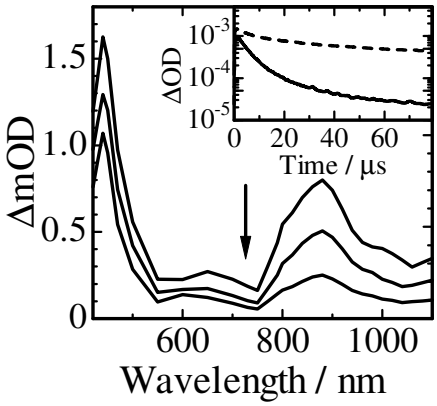

Figure 2-6. Transient absorption spectra of PCBM/TCNE solution in benzonitrile at 2, 5, and 10 μs after the laser excitation at 400 nm with a fluence of 30 μJ cm^{-2}. The molar concentration is [PCBM] = 1.3 mM and [TCNE] = 6.6 mM. The inset shows the transient decay at 900 nm (solid line) and 450 nm (broken line).

Finally, the transient absorption spectra of a benzonitrile solution dissolved with PCBM as an electron donor and TCNE as an electron acceptor were measured to assign the absorption of PCBM radical cation. These spectra were measured in solution rather than in film because a good common solution for fullerene and TCNE is not found. Photoexcitation of this blend solution will give PCBM radical cation and TCNE radical anion, because photoinduced electron transfer from fullerene triplet to TCNE has been reported.[21] Figure 2-6 shows the transient absorption spectra of a mixture of PCBM and TCNE in benzonitrile. Two distinct absorption peaks were observed at 450 and 890 nm. The absorption band at 450 nm is indistinguishable from the spectrum of TCNE radical anion previously reported[22] and the other band at 890 nm is slightly blue-shifted compared with that of fullerene radical cation (980 nm)[23,24] but rather similar to that of fullerene derivatives (960 nm).[25] These two bands were therefore assigned to the formation of PCBM radical cation and TCNE radical anion. As shown in the inset to the

figure, the transient signal at 890 nm decayed much faster than that at 450 nm while both decay dynamics were finally similar at the longer time stage. The decay at 450 nm was well fitted with a sum of the first and second order equations: $\Delta OD = A\, t^{-1} + B \exp(-t/\tau)$ while the band at 890 nm obeyed the second order kinetics: $\Delta OD = A\, t^{-1}$. The monoexponential lifetime of the transient signal at 450 nm was ~ 80 μs and significantly shortened under O_2 atmosphere. In a reference experiment, a similar transient absorption was observed at 450 nm with the same lifetime for a benzonitrile solution with TCNE alone. Thus, the first order decay component of the blend solution is due to TCNE in the excited triplet state. The second order decay is therefore assigned to bimolecular recombination of PCBM radical cation and TCNE radical anion. On the basis of the molar absorption coefficient of TCNE radical anion $\varepsilon = 5670\ M^{-1}\ cm^{-1}$ at 457 nm,[22] that of PCBM radical cation is evaluated to be $\varepsilon = 9000\ M^{-1}\ cm^{-1}$ at 890 nm, which is comparable to that of fullerene radical cation ($\varepsilon = 11000\ M^{-1}\ cm^{-1}$).[23]

2.3. Discussion

2.3.1. Charge Carriers Formed in MDMO-PPV/PCBM Blends

The author starts off the discussion by considering charge carriers formed in MDMO-PPV/PCBM blend films. For blend films with PCBM at a low concentration, as mentioned above, the transient spectra observed were tentatively assigned to the formation of MDMO-PPV hole polaron and PCBM radical anion. For confirmation of this assignment, the spectra for the film with 5 wt% PCBM were compared with a summation of each spectrum of MDMO-PPV polaron and PCBM radical anion obtained in the previous section. As shown in Figure 2-7a, the reproduced spectrum was in good agreement with that observed for the blend film with 5 wt% PCBM. Therefore, it is concluded that MDMO-PPV polaron and PCBM radical anion are formed as charge

carriers in the blend films with PCBM at a low concentration (<10 wt%). From the spectral simulation, the molar absorption coefficient of MDMO-PPV hole polaron is evaluated to be $\varepsilon_{\text{MDMO-PPV}}{}^{+}$ = 15000 M^{-1} cm^{-1} on the basis of that of PCBM radical anion $\varepsilon_{\text{PCBM}}{}^{-}$ = 6000 M^{-1} cm^{-1}. This value is comparable to an absorption cross section of polarons reported for a PPV derivative.[26]

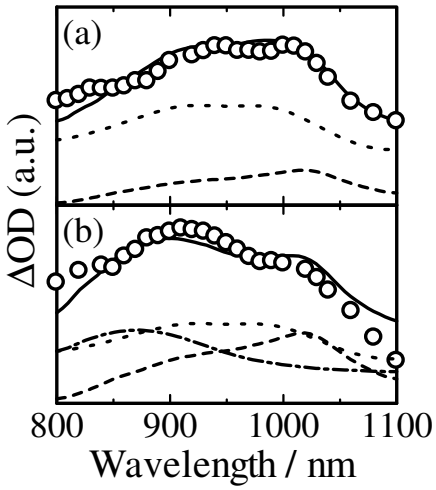

Figure 2-7. Transient absorption spectra of MDMO-PPV/PCBM blend films (open circles) at 1 μs after the laser excitation at 500 nm with a fluence of 30 μJ cm^{-2}. The PCBM concentration is (a) 5 wt% (b) 68 wt%. The solid lines represent absorption spectra simulated by a sum of each absorption spectrum of charge carriers: MDMO-PPV^{+} (broken lines), $PCBM^{-}$ (dotted lines), and $PCBM^{+}$ (dashed-dotted lines). The mole fraction of each spectrum is (a) MDMO-PPV^{+} : $PCBM^{+}$: $PCBM^{-}$ = 0.5 : 0 : 0.5, (b) 0.15 : 0.35 : 0.5.

On the other hand, two possible explanations were considered for the different transient spectra observed for blend films with high PCBM concentrations as mentioned above. As shown in Figure 2-3, the absorption spectrum of MDMO-PPV hole polaron at

~950 nm is essentially independent of TCNE dopant concentrations up to 50 wt% (corresponding to ~40% by volume).[27] This concentration is much higher than the 30 wt % PCBM concentration (corresponding to ~20% by volume)[30] above which spectral changes were observed in the transient measurements. Furthermore, no spectral change was observed for PS/TMPD/PCBM blend films with PCBM concentrations up to 60 wt%, suggesting that the absorption spectrum of PCBM radical anion is also essentially independent of the PCBM concentration as reported previously.[14] Therefore, it is concluded that neither MDMO-PPV polarons nor PCBM radical anion is related to the spectral change observed for blend films with PCBM at a high concentration (>30 wt%). Instead it is concluded that another charge carrier is formed in blend films at the high PCBM concentrations. The author considers PCBM radical cation as the most possible carrier formed at the high PCBM concentrations because, as mentioned before, MDMO-PPV electron polaron has negligible absorption in the wavelength region from 800 to 1000 nm.

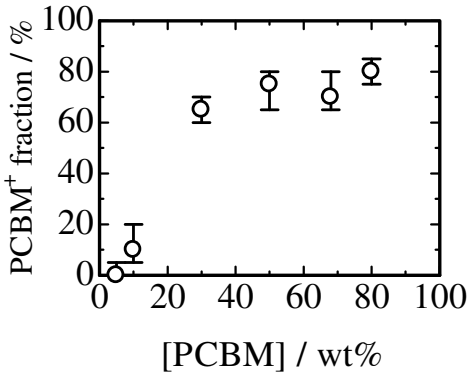

Figure 2-8. The mole fraction of $PCBM^+$ in hole carriers plotted against the weight concentration of PCBM in MDMO-PPV/PCBM blend films. The fraction is evaluated from the spectral simulation shown in Figure 2-7.

To verify the assumption that PCBM radical cation is formed in the blend films, transient spectra observed for blend films with a higher PCBM concentration were reproduced. In contrast to the spectrum at the low PCBM concentration, the spectrum at 68 wt% PCBM was irreproducible by a simple summation of each spectrum of MDMO-PPV hole polaron and PCBM radical anion. Rather, as shown in Figure 2-7b, it was well reproduced by a summation of each spectrum of MDMO-PPV hole polaron, PCBM radical anion, and PCBM radical cation. Therefore, it is concluded that PCBM radical cation is formed as a new charge carrier at the high PCBM concentrations. Furthermore, the mole fraction of PCBM radical cation formed in the blend films can be quantitatively evaluated on the basis of each molar absorption coefficient obtained in the previous section. Figure 2-8 shows the dependence of the evaluated mole fraction of PCBM radical cation in hole carriers on the PCBM concentration in blend films. At low PCBM concentrations (<10 wt%), the mole fraction of PCBM radical cation was negligible, which is indicative of the formation of MDMO-PPV hole polaron and PCBM radical anion pairs alone. Above 30 wt% PCBM, on the other hand, it drastically increased to 60 mol % and gradually up to 80 mol% at 80 wt% PCBM. In other words, most holes formed in blend films are located on PCBM molecules rather than MDMO-PPV chains. This finding seems contradictory to the prevailing view that MDMO-PPV serves as a hole-transporting material and PCBM as an electron-transporting material in blend films. However, this is consistent with ambipolar transport reported for fullerene derivatives including PCBM.[9–11] The field-effect hole mobility of PCBM is reported to be 8×10^{-3} $cm^2\ V^{-1}\ s^{-1}$ [11], which is much higher than the hole mobility of pristine MDMO-PPV (~ 10^{-7} $cm^2\ V^{-1}\ s^{-1}$)[8,9] but rather comparable to that of MDMO-PPV/PCBM blend films (~ 10^{-4} $cm^2\ V^{-1}\ s^{-1}$).[8,9] Thus, the finding can explain previous reports[9] that the hole mobility in MDMO-PPV/PCBM blend films increased at higher PCBM concentrations

(>50 wt%).

2.3.2. Mechanisms of PCBM Radical Cation Generation

Next, the author consider the formation mechanism of PCBM radical cation in MDMO-PPV/PCBM blend films at higher PCBM concentrations (>30 wt%). As shown in Figure 2-8, the mole fraction of PCBM radical cation sharply increased between 10 and 30 wt%. This turning point is in agreement with the theoretical percolation threshold of ~17 % by volume (corresponding to ~25 wt% PCBM) for random 3D network.[6] Furthermore, the abrupt increase is characteristic of the percolation probability. These results suggest that the formation of PCBM radical cation is closely correlated with the formation of the PCBM domain in the blend films. In other words, PCBM radical cation is likely to be formed in the PCBM domain by the direct photoexcitation, as long-lived charge carriers identified as spin 1/2 polarons ($C_{60}^{\pm}$) in fullerene solid films.[31] Previous studies of C_{60}[32,33] and PCBM solid films[34, 35] have revealed enhanced absorption in the visible region assigned to intermolecular charge transfer (CT) transitions.[31] For the PCBM pristine film, significantly greater absorption is observed in the visible region compared with 12 wt% PCBM dispersed in PS film where PCBM is likely to be more isolated.[34] In other words, the absorption of PCBM is more enhanced in the visible region than expected from the PCBM fraction because intermolecular CT transitions appear along with the formation of the PCBM domain. Therefore, it is concluded that the direct photoexcitation of PCBM is substantial for MDMO-PPV/PCBM blend films at higher PCBM concentrations, resulting in the formation of PCBM radical cation and anion pairs. However, the absorption of fullerene is not exceeds polymer absorption in absorption coefficient even in PCBM rich film. This suggests energy transfer path from other state (such as triplet exciton) might exist.

Another mechanism for the formation of PCBM radical cation is hole transfer from MDMO-PPV to the PCBM domain. On the basis of the reported ionization potentials for the two materials (IP = 5.1 eV for MDMO-PPV and IP = 6.1 eV for PCBM),[9] the hole transfer from MDMO-PPV to PCBM should be energetically forbidden because of the energy difference as large as 1 eV, which is consistent with the prevailing view that MDMO-PPV and PCBM serve as a hole-transporting material and an electron-transporting material, respectively, in the blend. Nelson and coworkers have estimated the Gibbs free energy for the hole transfer to be $\Delta G \approx 0.5 - 0.7$ eV considering interfacial dipole and higher polarizability and larger density of states of PCBM in addition to the simple energy difference of IPs.[9] They concluded that the hole transfer from MDMO-PPV to PCBM through a single charge transfer step was unlikely because their simulation for time of flight measurements suggested that hole transport through PCBM can dominate only for values of ΔG less than ~ 0.2 eV at room temperature. Instead they tentatively explained the hole transport in the blend films as hopping between CT states at the polymer/fullerene interface into which hole polarons generated in the MDMO-PPV phase may be transferred. However, the transient results demonstrate the formation of PCBM radical cation rather than such a new CT state, because the absorption spectrum of the interfacial CT state (MDMO-PPV$^{\delta+}$/PCBM$^{\delta-}$) is expected to be similar to MDMO-PPV hole polaron or PCBM radical anion rather than PCBM radical cation. Furthermore, no absorption ascribable to the CT state was observed for MDMO-PPV/TCNE blend films. The author therefore concludes that hole carriers in MDMO-PPV/PCBM blend films are MDMO-PPV polaron and PCBM radical cation rather than the interfacial CT states. Rather the interfacial CT states may be associated with the formation of PCBM radical cation to reduce energy barrier for the hole transfer from MDMO-PPV to PCBM. Furthermore, the effective energy difference may be smaller considering the relatively

wide bandwidth reported for fullerene solid (~ 0.4 – 0.6 eV).[36,37] However, the author has no clear evidence for such an unusual hole transfer. Further studies are needed to address the formation mechanism of PCBM radical cation in MDMO-PPV/PCBM blend films.

2.4. Conclusions

Photogenerated charge carriers in MDMO-PPV/PCBM blend films with a PCBM concentration ranging from 0 to 80 wt% have studied by transient absorption spectroscopy. To identify the charge carriers, the author measured transient absorption of each charge carrier separately using various combinations of electron donor and acceptor materials. MDMO-PPV hole polaron has a broad absorption at ~950 nm (15000 M^{-1} cm^{-1}), PCBM radical anion at 1020 nm (6000 M^{-1} cm^{-1}), and PCBM radical cation at 890 nm (9000 M^{-1} cm^{-1}). The transient absorption spectrum of the blend film (<10 wt% PCBM) was reproduced by a simple summation of the spectrum of MDMO-PPV hole polaron and PCBM radical anion, suggesting that charge carriers in the blend are MDMO-PPV hole polaron and PCBM radical anion alone. On the other hand, the transient absorption spectrum (>30 wt% PCBM) was reproduced by a summation of each spectrum of MDMO-PPV hole polaron, PCBM radical anion, and PCBM radical cation, suggesting that charge carriers in the blend are not only MDMO-PPV hole polaron and PCBM radical anion but also PCBM radical cation. Furthermore, it was confirmed that the transient absorption of MDMO-PPV hole polaron and PCBM radical anion is independent of dopant concentration. Thus, it was concluded that PCBM radical cation is formed as a hole carrier in the blend films with PCBM at a high concentration. Possible mechanisms of the formation of PCBM radical cation in the blend include the following: i) direct photoexcitation of intermolecular CT transitions of PCBM pronounced at higher PCBM

concentrations, resulting in the formation of PCBM radical cation and anion pairs at the PCBM domain in the blend, and ii) hole transfer from MDMO-PPV to PCBM domain via interfacial CT states. Further studies are required to resolve which mechanism is dominant. This study provided a spectroscopic evidence for ambipolar transport of PCBM in polymer–fullerene blend films, and provides a new strategy for designing of bulk heterojunction solar cells.

2.5. Experimental

Preparation: Polymer/fullerene blend films were prepared on glass substrates by spin-coating from a chlorobenzene solution of MDMO-PPV (Aldrich, M_n = 95,000 g mol^{-1}) and PCBM (Frontier Carbon, >99%) at a spin rate of 1000 rpm under ambient conditions. Film thickness was typically 150 – 200 nm. The weight fraction of PCBM was varied from 5 to 80 wt%. The blend solution was stirred at 35 °C overnight to be dissolved homogeneously. Before the spin-coating, the glass substrates were cleaned by ultrasonic treatment in toluene, acetone, and ethanol sequentially for 15 min each and then with a UV–ozone cleaner (Nippon Laser & Electronics Lab., UV253) for 1 h. For blend films of MDMO-PPV and TCNE (Aldrich, >98%), cyclohexanone was used as a solvent instead of chlorobenzene. The blend solution was stirred at 50 °C for 5 h. The weight fraction of TCNE was adjusted to 5 and 50 wt % in the final films. For blend films of PS (Aldrich, M_n = 280,000 g mol^{-1}) doped with PCBM and TMPD (Wako, >98%), chlorobenzene was used as a solvent. The PS was purified by reprecipitation from toluene solution into methanol three times. The blend solution was stirred at room temperature overnight. The weight ratio in the blend films was adjusted to PS : PCBM : TMPD = 5 : 3 : 2 (30 wt% PCBM) or 2 : 6 : 2 (60 wt% PCBM). For a blend solution of PCBM and TCNE, benzonitrile was used as a solvent. The molar concentration of PCBM

and TCNE was 0.2 mM and 1.5 mM, respectively.

Measurements: Transient absorption data were collected under Ar atmosphere with a highly sensitive microsecond transient absorption system and with a femtosecond transient absorption system as described below. The sample films were sealed in a quartz cuvette purged with Ar for 30 min. The sample solution in a quartz cell was deaerated by Ar bubbling for 30 min. For the microsecond transient absorption measurement, the sample was excited with a light pulse (500 nm, 30 μJ cm^{-2}, 4 Hz) from a dye laser (Photon Technology International, GL-301) that was pumped with a nitrogen laser (Photon Technology International, GL-3300), and probed with a monochromatic light from a 50-W quartz tungsten halogen lamp (Thermo-ORIEL, Model 66997) with a light intensity controller (Thermo-ORIEL, Model 66950), which was equipped with appropriate optical cut-filters and two monochromators (Ritsu, MC-10N) before and after the sample to reduce stray light, scattered light, and emission from the sample. The probe light was detected with a pre-amplified Si photodiode (Costronics Electronics). The detected signal was sent to the main amplification system with an electronic band-pass filter (Costronics Electronics) to improve the noise-to-signal ratio. The amplified signal was collected with a digital oscilloscope (Tektronix, TDS2022), which was synchronized with a trigger signal of the laser pulse from a photodiode (Thorlabs, DET10A). The detectable absorbance change ΔOD is as small as ~ 10^{-5} – 10^{-6} depending on the measuring time domain. The femtosecond transient absorption data were collected with a pump and probe transient absorption spectroscopy system (Ultrafast Systems, Helios). The pump light was second harmonic pulses (400 nm, 64 μJ cm^{-2}, fwhm 100 fs, 500 Hz) from a regeneratively amplified Ti-sapphire laser (Spectra-Physics, Hurricane). The probe beam was detected with a linear CCD array (Ocean Optics, S2000) for the visible wavelength range from 400 to 900 nm and with a digital line scan InGaAs camera (Sensors, SU-LDV) for the near-IR

wavelength range from 850 to 1600 nm. The typical noise level of this system is lower than 2×10^{-4}.

2.6. References and Notes

[1] N. S. Sariciftci, L. Smilowitz, A. J. Heeger, F. Wudl, *Science* **1992**, *258*, 1474–1476.

[2] S. Morita, A. A. Zakhidov, K. Yoshino, *Solid Stat. Comm.* **1992**, *82*, 249–252.

[3] C. J. Brabec, G. Zerza, G. Cerullo, S. De Silvestri, S. Luzzati, J. C. Hummelen, S. Sariciftci, *Chem. Phys. Lett.* **2001**, *340*, 232–236.

[4] S. E. Shaheen, C. J. Brabec, N. S. Sariciftci, F. Padinger, T. Fromherz, J. C. Hummelen, *Appl. Phys. Lett.* **2001**, *78*, 841–843.

[5] C. J. Brabec, S. E. Shaheen, C. Winder, N. S. Sariciftci, P. Denk, *Appl. Phys. Lett.* **2002**, *80*, 1288–1290.

[6] J. K. J. Duren, X. Yang, J. Loos, C. W. T. Bulle-Lieuwma, A. B. Sieval, J. C. Hummelen, R. A. J. Janssen, *Adv. Funct. Mater.* **2004**, *14*, 425–434.

[7] V. D. Mihailetchi, J. K. J. van Duren, P. W. M. Blom, J. C. Hummelen, R. A. J. Janssen, J. M. Kroon, M. T. Rispens, W. J. H. Verhees, M. M. Wienk, *Adv. Funct. Mater.* **2003**, *13*, 43–46.

[8] C. Melzer, E. J. Koop, V. D. Mihailetchi, P. W. M. Blom, *Adv. Funct. Mater.* **2004**, *14*, 865–870.

[9] S. M. Tuladhar, D. Poplavskyy, S. A. Choulis, J. R. Durrant, D. D. C. Bradley, J. Nelson, *Adv. Funct. Mater.* **2005**, *15*, 1171–1182.

[10] T. Nishikawa, S. Kobayashi, T. Nakanowatari, T. Mitani, T. Shimoda, Y. Kubozono, G. Yamamoto, H. Ishii, M. Niwano, Y. Iwasa, *J. Appl. Phys.* **2005**, *97*, 104509.

[11] T. D. Anthopoulos, C. Tanase, S. Setayesh, E. J. Meijer, J. C. Hummelen, P. W. M. Blom, D. M. de Leeuw, *Adv. Mater.* **2004**, *16*, 2174–2179.

[12] D. M. Guldi, M. Prato, *Acc. Chem. Res.* **2000**, *33*, 695–703.

[13] A. F. Nogueira, I. Montanari, J. Nelson, J. R. Durrant, C. Winder, N. S. Sariciftci, C. Brabec, *J. Phys. Chem. B* **2003**, *107*, 1567–1573.

[14] K. Kaneto, T. Abe, W. Takashima, *Solid State Commun.* **1995**, *96*, 259–264.

[15] V. A. Nadtochenko, N. N. Denisov, I. V. Rubtsov, A. S. Lobach, A. P. Moravskii, *Chem. Phys.*

Lett. **1993**, *208*, 431–435.

[16] I. Montanari, A. F. Nogueira, J. Nelson, J. R. Durrant, C. Winder, M. A. Loi, N. S. Sariciftci, C. Brabec, *Appl. Phys. Lett.* **2002**, *81*, 3001–3003.

[17] H. D. Burrows, J. S. de Melo, C. Serpa, L. G. Arnaut, M. da G. Miguel, A. P. Monkman, I. Hamblett, S. Navaratnam, *Chem. Phys.* **2002**, *285*, 3–11.

[18] J. Nelson, *Phys. Rev. B* **2003**, *67*, 155209.

[19] J. Steigman, W. Cronkright, *J. Am. Chem. Soc.* **1970**, *92*, 6736–6743.

[20] T. Kawaguchi, S. Seki, K. Okamoto, A. Saeki, Y. Yoshida, S. Tagawa, *Chem. Phys. Lett.* **2003**, *374*, 353–357.

[21] V. A. Nadtochenko, N. N. Denisov, I. V. Rubtsov, A. S. Lobach, A. P. Moravsky, *Russ. Chem. Bull.* **1993**, *42*, 1171–1173.

[22] O. W. Webster, W. Mahler, R. E. Benson, *J. Am. Chem. Soc.* **1962**, *84*, 3678–3684.

[23] R. D. Webster, G. A. Heath, *Phys. Chem. Chem. Phys.* **2001**, *3*, 2588–2594.

[24] S. Fukuzumi, H. Mori, H. Imahori, T. Suenobu, Y. Araki, O. Ito, K. M. Kadish, *J. Am. Chem. Soc.* **2001**, *123*, 12458–12465.

[25] K. Ohkubo, J. Ortiz, L. Martín-Gomis, F. Fernández-Lázaro, Á. Sastre-Santos, S. Fukuzumi, *Chem. Commun.* **2007**, 589–591.

[26] M. Ariu, D. G. Lidzey, M. Sims, A. J. Cadby, P. A. Lane, D. D. C. Bradley, *J. Phys.: Condens. Matter* **2002**, *14*, 9975–9986.

[27] The volume fraction was calculated by using $d_{\text{MDMO-PPV}}$ = 0.9 g cm^{-3} [28] and d_{TCNE} = 1.3 g cm^{-3} [29].

[28] C. W. T. Bulle-Lieuwma, W. J. H. van Gennip, J. K. J. van Duren, P. Jonkheijm, R. A. J. Janssen, J. W. Niemantsverdriet, *App. Surf. Sci.* **2003**, *203-204*, 547–550.

[29] V. D. Kiselev, G. G. Iskhakova, E. A. Kashaeva, L. N. Potapova, A. I. Konovalov, *Russ. Chem. Bull.* **2004**, *53*, 2490–2495.

[30] The volume fraction was calculated by using $d_{\text{MDMO-PPV}}$ = 0.9 g cm^{-3} [28] and d_{PCBM} = 1.5 g cm^{-3} [28].

[31] D. Dick, X. Wei, S. Jeglinski, R. E. Benner, Z. V. Vardeny, D. Moses, V. I. Srdanov, F. Wudl, *Phys. Rev. Lett.* **1994**, *73*, 2760–2763.

[32] S. Kazaoui, N. Minami, Y. Tanabe, H. J. Byrne, A. Eilmes, P. Petelenz, *Phys. Rev. B* **1998**, *58*, 7689.

[33] R. Könenkamp, G. Priebe, B. Pietzak, *Phys. Rev. B* **1999**, *60*, 11804.

[34] S. Cook, H. Ohkita, Y. Kim, J. J. Benson-Smith, D. D. C. Bradley, J. R. Durrant, *Chem. Phys. Lett.* **2007**, *445*, 276–280.

[35] L. Goris, K. Haenen, M. Nesládek, P. Wagner, D. Vanderzande, L. de Schepper, J. D'haen, L. Lutsen, J. V. Manca, *J. Mater. Sci.* **2005**, *40*, 1413–1418.

[36] G. Gensterblum, J. -J. Pireaux, P. A. Thiry, R. Caudano, T. Buslaps, R. L. Johnson, G. le Lay, V. Aristov, R. Günther, A. Taleb-Ibrahimi, G. Indlekofer, Y. Pertroff, *Phys. Rev. B* **1993**, *48*, 14756.

[37] P. J. Benning, C. G. Olson, D. W. Lynch, J. H. Weaver, *Phys. Rev. B* **1994**, *50*, 11239.

Chapter 3

Formation Mechanism of Fullerene Cation in Bulk Heterojunction Polymer Solar Cells

3.1. Introduction

In polymer/fullerene solar cells, semiconducting conjugated polymers and fullerene derivatives are generally considered to serve as a hole-transporting and electron-transporting materials, respectively.[1,2] Indeed, organic semiconductors with a shallow ionization potential tend to be *p*-type semiconductors and organic semiconductors with a deep ionization potential tend to be *n*-type semiconductors. On the other hand, ambipolar transport properties have been recently reported for not a few materials including fullerenes, pentacene, and conjugated polymers in the field effect transistor (FET) devices with appropriate electrodes and gate dielectrics.[3–8] These reports indicate that organic semiconducting materials are inherently capable to be ambipolar.[9]

Recently, there have been several studies indicative of ambipolar charge transport of fullerene derivatives even in polymer/fullerene blends. For blend films of poly[2-methoxy-5-(3,7-dimethyloctyloxy)-1,4-phenylenevinylene] (MDMO-PPV) and [6,6]-phenyl-C_{61}-butyric acid methyl ester (PCBM), the hole mobility increases as the increase in the PCBM fraction. The hole mobility of MDMO-PPV/PCBM blend films ($2 - 3 \times 10^{-4}$ cm^2 V^{-1} s^{-1})[10,11] is at least two orders of magnitude lager than that of a pristine MDMO-PPV film ($0.3 - 2 \times 10^{-6}$ cm^2 V^{-1} s^{-1}),[10,11] but rather comparable to the FET hole mobility of PCBM (8×10^{-3} cm^2 V^{-1} s^{-1}).[6] For blend films of poly[2,7-(9,9-dioctylfluorene)-*alt*-5,5-(5',8'-di-2-thienyl-(2',3'-bis-(3''-octyloxyphenyl)-

quinoxaline))] (APFO-15) and PCBM, the electroluminescence of PCBM emission has been observed in addition to that of charge transfer (CT) emission.[12] These findings suggest hole transport in the fullerene phase in polymer/fullerene blends. Previously, the author found the formation of fullerene radical cation in MDMO-PPV/PCBM blend films by transient absorption measurements: no PCBM radical cation is observed at low PCBM concentrations while PCBM radical cation is observed in addition to PCBM radical anion at high PCBM concentrations.[13] This is consistent with previous reports that the hole mobility in MDMO-PPV/PCBM blend films increases at higher PCBM concentrations (>50 wt%).[11] However, little is known about the formation mechanism of fullerene radical cation in polymer/fullerene blends.

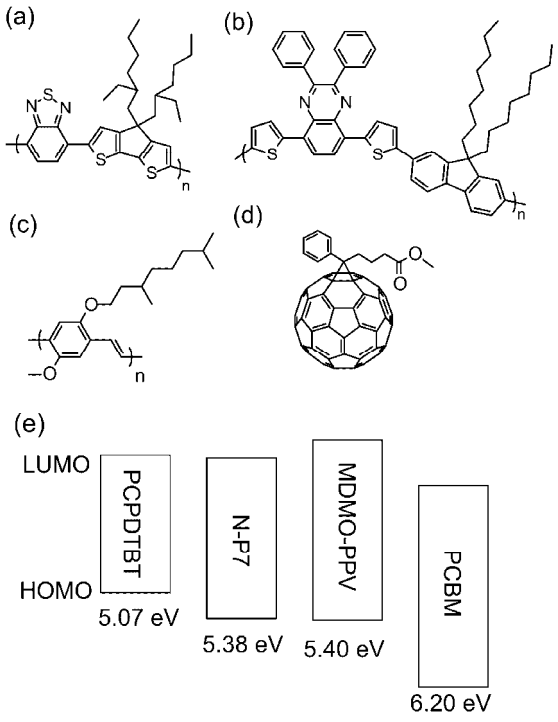

Figure 3-1. Chemical structures of conjugated polymers and a fullerene employed in this study: a) PCPDTBT, b) N-P7, c) MDMO-PPV, and d) PCBM. e) The energy diagrams of these materials. The HOMO energy is measured by the photoelectron yield spectroscopy.

Herein, the author systematically studies the charge carriers formed in blend films of PCBM and conjugated polymers with different ionization potentials in order to address the formation mechanism of fullerene cation in polymer/fullerene blends. Figure 3-1 shows conjugated polymers employed in this study: poly[2,6-(4,4-bis-(2-ethylhexyl)-4*H*-cyclopenta[2,1-b;3,4-b']dithiophene)-*alt*-4,7-(2,1,3-benzothiadiazole)] (PCPDTBT) and poly[2,7-(9,9-dioctylfluorene)-*alt*-5,5-(5',8'-di-2-thienyl-2',3'-diphenylquinoxaline)] (N-P7). PCPDTBT and N-P7 have smaller or similar ionization potential (I_p = 5.1 – 5.3 eV eV for PCPDTBT[14] and 5.37 eV for N-P7[15]) compared to MDMO-PPV. ($I_p \approx$ 5.3 eV[16]). Furthermore, polymer solar cells with them exhibit the optimized power conversion efficiency (~5.5%) at high weight fractions of fullerene (1 : 2 or 1 : 3),[17,18] as is the case of MDMO-PPV/PCBM (1 : 4).[19] The time evolution of PCBM radical cation formation is analyzed on the basis of the absorption coefficients of polymer polarons, PCBM radical anion, and PCBM radical cation. The formation time is dependent on polymer ionization potential and phase-separated domain size. The final fraction of PCBM radical cation F_{eq} is dependent on the polymer ionization but independent of the phase-separated domain size and the excitation wavelength. Furthermore, F_{eq} is calculated by the Monte Carlo simulation for hole injection from polymer to fullerene domains. The mechanism and energetic conditions of the formation of PCBM radical cation in polymer/PCBM blend films were discussed.

3.2. Results

3.2.1. Transient Absorption

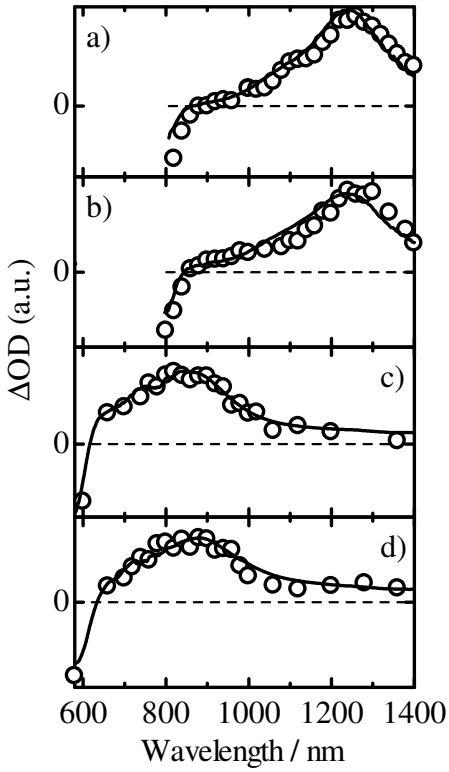

Figure 3-2. Transient absorption spectra of blend films: a) PCPDTBT/TCNB (95:5 w/w), b) PCPDTBT/TCNB (70 : 30 w/w), c) N-P7/TCNB (95 : 5 w/w), and d) N-P7/TCNB (70 : 30 w/w). The solid lines and open circles show the spectra measured at 3 ns and 0.5 μs after the laser excitation, respectively.

To assign the absorption spectrum of PCPDTBT and N-P7 hole polarons, transient absorption spectra of polymer films doped with tetracyanobenzene (TCNB) were measured: TCNB is a strong electron acceptor ($E_{1/2}(TCNB^-/TCNB)$ = −0.6 V vs SCE[20]) similar to C_{60} ($E_{1/2}(C_{60}^-/C_{60})$ = −0.3 – −0.4 V vs SCE[21]). No fluorescence was observed for the TCNB blended films, indicating that TCNB efficiently acts as an electron acceptor

in the blend films. Figures 3-2a and 3-2b show the transient absorption spectra of PCPDTBT/TCNB blend films with 5 and 30 wt% TCNB in the microsecond time region, which are almost the same as those in the nanosecond time region. A broad absorption was observed at ~1240 nm for both blend films with 5 wt% and 30 wt% TCNB. This absorption was not quenched in an oxygen atmosphere, and hence not ascribable to triplet exciton. Note that TCNB radical anion has no absorption band in this wavelength region.[20] Therefore, the absorption band at 1240 nm is safely assigned to the absorption of PCPDTBT hole polaron, which is consistent with previous reports.[22,23] Figures 3-2c and 3-2d show the transient absorption spectra of N-P7/TCNB blend films with 5 and 30 wt% TCNB in the microsecond time region, which are also almost the same as those in the nanosecond time region. The broad absorption band at ~850 nm is similarly ascribed to N-P7 hole polaron. In summary, the absorption spectra of both PCPDTBT and N-P7 hole polarons are independent of time and the dopant concentration.

Figure 3-3 shows the transient absorption spectra of PCPDTBT/PCBM and NP-7/PCBM blend films (5 and 50 wt% of PCBM) excited at 400 nm. The absorption spectra were normalized at 1240 nm for PCPDTBT/PCBM and at 700 nm for N-P7/PCBM blends where only polymer hole polarons have an absorption band (see the Appendix). For the blend films with 5 wt% PCBM, no spectral change was observed in this time region, suggesting no change in the charge carrier composition. For the blend with 50 wt% PCBM, on the other hand, distinct spectral changes were observed for blend films: the absorption at around 1000 nm increased for PCPDTBT/PCBM and the absorption at around 900 nm increased for N-P7/PCBM. The same results were obtained upon the selective excitation of polymers: PCPDTBT at 800 nm and N-P7 at 570 nm. In other words, these temporal changes in the absorption spectra are independent of the excitation wavelength. The absorption increase at 1000 nm in PCPDTBT/PCBM blend is

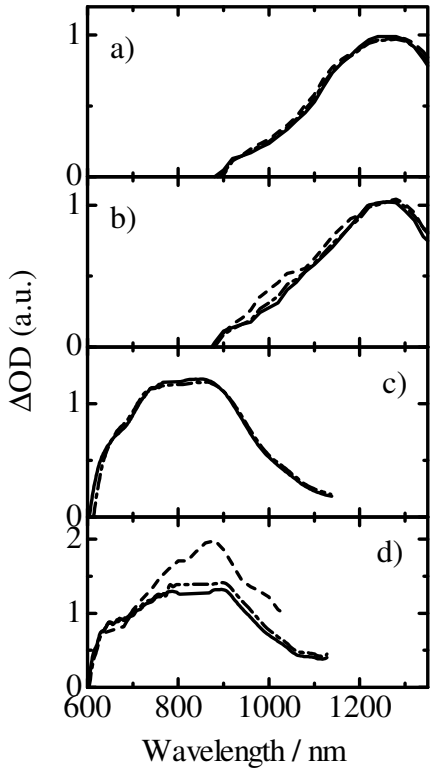

Figure 3-3. Transient absorption spectra of blend films excited at 400 nm with a fluence of 30 μJ cm^{-2}: a) PCPDTBT/PCBM (95 : 5 w/w), b) PCPDTBT/PCBM (50 : 50 w/w), c) N-P7/PCBM (95 : 5 w/w), and d) N-P7/PCBM (50 : 50 w/w). In the panels a) and b), the solid, dashed-dotted, and broken lines show the spectra at 0.5, 2, and 5 μs, respectively. In the panels c) and d), the solid, dashed-dotted, and broken lines show the spectra at 1, 3, and 500 ns, respectively.

indicative of the increase in the fraction of the PCBM radical anion because PCBM radical anion has a characteristic absorption at 1020 nm.[13] As described below, the relative increase in the fraction of the PCBM radical anion is due to the decrease in the fraction of PCPDTBT hole polaron caused by the formation of PCBM radical cation. On the other hand, the absorption increase at 900 nm in N-P7/PCBM blends is indicative of the increase

in the fraction of the PCBM radical cation because PCBM radical cation has a characteristic absorption at 890 nm.[13] In summary, both findings suggest hole injection from polymer to PCBM in blend films with high PCBM fractions as is discussed below.

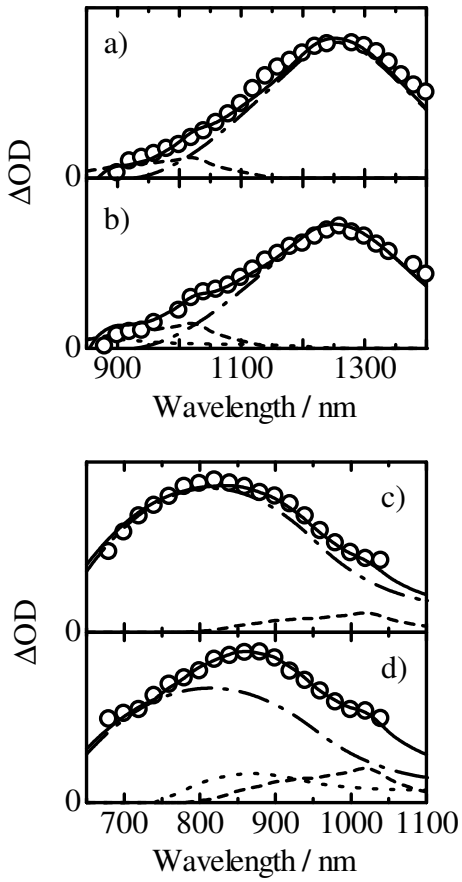

Figure 3-4. Transient absorption spectra of blend films (open circles) at 1 μs after the laser excitation at 400 nm with a fluence of 30 μJ cm^{-2}: a) PCPDTBT/PCBM (95 : 5 w/w), b) PCPDTBT/PCBM (50 : 50 w/w), c) N-P7/PCBM (95 : 5 w/w), and d) N-P7/PCBM (50 : 50 w/w). Solid lines represent the absorption spectra simulated by a sum of each absorption spectrum of charge carriers: $polymer^+$ (dashed-dotted lines), $PCBM^-$ (broken lines), and $PCBM^+$ (dotted lines). The mole fraction of each spectrum is as follows: a) $polymer^+ : PCBM^+ : PCBM^- = 0.5 : 0 : 0.5$, b) 0.35 : 0.15 : 0.5, c) 0.5 : 0 : 0.5, b) 0.3 : 0.2 :

0.5.

In order to analyze the temporal change in the absorption spectra quantitatively, the author resolved the transient absorption spectra by using each spectrum of polymer hole polarons, PCBM radical anion, and PCBM radical cation. For blend films with 5 wt% PCBM, as shown in Figures 3-4a and 3-4c, the observed spectra were well reproduced by the sum of the absorption spectra of polymer hole polaron and PCBM radical anion. Therefore, it is concluded that hole polaron and PCBM radical anion are formed as charge carriers in the blend films with 5 wt% PCBM. From the spectral simulation, the molar absorption coefficient of polymer hole polarons are estimated to be $\varepsilon_{PCPDTBT}^{+}$ = 40000 M^{-1} cm^{-1} at 1240 nm and $\varepsilon_{N\text{-}P7}^{+}$ = 40000 M^{-1} at 850 nm on the basis of that of PCBM radical anion ε_{PCBM}^{-} = 6000 M^{-1} cm^{-1} at 890 nm.[13] This is larger than that of MDMO-PPV hole polaron ($\varepsilon_{MDMO\text{-}PPV}^{+}$ = 15000 M^{-1} cm^{-1}), but rather comparable to that of polythiophene (ε = 34000 M^{-1} cm^{-1}).[13,24]

For blend films with 50 wt% PCBM, on the other hand, the transient spectra changed with time as shown in Figure 3-3. There are two possible explanations for the spectral change in polymer/PCBM blend films: (i) the absorption spectrum of charge carriers (polymer hole polarons and/or PCBM radical anions) is dependent on the PCBM concentration and (ii) the charge carrier composition is dependent on the PCBM concentration. As mentioned above, the absorption spectra of polymer hole polarons are independent on the dopant concentration. Furthermore, the previous study has demonstrated that the absorption spectrum of PCBM radical anion is also essentially independent of the PCBM concentration.[13] Therefore, it is assigned that another charge carrier is formed in blend films at high PCBM concentrations. To explain the spectral change, the author consider PCBM radical cation as the most possible carrier formed in blends at high PCBM concentrations. In contrast to the blend films with 5 wt% PCBM,

the absorption spectra of the blend films with 50 wt% of PCBM were not reproducible by the sum of each spectrum of polymer hole polaron and PCBM radical anion. Rather, as shown in Figures 3-4b and 3-4d, the whole spectra observed at 1 μs were well reproduced by the sum of each spectrum of polymer hole polaron, PCBM radical anion, and PCBM radical cation. Thereafter, no spectral change was observed, suggesting that thermodynamic equilibrium is established. The author therefore conclude that PCBM radical cation is formed with time in the blend films with 50 wt% PCBM. On the basis of the molar absorption coefficient of each carrier, the equilibrium fraction of PCBM radical cation formed in the blend films can be quantitatively evaluated to be F_{eq} = 0.3 for PCPDTBT and F_{eq} = 0.6 for N-P7 blend films at 1 μs.

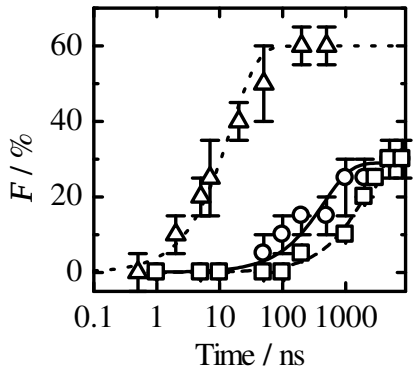

Figure 3-5. The mole fraction of $PCBM^+$ to the total hole carriers in blend films plotted against the delay time after pulse laser excitation: PCPDTBT/PCBM fabricated without DIO (circles), PCPDTBT/PCBM fabricated with DIO (squares), and N-P7/PCBM (triangles).

The spectral changes before the thermodynamic equilibrium were well reproduced by the sum of each spectrum of polymer hole polaron, PCBM radical anion, and PCBM

radical cation with different fractions. Figure 3-5 shows the time dependence of the fraction $F(t)$ of PCBM radical cation in the blend films. The time evolution of $F(t)$ was well fitted with a exponential function: $F(t) = a[1-\exp(-t/\tau)]$. As a result, the time constant of the PCBM radical cation formation is estimated to be τ = 450 ns for PCPDTBT/PCBM and τ = 15 ns for N-P7/PCBM blend films. These rise constants are in good agreement with the decay constants of polymer hole polarons, suggesting that PCBM radical cations are formed from polymer hole polarons.

The hole injection from polymer to PCBM domains should be dependent on phase-separated domain size. The author therefore analyzed the formation time of PCBM cations in PCPDTBT/PCBM blend films fabricated with 1,8-diiodooctane (DIO) as an additive for the spincast solution. The averaged domain size was evaluated to be 59 nm by AFM measurements that are larger than 31 nm evaluated for PCPDTBT/PCBM blend films fabricated without DIO (see the Appendix). This additive effect is consistent with previous reports.[25–27] It is noted that each phase-separated polymer domain observed by AFM is not pure but contains PCBM molecules because polymer fluorescence is highly quenched for both films. It is also noted that the additive has no impact on the HOMO level of PCPDTBT in the blend. As shown in the open squares in Figure 3-5, the formation time of PCBM radical cation is ~2 μs, which is slower than that observed for PCPDTBT/PCBM blend films fabricated without DIO. The final fraction of PCBM radical cation is F_{eq} = 0.3, which is the same as that observed for the blend films fabricated without DIO. These results also suggest the hole injection from polymer to PCBM domains.

3.2.2 Monte Carlo Simulation

To address the origin of the hole injection from polymer to PCBM domains, the

author simulated hole hopping in a semi-infinite donor/acceptor planar heterojunction by the Monte Carlo analysis. The calculation is based on the Miller–Abraham model for hopping in a disordered material.[28,29] In this model, the hopping probability P_{ij} from site i to site j is given by

$$P_{ij} = \frac{\nu_{ij}}{\sum_{l} \nu_{il}} \tag{3-1}$$

$$\nu_{ij}(\Delta E_{il}) = \begin{cases} \exp\left(\frac{-\Delta E_{il}}{k_{\mathrm{B}}T}\right) & \text{for } \Delta E_{il} > 0 \\ 1 & \text{for } \Delta E_{il} \le 0 \end{cases} \tag{3-2}$$

where ΔE_{il} is the energy difference between site i and l, k_{B} is the Boltzmann constant, and T is temperature. All the site energy is generated randomly on the basis of the following Gaussian distribution function $D(E)$[30]

$$D_{\mathrm{X}}(E) = \frac{d_{\mathrm{X}}}{\sqrt{2\pi}\sigma_{\mathrm{X}}} \exp\left[-\frac{(E - E_{\mathrm{X}}^{0})^{2}}{2\sigma_{\mathrm{X}}^{2}}\right] \tag{3-3}$$

where E_{X}^{0} is the HOMO energy level of the domain X, d_{X} is the degeneracy in the HOMO levels of the domain X, σ_{X} is the width of the energetic Gaussian distribution of the HOMO levels for the domain X, and the subscripts of D and A stand for donor and acceptor, respectively. The HOMO energy E_0^{X} is evaluated by the photoelectron yield spectroscopy. Here, the author set $d_{\mathrm{A}} = 5$ for PCBM, which has fivefold degeneracy in the HOMO levels,[31] and $d_{\mathrm{D}} = d_{\mathrm{A}} = 1$ for polymers. The width σ_{X} is taken from previous studies. For most conjugated polymer films, the width due to energetic disorders has been reported to be around 0.1 eV.[32–40] Thus, the author set $\sigma_{\mathrm{D}} = \sigma_{\mathrm{A}} = 0.1$ eV for polymers as a typical value. For fullerene and its derivatives, the band width (full width half mean) has been reported to range from 0.8 to 1.1 eV.[41–48] Thus, the author set $\sigma_{\mathrm{A}} =$ 0.4 eV for PCBM as a minimum value. In the simulation, a hole is generated at the nearest neighbor site at the heterojunction. The hole is iteratively hopping in a simple

cubic lattice: it moves from a site i to an adjacent site j with a probability of P_{ij} or stays at the original site with a probability of P_{ii}. It is determined whether the hole finally stays at the donor or acceptor domain. This calculation is independently performed for 3000 holes. As a result, the equilibrium fractions F_{eq} of holes in the acceptor domain is obtained as a function of ΔE_{HOMO}.

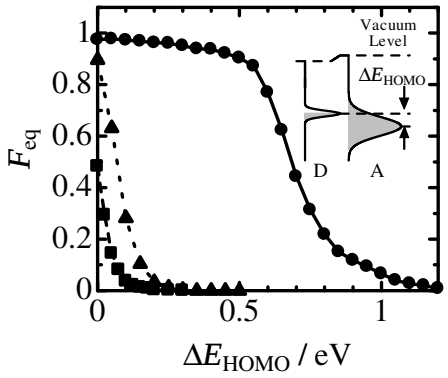

Figure 3-6. The calculated equilibrium fraction of PCBM radical cation F_{eq} plotted against ΔE_{HOMO}: polymer/fullerene blends with a high fullerene density with σ_D = 0.1 eV, σ_A = 0.4 eV, d_D = 1, d_A = 5 (solid line and circles), polymer/fullerene blends at a low fullerene density with σ_D = σ_A = 0.1 eV, d_D = 1, d_A = 5 (dotted line and triangles), and polymer/polymer blends with σ_D = σ_A = 0.1 eV, d_D = d_A = 1 (broken line and squares),. The inset shows the conceptual energy diagram of the HOMO levels.

Figure 3-6 shows the simulation results with the typical parameters of polymer/fullerene (σ_D = 0.1 eV and σ_A = 0.4 eV) and polymer/polymer (σ_D = σ_A = 0.1 eV) heterojunctions. For polymer/fullerene blend films, F_{eq} is as high as >0.9 for ΔE_{HOMO} < 0.3 eV, steeply decreases at around ΔE_{HOMO} = 0.5 eV, and then is as small as <0.1 for ΔE_{HOMO} > 0.7 eV. For polymer/polymer blend films, on the other hand, F_{eq} is ~0.5 for

ΔE_{HOMO} = 0 eV, but steeply decreases, and then is negligibly small for ΔE_{HOMO} > 0.1 eV. This result shows that the distribution width has critical impact on the hole injection from polymer to fullerene domains. The author will discuss the energetic conditions for holes injection into acceptor domains.

3.3. Discussion

3.3.1. Formation Mechanism of PCBM Cation

In the previous study, the author proposed two possible mechanisms for the formation of the PCBM radical cation in blend films. One is the formation of the PCBM radical cation and anion pairs at the PCBM domain in the blend, which would be caused by the direct or indirect photoexcitation of intermolecular CT transitions of PCBM. The other is the formation of the PCBM radical cation by hole injection from hole polarons in polymer domains. If the former mechanism were dominant, the PCBM radical cation should be observed immediately after the laser excitation and some of them would rapidly decay because of the geminate recombination. As shown in Figure 3-3, this is not the case. In reality, no PCBM radical cation is observed on a time scale of nanoseconds, but the fraction of PCBM radical cation rather increases with time in parallel with the fraction of polymer polarons decreases with the same time constant. Furthermore, if the former mechanism were dominant, the final fraction of the PCBM radical cation should be dependent on the excitation wavelength. This is also not the case as described above. These transient results strongly suggest the hole injection from polymer to PCBM domains. If the latter mechanism is dominant, the hole injection time should be dependent on the domain size. Indeed, the author observed the different formation dynamics of PCBM radical cation in PCPDTBT/PCBM blend films with different phase-separated domain sizes: PCBM radical cation is generated faster (450 ns) in smaller domains (31 nm) but

slower (2 μs) in larger domains (59 nm). If the hole mobility $\mu_h = 10^{-4}$ cm^2 V^{-1} s^{-1} is assumed,[27,49,50] the diffusion constant of the hole carrier is calculated by the Einstein's relationship $D = (k_B T/q)\mu$ where q is the elementary charge. Thus, we can estimate the 3D diffusion length $\langle x^2 \rangle^{1/2} = (6Dt)^{1/2} \approx 25$ nm for 450 ns and 55 nm for 2 μs, which is in good agreement with the domain size observed. On the basis of these findings, it is therefore concluded that PCBM radical cation is formed mainly by the hole injection from polymer polarons in polymer domains.

3.3.2. Energetic Conditions

Next, the author discuss the energetic conditions for the hole injection to acceptor domains even in polymer/fullerene blend films. As shown in Figure 3-1, the HOMO levels of all the conjugated polymers studied are higher than that of PCBM. In other words, hole carriers should be energetically more stable in conjugated polymers than in PCBM molecules in terms of the simple energetic scheme. Thus, it is necessary to consider energetic distribution in the HOMO levels or energetic realignment at the interface in order to explain the hole injection from polymer to PCBM domains. As mentioned above, most organic semiconductors exhibit energetic disorder in the range of 0.1 eV for charge transport.[32–40] However, as shown by the broken line in Figure 3-6, F_{eq} is negligible for the parameters ($\sigma_D = \sigma_A = 0.1$ eV, $d_D = d_A = 1$), suggesting no hole injection from donor to acceptor domains. These parameters are typical for most polymer/polymer blends. In other words, the hole injection from donor to acceptor would be negligible for polymer/polymer blend films. On the other hand, as mentioned above, fullerene derivatives have fivefold degenerated HOMO levels ($d_A = 5$). As shown by the dotted line in Figure 3-6 ($\sigma_D = \sigma_A = 0.1$ eV, $d_D = 1$, $d_A = 5$), F_{eq} is still negligible for $\Delta E_{HOMO} > 0.2$ eV. These parameters correspond to polymer/fullerene blends at low

fullerene fractions because energetic distribution of isolated fullerenes would be dependent on the energetic disorder of the polymer matrix. Indeed, no hole injection from polymer to PCBM domains is observed for the blends at low PCBM fractions (<30 wt%). At a higher PCBM concentration, PCBM molecules are likely to form aggregated clusters or nanocrystals. As reported previously,[51] the intermolecular CT absorption band at 500 nm becomes prominent at high PCBM concentrations, suggesting substantial intermolecular interaction in the ground state. Large intermolecular interactions generally cause crystallization, resulting in band structures in the electronic state. For C_{60} crystals, there are many studies on the band structure. The band width of the valence band has been estimated to be 0.8 to 1.2 eV by the photoemission spectra.[41–48] For PCBM, a recent calculation suggests that the simple cubic structure is the most stable and causes a broadening of the energy levels resulting from the overlap of neighboring PCBM orbital due to the compact packing.[52] As shown by the solid line in Figure 3-6 (σ_D = 0.1 eV, σ_A = 0.4 eV, d_D = 1, d_A = 5), F_{eq} is as large as 0.8 for $\Delta E_{HOMO} < 0.4$ eV, start to decrease at around $\Delta E_{HOMO} \approx 0.5$ eV, and negligible for $\Delta E_{HOMO} > 0.8$ eV. This is qualitatively consistent with F_{eq} obtained from the transient measurements. Therefore, it is concluded that the hole injection from polymer to PCBM domains is primarily due to the large band width of PCBM nanocrystals and secondarily due to the fivefold degeneracy in the HOMO levels of PCBM.

Finally the author note the energy difference Δ between ΔE_{HOMO} and $E_A^0 - E_D^0$. As shown in Figure 3-7, ΔE_{HOMO} corresponding to the observed F_{eq} is different from $E_A^0 - E_D^0$. The difference is Δ = 0.37 eV for PCPDTBT/PCBM, Δ = 0.17 eV for N-P7/PCBM, and Δ = 0.20 eV for MDMO-PPV/PCBM. This is probably because other important factors are neglected in this simple simulation. For example, interfacial dipoles at the heterojunction have been reported to cause 0.2 – 0.6 eV of vacuum level shift.[53,54] Such

interfacial dipoles have been found for many polymer/fullerene blend films: 0.4 eV for P3HT/PCBM,[55] 0.6 eV for P3HT/C_{60},[56] and 0.25 eV for PPV oligomer/C_{60}.[57] These values are in range of estimated Δ as mentioned above. Therefore, it is thought that the most of part in Δ can be explained by the vacuum level shift.

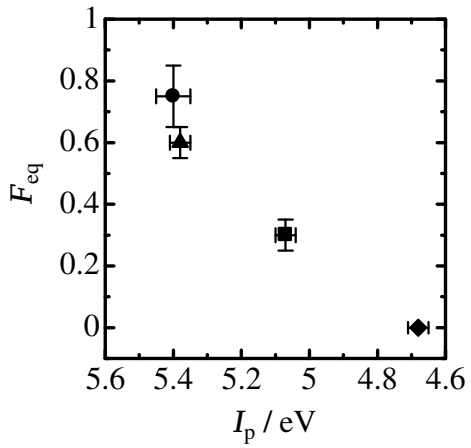

Figure 3-7. F_{eq} obtained from the transient study plotted against the ionization potential I_p of conjugated polymer: MDMO-PPV/PCBM (circle), N-P7/PCBM (triangle), PCPDTBT/PCBM (square), and P3HT/PCBM (diamond) blends.

3.4. Conclusions

The formation dynamics of PCBM radical cation in polymer/PCBM blends was studied by transient absorption measurements. As a result, the author obtained the key findings as follows. At an early time stage after the photoexcitation, polymer hole polaron and PCBM radical anion were observed but no PCBM radical cation was found. On a time scale of nanoseconds, the fraction of PCBM radical cation increased with time while the fraction of polymer hole polaron decreased with the same time constant. Finally, the fraction of PCBM radical cation became constant on a time scale of microseconds, suggesting that thermodynamic equilibrium is established. The formation

time of PCBM radical cation is dependent on the phase-separated domain sizes: the slower formation of PCBM radical cation was observed for the larger domains. The final fraction of PCBM radical cation F_{eq} is dependent on the ionization potential of donor polymers but independent of the domain size and the excitation wavelength: F_{eq} = 30% for PCPDTBT/PCBM and F_{eq} = 60% for N-P7/PCBM blends. It is therefore concluded that PCBM radical cation is generated mainly by the hole injection from polymer to PCBM domains in polymer/PCBM blends. In order to discuss the energetic conditions for the hole injection to acceptor in donor/acceptor blends, hole hopping at donor/acceptor heterojunction was simulated by the Monte Carlo analysis based on the Miller–Abraham model. In this simulation, the author considers the energetic distribution and the degeneracy in the HOMO levels. As a result, the hole injection would be negligible for polymer/polymer blends because the energetic distribution is as small as 0.1 eV and the degeneracy is typically unity. Even for polymer/PCBM with the fivefold degeneracy in the HOMO of PCBM, the hole injection would be negligible for lower PCBM fractions because of the small energetic distribution. In contrast, the hole injection is energetically favorable for higher PCBM fractions because of the large band width due to the formation of aggregated PCBM nanocrystals and the fivefold degeneracy in the HOMO levels of PCBM. This is consistent with the final fraction obtained from the transient study. It is therefore concluded that the hole injection from polymer to PCBM domains is primarily due to the large band width of PCBM nanocrystals and secondarily due to the fivefold degeneracy in the HOMO levels of PCBM. The author believes that such conditions would be true for other polymer/fullerene solar cells in particular employing polymers with deeper HOMO levels.

3.5. Experimental

Materials: Chemical regents for PCPDTBT synthesis were used without further purification: 2,1,3-benzothiadiazole-4,7-bis(boronic acid pinacol ester) (Aldrich, 95%), 2,6-dibromo-4,4-bis(2-ethylhexyl)-4*H*-cyclopenta[2,1-b:3,4-b']dithiophene (Luminescence Technology Corp.), potassium carbonate (Aldrich, 99.995%), Aliquat(R)336 (Aldrich, 99.995%), toluene (Wako, Organic synthesis grade), tetrakis(triphenylphosphine)palladium(0) (Aldrich, 99%), bromobenzene (Aldrich, >99.5%), and phenylboroic acid (Aldrich, >97.0%). Details of the synthesis of PCPDTBT are described in the Appendix. The other polymer N-P7 was provided by Toray Industries, Inc. The acceptor PCBM (99.9%) was purchased from Frontier Carbon and used without further purification. The other acceptor TCNB (98%) was purchased from Tokyo Chemical Industry Co., Ltd and recrystallized from ethanol prior to the experiment.

Sample Fabrication: Polymer/fullerene blend films were prepared on glass substrates by spin-coating from a chlorobenzene solution of polymer and PCBM at a spin rate of 1000 rpm after the spin rate of 400 rpm (10 s) under ambient conditions. The film thickness was typically 200 nm. The weight fraction of PCBM was varied from 5 to 80 wt%. The blend solution was stirred at 40 °C overnight to be dissolved homogeneously. Before the spin-coating, the glass substrates were cleaned by ultrasonic treatment in toluene, acetone, and ethanol sequentially for 15 min each, and then with a UV–ozone cleaner (Nippon Laser & Electronics Lab., UV253) for 1 h. For blend films of polymer and TCNB, tetrahydrofuran (for PCPDTBT) or cyclohexanone (for N-P7) was used as solvent instead of chlorobenzene. The blend solution was stirred at room temperature over night. The weight fraction of TCNB was adjusted to 5 and 30 wt% in the final films.

Measurements: Transient absorption data were collected under N_2 atmosphere with a

highly sensitive a nano/microsecond transient absorption system and with a femtosecond transient absorption system as described below. For the microsecond transient absorption measurement, the sample was excited with a light pulse (400 nm, 30 μJ cm^{-2}, 4 Hz) from a dye laser (Photon Technology International, GL-301) that was pumped with a nitrogen laser (Photon Technology International, GL-3300), and probed with a monochromatic light from a 50-W quartz tungsten halogen lamp (Thermo–ORIEL, Model 66997) with a light intensity controller (Thermo–ORIEL, Model 66950), which was equipped with appropriate optical cut-filters and two monochromators (Ritsu, MC-10N) before and after the sample to reduce stray light, scattered light, and emission from the sample. The probe light was detected with a pre-amplified Si photodiode (Costronics Electronics) for the visible wavelength range from 700 to 1100 nm or a pre-amplified InGaAs photodiode (Newport 1811) for the near-IR wavelength range from 900 to 1500 nm. The detected signal was sent to the main amplification system with electronic band-pass filters (Costronics Electronics) to improve the noise-to-signal ratio. The amplified signal was collected with a 200-MHz digital oscilloscope (Tektronix, TDS2022), which was synchronized with a trigger signal of the laser pulse from a photodiode (Thorlabs, DET10A). The detectable absorbance change ΔOD is as small as ~10^{-5} – 10^{-6} depending on the measuring time region. For the nanosecond time region, the optical line was the same as the microsecond spectrometer mentioned above. The probe light was detected with a pre-amplified Si photodiode (Newport, 1801) for visible region or a pre-amplified InGaAs photodiode (Newport, 1811) for the near-IR region. The detected signal was amplified with a voltage amplifier (Femto, DHPVA-200) and collected with a 500-MHz digital oscilloscope (Tektronix, TDS3022). The femtosecond transient absorption data were collected with a pump and probe transient absorption spectroscopy system (Ultrafast Systems, Helios). The pump light was second harmonic pulses (400 nm, 30 μJ cm^{-2}, fwhm 100 fs, 1 kHz)

from a regeneratively amplified Ti-sapphire laser (Spectra-Physics, Hurricane). The probe beam was detected with a linear CMOS array (Ultrafast Systems, SPEC-VIS) for the visible wavelength range from 400 to 900 nm and with an InGaAs linear diode array (Ultrafast Systems, SPEC-NIR) for the near-IR wavelength range from 850 to 1600 nm. The typical noise level of this system is lower than 2×10^{-4}.

3.6. Appendix

3.6.1. Synthetic Scheme

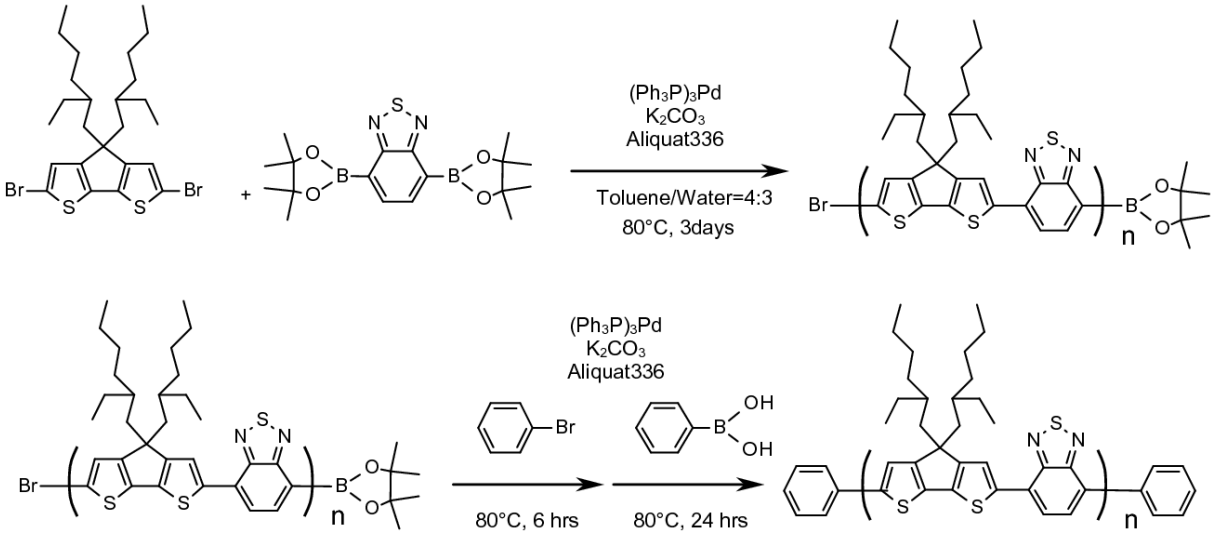

Figure 3-A1. Synthetic scheme of PCPDTBT.

According to the procedures reported in the previous reports,[A1–A4] PCPDTBT was synthesized by the Suzuki–Miyaura coupling reaction.[A5] 2,1,3-Benzothiadiazole-4,7-bis(boronic acid pinacol ester) (115.87mg, 0.300 mmol) and tetrakis(triphenylphosphine)palladium(0) (6.33 mg, 5.47 μmol, 1.8 mol%) were placed in a two-necked recovery flask and purged with Ar gas. Subsequently, 6 mL of Ar-bubbled toluene dissolved with 2,6-dibromo-4,4-bis(2-ethylhexyl)-4*H*-cyclopenta[2,1-b:3,4-b']dithiophene (173.07 mg, 0.309 mmol), 4.5 mL of Ar-bubbled

water dissolved with potassium carbonate (844.34 mg, 6.10 mmol), and two drops of Aliquat336 were poured into the flask. The solution in the flask was again bubbled with Ar gas for 30 min, and then was stirred for 3 days at 80 °C. To the solution Ar-bubbled bromobenzene (53.36 mg, 0.340 mmol) and 2 mL of Ar-bubbled toluene solution of phenylboroic acid (38.60 mg, 0.3176 mmol) were added every 6 h, which was stirred again over night. The solution was subsequently poured into a mixture of 3 mL of 2 M hydrochloric acid and 300 mL of methanol and stirred over night. The residue collected by filtering was dissolved in toluene, and reprecipitated in water/methanol. The crude product was purified by soxlet extraction with acetone for 6 h. A total of 75.37 mg (yield = 26%) of PCPDTBT was obtained as pure product. The molecular weight was estimated by GPC measurement with tetrahydrofuran as an eluent on the basis of polystyrene standard: M_n = 12,380, M_w = 21,580, M_w/M_n = 1.74. ^{1}H-NMR (CD_2Cl_2, 400 MHz): δ (ppm) 8.14 (s, 2H), 7.86 (s, 2H), 2.07 (s, 4H), 1.02 (m, 20H), 0.68 (m, 12H).

3.6.2. Absorption Spectra of Charge Carriers

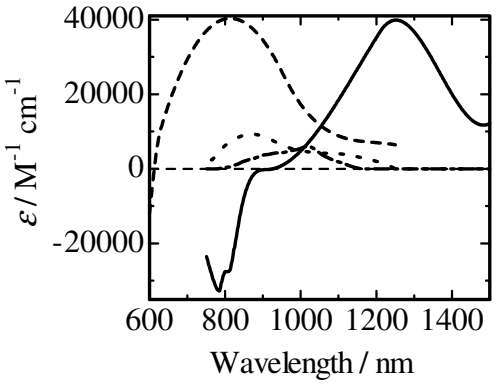

Figure 3-A2. Molar absorption coefficient spectra of PCPDTBT hole polaron (solid line) N-P7 hole polaron (broken line), PCBM anion (dashed-dotted line), and PCBM cation (dotted line).

3.6.3. Ionization Potentials of Materials

Figure 3-A3 shows the photoelectron yield spectra of PCBM, PCPDTBT, N-P7, and MDMO-PPV neat films. The threshold energy was estimated from the cut-off in cubic root of the photoelectron yield plotted against the incident photon energy.

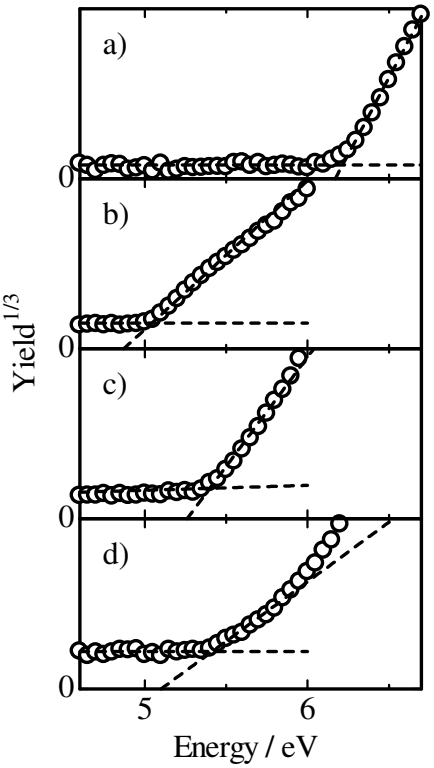

Figure 3-A3. Plots of the cubic root of the photoelectron yield of (a) PCBM, (b) PCPDTBT, (c) N-P7, and (d) MDMO-PPV.

3.6.4. Transient Absorption Spectra of PCPDTBT/PCBM

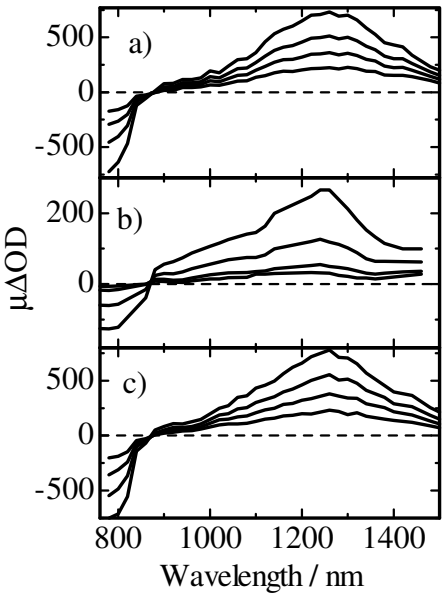

Figure 3-A4. Transient absorption spectra of PCPDTBT/PCBM blend films with different PCBM fractions: a) 5, b) 30 c) 50 wt% of PCBM. The delay times are 0.5, 1, 2, 5 μs after the laser excitation at 400 nm with a fluence of 30 μJ cm^{-2}.

3.6.5. Domain Size Estimation

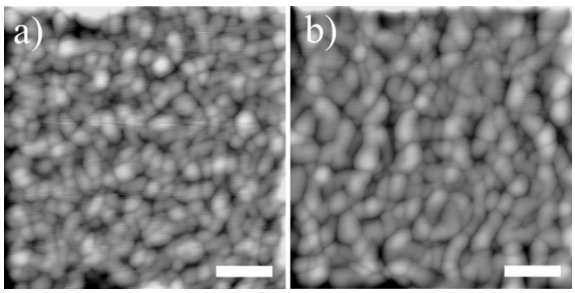

Figure 3-A5. The AFM topographic image measured by dynamic mode of PCPDTBT/PCBM blend films (50:50 w/w) without (a) and with (b) 1,8-diiodooctane. These films were washed by 1,8-octanedithiol to remove PCBM. The scale bars correspond to 100 nm in length.

From the AFM images, the major and minor axis length (x and y, respectively) for each domain were estimated by ellipsoid fittings. Figure 3-A6 shows the histograms of domain sizes using $(x^2+y^2)^{1/2}$. From these histograms, the domain sizes are estimated by Gaussian fittings.

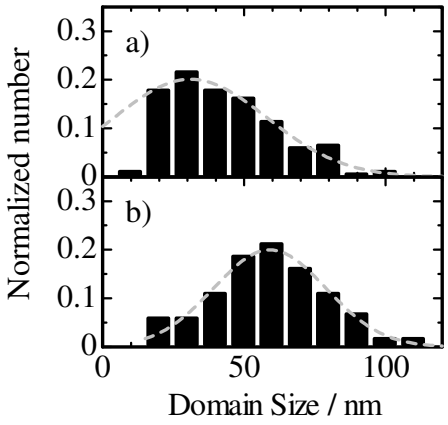

Figure 3-A6. Histograms of domain size estimated from AFM images of PCPDTBT/PCBM blend films (50:50 w/w) without (c) and with (d) 1,8-diiodooctane. The gray dash lines show Gaussian fittings for each histogram. The domain sizes are estimated by the mean square of major and minor axis of domain which was obtained by ellipsoid fittings.

3.7. References

[1] P. Haremans, D. Cheyns, B. P. Rand, *Acc. Chem. Res.* **2009**, *42*, 1740–1747.

[2] B. Kippelen, J.-L. Brédas, *Energy Environ. Sci.* **2009**, *2*, 251–261.

[3] J. Zaumseil, H. Sirringhaus, *Chem. Rev.* **2007**, *107*, 1296–1323.

[4] E. J. Meijer, D. M. de Leeuw, S. Setayesh, E. van Veenendaal, B. –H. Huisman, P. W. M. Blom, J. C. Hummelen, U. Scherf, T. M. Klapwijk, *Nat. Mater.* **2003**, *2*, 678–682.

[5] T. Yasuda, T. Goto, K. Fujita, T. Tsutsui, *Appl. Phys. Lett.* **2004**, *85*, 2098–2100.

[6] T. D. Anthopoulos, C. Tanase, S. Setayesh, E. J. Meijer, J. C. Hummelen, P. W. M. Blom, D. M. de Leeuw, *Adv. Mater.* **2004**, *16*, 2174–2179.

[7] L. -L. Chua, J. Zaumseil, J. –F. Chang, E. C –W. Ou, P. K. –H. Ho, H. Sirringhaus, R. H. Friend, *Nature* **2005**, *434*, 194–199.

[8] E. C. P. Smits, T. D. Anthopoulos, S. Setayesh, E. Van Veenendaal, R. Coehoorn, P. W. M. Blom, B. De Boer, D. M. De Leeuw, *Phys. Rev. B* **2006**, *73*, 205316.

[9] H. Sirringhaus, *Nature* **2009**, *457*, 667–668.

[10] C. Melzer, E. J. Koop, V. D. Mihailetchi, P. W. M. Blom, *Adv. Funct. Mater.* **2004**, *14*, 865–870.

[11] S. M. Tuladhar, D. Poplavskyy, S. A. Choulis, J. R. Durrant, D. D. C. Bradley, J. Nelson, *Adv. Funct. Mater.* **2005**, *15*, 1171–1182.

[12] A. Gadisa, K. Tvingstedt, K. Vandewal, F. Zhang, J. V. Manca, O. Inganäs, *Adv. Mater.* **2010**, *22*. 1008–1011.

[13] see the Chapter 2.

[14] A. Maurano, R. Hamilton, C. G. Shuttle, A. M. Ballantyne, J. Nelson, B. O'Regan, W. Zhang, I. McCulloch, H. Azimi, M. Morana, C. J. Brabec, J. R. Durrant, *Adv. Funct. Mater.* **2010**, *22*, 4987–4992.

[15] D. Kitazawa, N. Watanabe, S. Yamamoto, J. Tsukamoto, *J. Photopolym. Sci. Technol.* **2010**, *23*, 293–296.

[16] M. C. Scharber, D. Mühlbacher, M. Koppe, P. Denk, C. Waldauf, A. J. Heeger and C. J. Brabec, *Adv. Mater.*, **2006**, *18*, 789–794.

[17] J. Peet, J. Y. Kim, N. E. Coates, W. L. Ma, D. Moses, A. J. Heeger, and G. C. Bazan, *Nat. Mater.*, **2007**, *6*, 497–500.

[18] D. Kitazawa, N. Watanabe, S. Yamamoto, J. Tsukamoto, *Appl. Phys. Lett.* **2009**, *95*, 053701.

[19] J. K. J. Duren, X. Yang, J. Loos, C. W. T. Bulle-Lieuwma, A. B. Sieval, J. C. Hummelen, R. A. J. Janssen, *Adv. Funct. Mater.* **2004**, *14*, 425–434.

[20] A. Tsuchida, M. Yamamoto, Y. Nishijima, *J. Phys. Chem.* **1984**, *88*, 5062–5064.

[21] D. M. Guldi, M. Prato, *Acc. Chem. Res.* **2000**, *33*, 695–703.

[22] I.-W. Hwang, C. Soci, D. Moses, Z. Zhu, D. Waller, R. Gaudiana, C. J. Brabec, A. J. Heeger, *Adv. Mater.* **2007**, *19*, 2307–2312.

[23] T. Clarke, A. Ballantyne, F. Jamieson, C. Brabec, J. Nelson, J. Durrant, *Chem. Commun.* **2009**, 89–91.

[24] J. Guo, H. Ohkita, S. Yokoya, H. Benten, S. Ito, *J. Am. Chem. Soc.* **2010**, *132*, 9631–9637.

[25] A. Moulé, K. Meerholz, *Adv. Funct. Mater.* **2009**, *19*, 3028–3036.

[26] J. K .Lee, W. L. Ma, C. J. Brabec, J. Yuen, J. S. Moon, J. Y. Kim, K. Lee, G. C. Bazan, A. J. Heeger, *J. Am. Chem. Soc.* **2008**, *130*, 3619–3623.

[27] M. Dante, A. Garcis, T. –Q. Nguyen, *J. Phys. Chem. C* **2009**, *113*, 1596–1600.

[28] A. Miller, E. Abrahams, *Phys. Rev.* **1960**, *120*, 745–755.

[29] N. Tessler, Y. Preezant, N. Rappaport, Y. Roichman, *Adv. Mater.* **2009**, *21*, 2741–2761.

[30] G. Garcia-Belmonte, J. Bisquert, *Appl. Phys. Lett.* **2010**, *96*, 113301.

[31] H. W. Kroto, A. W. Allaf, S. P. Balm, *Chem. Rev.* **1991**, *91* 1213–1235.

[32] H. Bässler *Phys.Stat. Sol. (b)*, **1993**, *175*, 15–56.

[33] C. Tanase, P. W. M. Blom, D. M. De Leeuw, E. J. Meijer, in *Physics of Organic Semicondutors* (Ed.: W. Brütting), Wiley-VCH, Weinheim, Germany **2005**.

[34] P. W. M. Blom, M. C. J. M. Vissenberg, *Mater. Sci. Eng.*, **2000**, *27*, 53–94.

[35] W. Tang, V. Chellappan, M. Liu, Z.-K. Chen, L. Ke, *ACS Appl. Mater. Interfaces*, **2009**, *1*, 1467.

[36] L. M. Anderson, W. Osikowicz, F. L. E. Jakobsson, M. Berggren, L. Lindgren, M. R. Anderson, O. Inganäs, *Org. Electron.* **2008**, *9*, 569–574.

[37] F. Laquai, G. Wegner, C. Im, H Bässler, S. Heun, *Appl. Phys. Lett.* **2006**, *99*, 023712.

[38] A. M. Ballantyne, L .Chen, J. Dane, T. Hammant, F. M. Braun, M. Heeney, W. Duffy, I. McCulloch, D. D. C. Bradley, J. Nelson, *Adv. Funct. Mater.* **2008**, *18*, 2373–2380.

[39] I. I. Fishchuk, A. K. Kadashchuk, J. Genoe, M. Ullah, H. Sitter, Th. B. Singh, N. S. Sariciftci, H Bässler, *Phys. Rev. B.* **2010**, *81*, 045202.

[40] Y. Zhang, P. W. M. Blom, *Appl.Phys. Lett.* **2011**, *98*, 143504.

[41] M. S. Golden, M. Knupfer, J. Fink, J. F. Armbruster, T. R. Cummins, H. A. Romberg, M. Roth, M. Sing, M. Schmidt, E. Sohmen, *J. Phys.: Condens. Matter.* **1995**, *7*, 8219–8247.

[42] W. Y. Ching, M. –Z. Huang, Y. –N. Xu, W. G. Harter, F. T. Chan, *Phys. Rev. Lett.* **1991**, *67*, 2045–2048.

[43] E. L. Shirley, S. G. Louie, *Phys. Rev. Lett.* **1993**, *71*, 133–136.

[44] M. Merkel, M. Knupfer, M. S. Goldewn, J. Fink, R. Seemann, R. L. Johnson, *Phys. Rev. B* **1993**, *47*, 11470.

[45] P. J. Benning, C. G. Olson, D. W. Lynch, J. H. Weaver, *Phys. Rev. B* **1994**, *50*, 11239.

[46] G. K. Wertheim *Phys. Rev. B*, **1995**, *51*, 10248.

[47] K. Akaike, K. Kanai, H. Yoshida, J. Tsutsumi, T. Nishi, N. Sato, Y. Ouchi, K. Seki, *J. Appl. Phys.* **2008**, *104*, 023710.

[48] Q. Wei, K. Tajima, Y. Tong, S. Ye, K. Hashimoto, *J. Am. Chem. Soc.* **2009**, *131*, 17597–17604.

[49] M. Lenes, M. Morana, C. J. Brabec, P. W. M. Blom, *Adv. Funct. Mater.* **2009**, *19*, 1106–1111.

[50] C. H. Chen, C. H. Hsieh, M. Dubosc, Y. J. Cheng, C. S. Hsu, *Macromolecures* **2010**, *43*, 697–708.

[51] S. Cook, H. Ohkita, Y. Kim, J. J. Benson-Smith, D. D. C. Bradley, J. R. Durrant, *Chem. Phys. Lett.* **2007**, *445*, 276–280.

[52] J. M. Nápoles-Duarte, M. Reyes-Reyes, J. L. Ricardo-Chavez, R. Garibay-Alonso, R. López-Sandoval, *Phys. Rev. B* **2008**, *78*, 035425.

[53] H. Ishii, K. Sugiyama, E. Ito, K. Seki, *Adv. Mater.* **1999**, *11*, 605–625.

[54] S. Braun, W. R. Salaneck, M. Fahlman, *Adv. Mater.* **2009**, *21*, 1450–1472.

[55] Z. Xu, L.-M. Chen, M.-H. Chen, G. Li, Y. Yang, *Appl. Phys. Lett.* **2009**, *95*, 013301.

[56] W. Osikowicz, M. P. de Jong, W. R. Salaneck, *Adv. Mater.* **2007**, *19*, 4213–4217.

[57] S. C. Veenstra, H. T. Jonkman, *J. Polym. Sci B* **2003**, *41*, 2549–2560.

[A1] M. Zhang, H. N. Tsao, W. Pisula, C. Yang, A. K. Mishra, K. Müllen, *J. Am. Chem. Soc.* **2007**, *129*, 3472–3473.

[A2] H. N. Tsao, D. Cho, J. W. Andersen, A. Rouhanipour, D. W. Breiby, W. Pisula, K. Müllen, *Adv. Mater.* **2009**, *21*, 209–212.

[A3] K.-C. Li, Y.-C. Hsu, J.-T. Lin, C.-C. Yang, K.-H. Wei, H.-C. Lin, *J. Polym. Sci. A* **2009**, *47*, 2073–2092.

[A4] J. C. Bijleveld, M. Shaid, J. Gilot, M. M. Wienk, R. A. J. Janssen, *Adv. Funct. Mater.* **2009**, *21*, 3262–3276.

[A5] N. Miyaura, A. Suzuki, *J.Chem. Soc., Chem. Commun.* **1979**, 866–867.

Part II

Chapter 4

Molecular Understanding of the Open-Circuit Voltage of Polymer:Fullerene Solar Cells

4.1. Introduction

The power conversion efficiency (PCE) of bulk heterojunction organic solar cells based on conjugated polymer and fullerene derivatives has been steadily improved during the last decade. Recently, PCE in excess of 8% has been reported.[1,2] In general, there are two strategies for improving the device performance: one is to increase the short-circuit current density (J_{SC}) and the other is to increase the open-circuit voltage (V_{OC}). The maximum photocurrent is primarily limited by the number of photons absorbed by the solar cells. In other words, J_{SC} can be improved by using materials that have wider absorption bands to collect more photons from the solar light. For this purpose, a C_{70} fullerene derivative has been employed with conjugated polymers instead of C_{60} fullerene derivatives because of the larger extinction coefficient in the visible region.[3] Currently, various low-bandgap polymers have been developed to harvest the near-IR light and primarily contribute to the recent progress in PCE of polymer solar cells.[4–6] The incorporation of near-IR dye molecules into polymer:fullerene solar cells also has been reported to effectively improve the light-harvesting efficiency and hence boost J_{SC} substantially.[7–10] On the other hand, the maximum photovoltage is considered to be limited by the energy gap between the highest occupied molecular orbital (HOMO) level of a donor polymer and the lowest unoccupied molecular orbital (LUMO) level of an acceptor fullerene (ΔE_{DA}). Indeed, V_{OC} has been reported to increase with lowering

HOMO level of polymers and raising LUMO level of fullerenes.[11–14] Currently, remarkable progress in the device performance has been made using these strategies.[15,16]

Although there have been several studies showing a linear relationship between V_{OC} and ΔE_{DA} experimentally, V_{OC} is generally 0.2 – 0.5 V smaller than ΔE_{DA}.[11–14] Recently, the difference between V_{OC} and ΔE_{DA} has been discussed. For example, Koster *et al.* reported that the difference is related to the dissociation probability of bound electron–hole pair and the Langevin recombination of free carriers assuming that the quasi-Fermi levels are constant throughout the device.[17,18] A recent study on the light intensity dependence of photocurrent has shown that the recombination dynamics is the voltage dependent: first-order recombination under an short-circuit condition and bimolecular recombination under an open-circuit condition. From the temperature/intensity dependence of V_{OC}, the difference between V_{OC} and ΔE_{DA} is ascribed to the temperature dependence of the quasi-Fermi levels in the polymer and fullerene domains.[19] Similarly, Durrant *et al.* reported that the charge dynamics is dominated by bimolecular recombination at V_{OC} by transient photovoltage and absorption measurements. They note that the bimolecular rate constant is 2–3 orders of magnitude smaller than the Langevin recombination rate.[20] Furthermore, they recently demonstrated that V_{OC} varies only by ~0.1 V between P3HT and bridged thiophene-based polymers with a difference of 0.2 – 0.4 eV in ionization potentials, and assigned this mismatch to a faster recombination rate in bridged thiophene-based devices. Consequently, they proposed that V_{OC} depends not only on ΔE_{DA} but also on the magnitude bimolecular recombination rate.[21] On the other hand, V_{OC} is dependent on the saturation current density J_0 in terms of the diode-based equivalent circuit model. Recently, the molecular structures have been reported to affects V_{OC} in small molecule-based organic solar cells.[22–24] This suggests that V_{OC} is dependent on the electron transfer at the interface because of the difference in

the electronic coupling between donor and acceptor molecules. From another point of view, Inganäs *et al.* reported a linear relationship between V_{OC} and the charge transfer (CT) emission energy E_{CT} for blend films based on various conjugated polymers and PCBM. In this relationship, V_{OC} is reduced by 0.5 – 0.6 V compared to E_{CT},[25–27] which is similar to the difference between V_{OC} and ΔE_{DA}. They ascribed ~0.25 V of the reduction to radiative losses that are related to the formation of CT complex, and the rest (~0.35 V) to nonradiative losses.[27] As described above, the difference between V_{OC} and ΔE_{DA} has been discussed in terms of the bimolecular recombination dynamics and the interfacial electron transfer separately. However, the origin of V_{OC} in polymer solar cells is not fully understood.

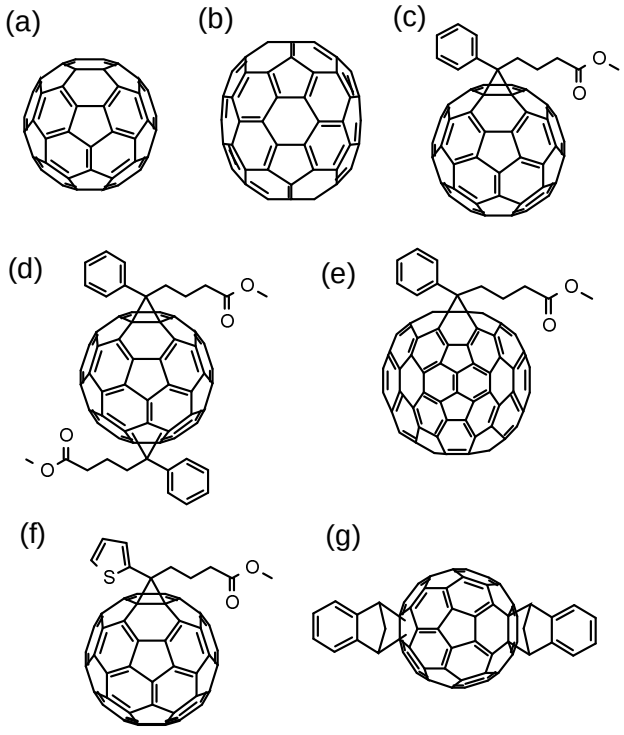

Figure 4-1. Chemical structures of fullerenes: (a) C_{60}, (b) C_{70}, (c) PCBM, (d) bis-PCBM, (e) $PC_{84}BM$, (f) ThCBM, and (g) ICBA.

To address the origin of V_{OC}, the author carefully analyzed *J*–*V* characteristics in the dark on the basis of the one-diode equivalent circuit model.[22,24,26,28-32] This simple equivalent circuit model have been widely used for analysis of open-circuit voltage of organic solar cells and succeeded in explaining the open-circuit voltage. It is noteworthy that the dark current properties strongly related to the open-circuit voltage which is measured under illumination. For example, Perez ***et al.*** discussed open-circuit voltages of organic solar cells with low molecular weight materials based on this model and showed that donor materials with structures that hinder intermolecular interaction leads high open-circuit voltages[22]. Kirchartz et al. discussed open-circuit voltages of P3HT-based polymer solar cells and indicated that charge recombination takes place between free charge carriers and charge carriers trapped in exponential tail of localized states.[32] In this study, the author employed seven fullerene derivatives with different LUMO levels as shown in Figure 4-1 in order to discuss the relationship between V_{OC} and ΔE_{DA} systematically. Five of them are fullerene derivatives with attached groups: [6,6]-phenyl-C_{61}-butyric acid methyl ester (PCBM), [6,6]-diphenyl-C_{62}-bis(butyric acid methyl ester) (bis-PCBM),[30,31] [6,6]-phenyl-C_{85}-butyric acid methyl ester ($PC_{84}BM$),[32] [6,6]-1-thienyl-C_{61}-butyric acid methyl ester (ThCBM),[33] [6,6]-bis[3,5-([1',2']-benzeno)-4*H*-cyclopenta]-C_{60} (Indene-C_{60}-bisadduct, ICBA).[34] The other two are pristine fullerenes of C_{60} and C_{70}, which are employed to discuss the effect of the side chain on V_{OC}.

4.2. Results

4.2.1. *J*–*V* Characteristics

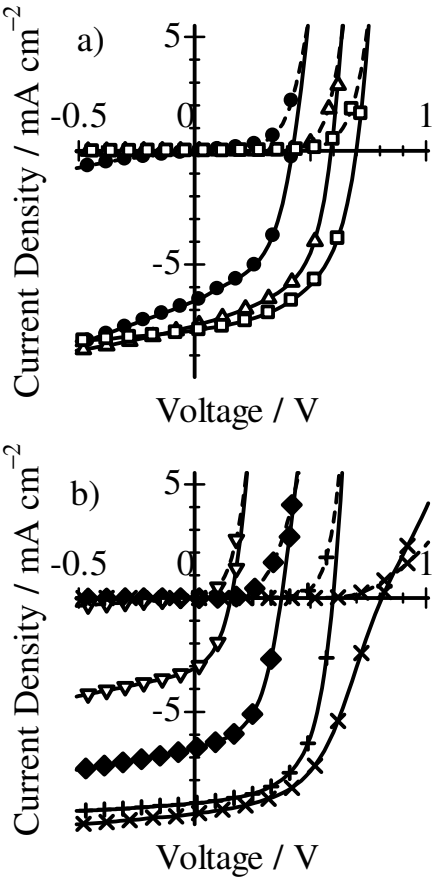

Figure 4-2. *J*–*V* characteristics of each P3HT:fullerene solar cell in the dark (broken lines) and under AM1.5G simulated solar illumination at 100 mW cm^{-2} (solid lines): C_{60} (●), PCBM (△), bis-PCBM (□), C_{70} (◆), $PC_{84}BM$ (▽), ThCBM (+), and ICBA (×). The opened and closed symbols show blend films with pristine fullerenes and fullerene derivatives with attached groups, respectively.

Table 4-1. The HOMO–LUMO energy gap ΔE_{DA}, device parameters, hole mobility μ_h, and quenching efficiency Φ_q of each P3HT:fullerene blend.

	ΔE_{DA} / eV	J_{SC} / mA cm^{-2}	V_{OC} / V	FF	PCE / %	μ_h / cm^2 V^{-1} s^{-1} [a]	Φ_q / % [b]
$PC_{84}BM$	0.58	3.09	0.16	0.40	0.19	5.0×10^{-5}	95
C_{70}	0.84	6.60	0.37	0.52	1.26	3.0×10^{-5}	86
C_{60}	0.86	6.60	0.42	0.49	1.36	5.0×10^{-5}	93
PCBM	0.94	7.70	0.59	0.53	2.41	3.0×10^{-5}	92
ThCBM	0.93	9.01	0.60	0.60	3.22	2.3×10^{-5}	92
bis-PCBM	1.02	7.89	0.70	0.53	2.95	6.0×10^{-5}	87
ICBA	1.09	9.48	0.81	0.50	3.83	3.5×10^{-5}	95

[a] The hole mobility is evaluated from the space charge limited current for the devices with a layer structure of ITO/PEDOT:PSS/P3HT:fullerene/Au.

[b] The quenching efficiency is evaluated by the PL intensity ratio of P3HT:fullerene blends to that of a P3HT pristine film.

Figure 4-2 shows the *J*–*V* characteristics of seven P3HT-based solar cells with different fullerene derivatives. All the devices showed reproducible diode characteristics in the dark and photovoltaic performance under the AM1.5G simulated solar illumination. The J_{SC} and FF were slightly smaller than those reported in the literatures[7–10,30–36] because each device was not fully optimized but just the active layer was fabricated in the same thickness. On the other hand, V_{OC} was in good agreement with the reported values:[7–10,30–36] that ranged from 0.16 V for $PC_{84}BM$ to 0.81 V for ICBA. The device parameters of these cells are summarized in Table 4-1. The energy level of the HOMO of P3HT was evaluated to be 4.68 eV by the photoemission yield spectroscopy measurement (see the Appendix). The energy levels of the LUMO of the fullerene derivatives were evaluated by cyclic voltammetry in solution with a ferrocene/ferrocenium (Fc/Fc^+) redox

couple as an internal standard using Ag/AgCl reference electrode (see the Appendix).[37] The energy differences between the HOMO level of P3HT and the LUMO level of fullerenes $\Delta E_{DA} = E_{HOMO}(P3HT) - E_{LUMO}(fullerene)$ are summarized in Table 4-1. Figure 4-3 shows a linear relationship between V_{OC} and ΔE_{DA}. This linear relationship is consistent with previous studies.[11–14] Interestingly, the plots for pristine fullerenes (C_{60} and C_{70}) deviate from the linear relationship: the V_{OC} of pristine fullerenes is smaller by ~0.1 V than that predicted from the linear relationship. This finding suggests that V_{OC} of polymer:fullerene solar cells cannot be explained by ΔE_{DA} alone as is discussed later. Furthermore, the hole mobility μ_h and photoluminescence (PL) quenching efficiency Φ_q of each blend film were evaluated by the space charge limited current measurement for the hole only devices and by the fluorescence measurement for the P3HT:fullerene blend and P3HT pristine films on a glass substrate, respectively. As summarized in Table 4-1, μ_h and Φ_q of blend films were independent of the fullerene derivatives. These results suggest that fullerene derivatives have little impact on the blend morphology of P3HT in the blend.

As shown in Figure 4-2, V_{OC} is closely related to the turn-on voltage in the dark current, suggesting that V_{OC} is strongly dependent on the diode characteristics. Therefore the dark current characteristics of these devices were analyzed by the equivalent circuit model based on a diode $J_0[\exp(qV/nk_BT) - 1]$, a series resistor R_s, and a parallel resistor R_p as shown in Figure 4-4a. In this model, J–V characteristics can be derived by Equation 4-1[28,29]

$$J = J_0\left\{\exp\left[\frac{q(V - JR_sA)}{nk_BT}\right] - 1\right\} + \frac{(V - JR_sA)}{R_pA} - J_{ph} \qquad (4\text{-}1)$$

where J_0 is the saturation current density, n is the ideality factor, R_s is the series resistance, R_p is the parallel resistance, q is the elementary charge, k_B is the Boltzmann constant, T is

the temperature, A is the active area of the device, and J_{ph} is the photocurrent density. As shown in Figure 4-4b, the dark J–V characteristics are well fitted with Equation 4-1. All the diode parameters are summarized in Table 4-2. Assuming that J_{ph} is equal to J_{SC}, Equation 4-1 can be simplified into Equation 4-2 under the open-circuit condition because of $V_{OC} << J_{SC}R_pA$ and $J_0 << J_{SC}$.

$$V_{OC} = \frac{nk_BT}{q}\ln\left[1+\frac{J_{SC}}{J_0}\left(1-\frac{V_{OC}}{J_{SC}R_pA}\right)\right] \approx \frac{nk_BT}{q}\ln\left(\frac{J_{SC}}{J_0}\right) \qquad (4\text{-}2)$$

The V_{OC}^{calc} calculated by the simplified Equation 4-2 with the diode parameters is in good agreement with the V_{OC} observed within a relative error of 7%, which is consistent with the previous report.[38] The agreement shows that this equation is valid for P3HT:fullerene solar cells employed in this study. In other words, V_{OC} of P3HT:fullerene solar cells is independent of R_s and R_p but essentially dependent on n, J_{SC}, and J_0. For different fullerenes, as shown in Table 4-2, J_0 differs by six orders of magnitude while variations in n and J_{SC} are negligibly small. Thus, it can safely be said that V_{OC} of P3HT:fullerene solar cells is primarily dependent on J_0.

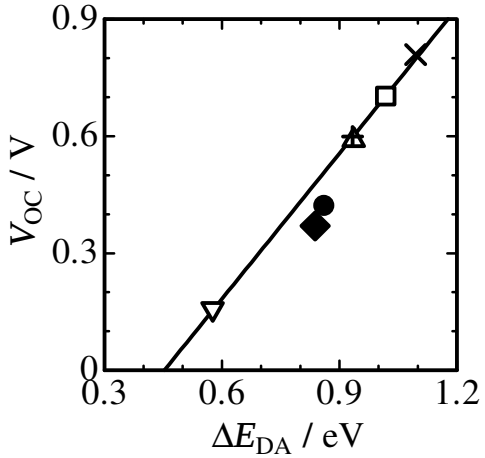

Figure 4-3. Relationship between V_{OC} and ΔE_{DA} for seven P3HT:fullerene solar cells. The symbols are the same as those in Figure 4-2.

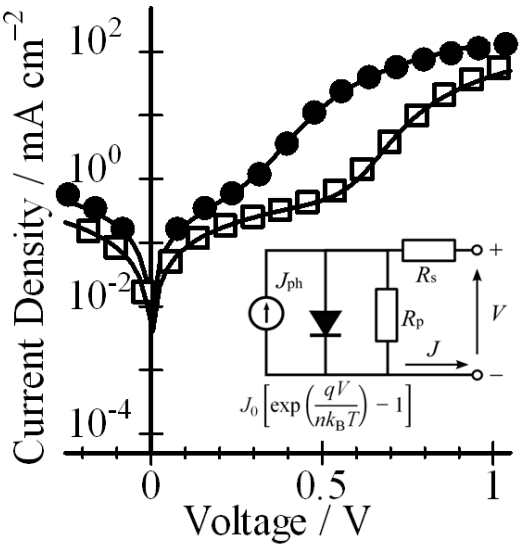

Figure 4-4. Log plots of the dark current density against applied voltage: C_{60} (●) and bis-PCBM (□). The inset shows the equivalent circuit, which consists of a diode $J_0[\exp(qV/nk_BT) - 1]$, a series resistor R_s, and a pallarel resistor R_p. The solid lines are fitting curves by Equation 4-3. The other data are shown in the Appendix.

Table 4-2. Diode parameters of P3HT:fullerene blend devices.

	n	R_sA / Ω cm^2	R_pA / kΩ cm^2	J_0 / mA cm^{-2}	J_{00} / mA cm^{-2}	E_A / eV
$PC_{84}BM$	1.73	2.6	2.7	6.0×10^{-2}	1.3×10^{2}	0.21
C_{70}	1.6	8	1	6.0×10^{-4}	6.4×10^{3}	0.45
C_{60}	1.54	8	70	1.5×10^{-4}	1.0×10^{4}	0.47
PCBM	1.7	3.5	75	3.0×10^{-6}	3.7×10^{2}	0.48
ThCBM	1.67	2.8	40	3.5×10^{-6}	3.4×10^{2}	0.47
bis-PCBM	1.7	5	1.2	2.5×10^{-7}	1.6×10^{2}	0.52
ICBA	1.75	100	1100	6.0×10^{-8}	2.2×10^{2}	0.60

4.2.2. Temperature Dependence of J_0

To address the origin of J_0, J–V characteristics in the dark were measured over the

temperature range from 180 to 310 K. Figure 4-5a shows the temperature dependence of J_0 of P3HT:fullerene solar cells. As reported previously,[29] J_0 can be expressed by the Arrhenius equation.

$$J_0 = J_{00} \exp\left(-\frac{E_A}{k_B T}\right) \tag{4-3}$$

where J_{00} is the pre-exponential factor and E_A is the activation energy. From the ordinate intercept and slope of the Arrhenius plots, J_{00} and E_A can be evaluated. Figure 4-5b shows these two parameters J_{00} and E_A plotted against V_{OC}. As shown in the figure, no correlation is found between J_{00} and V_{OC} but a linear relationship is observed between E_A and V_{OC}. Interestingly, J_{00} is classified based on the presence or absence of attached groups to the fullerene unit. The J_{00} of pristine fullerenes is almost two orders of magnitude larger than that of fullerene derivatives with attached groups. The contribution of J_{00} and E_A to V_{OC} is evaluated by Equation 4-4, which can be obtained from Equations 4-2 and 4-3.

$$qV_{OC} = nE_A - nk_B T \ln\left(\frac{J_{00}}{J_{SC}}\right) \tag{4-4}$$

Figure 4-5c shows the proportion of each term in Equation 4-4 for various fullerene derivatives. As shown in the figure, the first term on the right side is the largest and increases with increasing V_{OC} of polymer solar cells. On the other hand, the percentage of the second term to nE_A is ~30% for fullerene derivatives with attached groups and as large as ~50% for pristine fullerenes. In other words, E_A is the primary factor controlling V_{OC}, and J_{00} in the second term is a secondary factor but is not negligible for controlling V_{OC}. The second term is clearly dependent on the presence or absence of attached groups to the fullerene unit: $nk_B T \ln(J_{00}/J_{SC})$ is ~0.2 eV for fullerene derivatives with attached groups and is ~0.3 eV for pristine fullerenes.

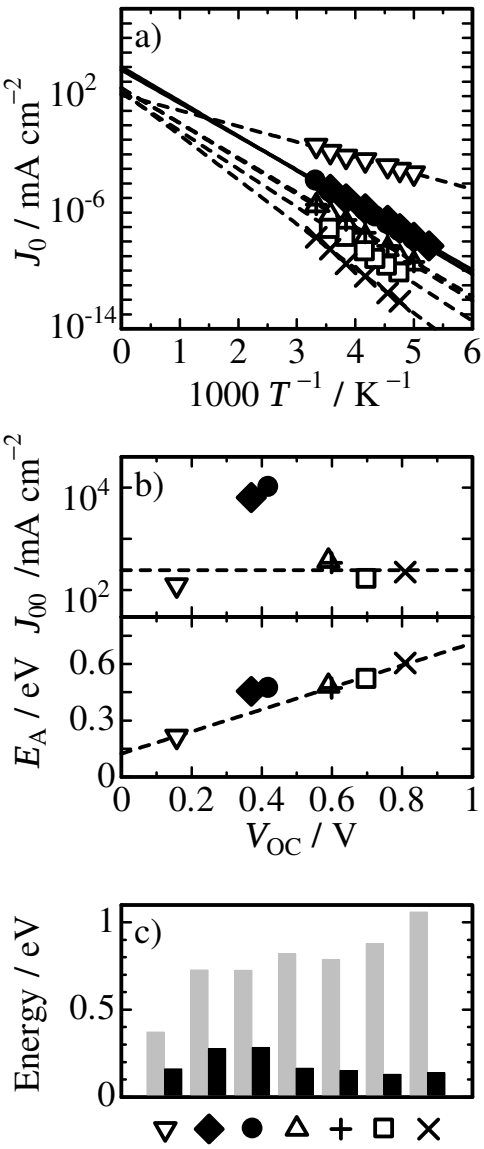

Figure 4-5. a) Arrhenius plots of the saturation current J_0 for each fullerene system. The symbols are the same as those in Figure 4-2. b) Plots of the pre-exponential factor J_{00} and activation energy E_A for J_0. The broken lines are fitting curves for fullerene derivatives with attached groups. c) Relative proportion of the two terms of nE_A (gray bars) and $nk_BT\ln(J_{00}/J_{SC})$ (black bars) in Equation 4-4. The difference between the gray and black bars corresponds to qV_{OC}. The temperature T is set at 300 K.

4.3. Discussion

4.3.1. Recombination Current

First, the author will consider the dark current density, as described above, which is closely related to V_{OC}. In the recombination via a bound electron–hole pair at a donor/acceptor interface, the recombination rate is given by $R = \gamma(n_e n_h - n_i^2)(1 - P_{dis})$ where γ is the Langevin recombination rate, P_{dis} is the dissociation probability of a bound electron–hole pair into free charge carriers at the interface, and n_e, n_h, and n_i are the concentrations of free electrons and holes, and intrinsic carriers, respectively.[17,18] The Langevin recombination rate γ is given by $q(\mu_e + \mu_h)/\varepsilon$ where μ_e and μ_h are electron and hole mobility, respectively, and ε is the permittivity. The dissociation probability is given by $P_{dis} = k_{dis}/(k_{rec} + k_{dis})$ where k_{rec} and k_{dis} are the recombination and dissociation rate of bound electron–hole pairs, respectively. Thus, the recombination current density J_{rec} can be written as the spatial integration of R[39]

$$J_{rec} = q\int_0^d \gamma(n_e n_h - n_i^2)(1-P_{dis})\mathrm{d}x = qd\gamma n_i^2(1-P_{dis})\left[\exp\left(\frac{qV}{k_B T}\right)-1\right] \quad (4\text{-}5)$$

where d is the thickness of the active layer. In other words, the saturation current density is equal to $qd\gamma n_i^2(1 - P_{dis})$, which is dependent on the carrier mobility and the recombination and dissociation rate of bound electron–hole pairs. In the diffusion-limited case $P_{dis} << 1$ ($k_{rec} >> k_{dis}$), the saturation current density is equal to $qd\gamma n_i^2$, which is dependent only on the carrier mobility. Thus, the author obtain the following Equation 4-6 from Equation 4-2, assuming that $J_0 = qd\gamma n_i^2(1 - P_{dis})$, $J_{SC} = P_{dis}Gqd$, and $n_i^2 = N_C^2\exp(E_g/k_B T)$ where G is the generation rate of bound electron–hole pairs, N_C is the effective density of states, and E_g is the energy difference between the valence band of donor material and the conduction band of acceptor material.[29]

$$V_{OC} = \frac{nE_g}{q} - \frac{nk_B T}{q} \ln\left(\frac{qd\gamma(1-P_{dis})N_C{}^2}{J_{SC}} \right) = \frac{nE_g}{q} - \frac{nk_B T}{q} \ln\left(\frac{\gamma(1-P_{dis})N_C{}^2}{P_{dis} G} \right) \quad (4\text{-}6)$$

Note that Equation 4-6 is identical to the one derived in previous studies[17,18] except for the ideality factor. The ideality factor $n \approx 1.6$ suggests that a recombination mechanism in P3HT:fullerene solar cells other than a direct recombination, such as the Shockley–Read–Hall (SRH) recombination as reported recently.[39,40] Indeed, Guo *et al.* found recently that there are two types of P3HT polarons (trap-free and trapped P3HT polarons) in P3HT:PCBM blend films.[41] The bimodal recombination may be related to the ideality factor $1 < n < 2$, which is a typical value for polymer solar cells. This study, however, is focused on the origin of J_0, and the author will not discuss the difference in the ideality factor any further.

4.3.2. Origin of Open-Circuit Voltage

From the comparison of Equation 4-4 with Equation 4-6, it was obtained the following relation: $E_A = E_g$ and $J_{00} = qd\gamma(1 - P_{dis})N_C{}^2$, which are indicative of the molecular origin of J_0 (J_{00} and E_A). In most studies, E_g is considered to be ΔE_{DA}.[12,14,17,24] This is consistent with the experimental relationship $V_{OC} \propto \Delta E_{DA}$, and it is concluded that E_A is its origin. However, as shown in Figure 4-5b, E_A is much smaller than ΔE_{DA}. This is partly because the formation of interfacial dipole would reduce the effective E_g as reported previously. The offset energy due to the interfacial dipole Δ is reported to be 0.4 eV for P3HT:PCBM blend films.[42] In this case, $E_A + \Delta$ is nearly equal to ΔE_{DA}.

Next the author focus on the difference in J_{00} between pristine fullerenes and fullerene derivatives with attached groups. As mentioned above, J_{00} is dependent only on

the charge mobility for the diffusion-limited recombination, and on the carrier mobility and the recombination and dissociation rate of bound electron–hole pairs for the non-diffusion-limited recombination. The electron mobility μ_e of pristine fullerenes is reported to be as high as ~0.1 $cm^2\ V^{-1}\ s^{-1}$,[43] which is one order of magnitude higher than that of fullerene derivatives with attached groups (~0.01 $cm^2\ V^{-1}\ s^{-1}$).[31,33,44,45] On the other hand, as shown in Table 4-1, μ_h of P3HT is as low as ~10^{-4} $cm^2\ V^{-1}\ s^{-1}$ in P3HT:fullerene blend films, which is comparable to time-of-flight mobility of P3HT films.[46] Thus, the two orders of magnitude difference in J_{00} cannot be explained in terms of the charge mobility alone.[47,48] This suggests that the recombination in P3HT:fullerene blends is non-diffusion-limited reaction.

For the non-diffusion-limited recombination, J_{00} is given by $qd\gamma(1 - P_{dis})N_C^2 = qd\gamma k_{rec}N_C^2/(k_{rec} + k_{dis})$. Previously, Guo *et al.* found by transient absorption spectroscopy that P3HT polarons are promptly generated within <100 fs in P3HT:PCBM blend films and a small part of them recombines to the ground state on a nanosecond time scale.[49] In other words, k_{rec} and k_{dis} are roughly estimated to be ~10^9 s^{-1} and >10^{13} s^{-1}, respectively. Recent spectroscopic studies have shown similar results even for other polymer:fullerene blends.[50–53] Thus, $k_{rec} << k_{dis}$ can be assumeumed for all the P3HT:fullerene blends studied here. Consequently, J_{00} can be simplified into $J_{00} = qdN_C^2\gamma k_{rec}/k_{dis} = qdN_C^2\gamma_a$ where γ_a is the apparent recombination rate ($\gamma k_{rec}/k_{dis}$). Considering the high PL quenching and the large J_{SC} for all the blends, k_{dis} can be assumed to be high enough to yield the high dissociation efficiency independently of fullerene derivatives. It is therefore concluded that the large difference in J_{00} is ascribed mainly to γ and k_{rec}.

According to the Marcus theory,[54] the electron transfer rate k_{ET} can be described by Equation 4-7

$$k_{ET} = \frac{4\pi^2}{h} \frac{H_{AB}^2}{\sqrt{4\pi\lambda k_B T}} \exp\left(-\frac{(\Delta G^0 + \lambda)^2}{4\lambda k_B T} \right) \quad (4\text{-}7)$$

where h is the Planck constant, H_{AB} is the electronic coupling matrix element between the reactant A and the product B, λ is the reorganization energy, ΔG_0 is the free energy difference between the reactant and the product. In the case of the charge transport in the same molecules, the charge transfer rate k_{CT} is given by Equation 4-8

$$k_{CT} = \frac{4\pi^2}{h} \frac{H_{AA}^2}{\sqrt{4\pi\lambda k_B T}} \exp\left(-\frac{\lambda}{4k_B T} \right) \quad (4\text{-}8)$$

The Langevin recombination rate γ is proportional to the diffusion constant, which is proportional to k_{CT} assuming that the charge diffusion is repetitive hopping between two neighbors.[55,56] On the other hand, as mentioned above, γ is given by $q(\mu_e + \mu_h)/\varepsilon \approx q\mu_e/\varepsilon$. Thus, the author ascribe the difference in μ_e by one order of magnitude to the electronic coupling matrix element H_{AA} because it is the most sensitive to the presence or absence of attached groups to fullerenes. In other words, the difference in γ (or μ_e) by one order of magnitude suggests that H_{AA}^2 between pristine fullerenes is about 10 times larger than that between fullerene derivatives with attached groups. The author therefore ascribes the remaining difference in J_{00} by one order of magnitude to k_{rec}. Similarly, the difference in k_{rec} suggests that H_{AB}^2 between P3HT and pristine fullerenes is about 10 times larger than that between P3HT and fullerene derivatives with attached groups.[57] This is reasonable because the presence or absence of attached groups to fullerenes would change the intermolecular distance and hence would have comparable impact on H_{AA} and H_{AB}. Furthermore, recent studies have shown that weak intermolecular interaction due to bulky substituents leads to higher V_{OC} for small molecule organic solar cells.[22,23] Therefore, it is concluded that the V_{OC} is dependent on both electronic couplings of fullerene/fullerene and polymer/fullerene.

It is noteworthy that V_{OC} is dependent on the charge recombination at the P3HT/PCBM interface. This is inconsistent with the Langevin recombination that is limited only by diffusion. In the Langevin recombination, the reaction radius is assumed to be a critical distance r_c at which the thermal energy of a charge carrier is equal to the Coulombic attractive potential energy. In P3HT:PCBM blends, r_c is estimated to be as long as 16 nm with a dielectric constant of 3.4. This is significantly larger than the separation distance of the interfacial charge recombination r_0, which would be a few nanometers at most. If r_0 were employed instead of r_c, the diffusion-limited recombination rate would be almost one order of magnitude smaller than the Langevin recombination rate γ. Furthermore, as mentioned above, the apparent recombination rate γ_a is reduced by a factor of k_{rec}/k_{dis} compared to γ for the non-diffusion-limited reaction. In other words, the large difference between k_{rec} and k_{dis} may be related to the reduced recombination rate reported for polymer:fullerene blends. Such electron-transfer-dependent recombination has been reported for dye-sensitized solar cells.[58]

Finally, the author discusses the molecular design for improving V_{OC} on the basis of the findings in this study. It was found that V_{OC} is essentially dependent on E_A and J_{00} from the detailed analysis of the dark current characteristics of the devices. The activation energy E_A is closely related to ΔE_{DA}, which is consistent with the experimental relation $V_{OC} \propto \Delta E_{DA}$. The relation provides the guideline for the molecular design that lowers HOMO donors and higher LUMO acceptors are desirable for higher V_{OC}. This strategy has already been great successful in improving V_{OC} in polymer solar cells mentioned before.[59,60] On the other hand, J_{00} is essentially related to the electronic couplings of polymer/polymer or fullerene/fullerene H_{AA} and of polymer/fullerene H_{AB}. In other words, lower H_{AA} or H_{AB} could lead to a higher V_{OC}. However, a lower H_{AA}

results in lower charge mobility, which would cause lower charge collection efficiency and hence lower device performance. Thus, the molecular design for lowering H_{AA} is not appropriate for improving the overall device performance. Similarly, a lower H_{AB} results in the decrease in the electron transfer rate at the polymer/fullerene interface. In other words, a lower H_{AB} seems to cause not only a lower k_{rec} but also a lower charge separation rate k_{cs}, the latter of which would result in lower charge generation efficiency. However, this is not always true because H_{AB} is different between k_{rec} and k_{cs}. The electronic coupling in the charge separation H_{AB}^{CS} is taken to be the coupling between the LUMO of the donor and the acceptor and that in the charge recombination H_{AB}^{CR} is taken to be the coupling between the HOMO of the donor and the LUMO or LUMO + 1 of the acceptor.[61] For example, H_{AB}^{CS} can be larger than H_{AB}^{CR} by controlling the spatial distribution of HOMO and LUMO of the donor material as reported for dye-sensitized solar cells.[58,62,63] The LUMO of the Ru complex sensitizer is concentrated on bipyridine ligands attached with the anchoring carboxylic groups while the HOMO is shifted in weight from the Ru atom towards the NCS ligands. Consequently, H_{AB}^{CS} is significantly larger than H_{AB}^{CR}, resulting in ultrafast electron injection into TiO_2 and slow recombination at the interface simultaneously. Furthermore, a recent *ab initio* calculation has shown that the electronic coupling at the P3HT/C_{60} heterojunction is much larger in the excited state than in the ground state.[64] The author therefore proposes that the molecular design with a large H_{AB}^{CS} and small H_{AB}^{CR} would enhance V_{OC} effectively without any loss of the charge generation efficiency.

4.4. Conclusion

The origin of open-circuit voltage of polymer:fullerene solar cells have studied by analyzing the *J–V* characteristic in the dark and under the illuminaiton. Seven different

polymer solar cells were fabricated by using different fullerene derivatives with the LUMO levels ranging from 3.53 to 4.10 eV. From the photocurrent measurement, the linear relationship between V_{OC} and ΔE_{DA} is observed as reported priviously, but not between fullerene derivatives with attached groups and pristine fullerenes. To understand the different linear relationship between V_{OC} and ΔE_{DA}, the author carefully analyzed the diode characteristics in the dark on the basis of the equivalent circuit model. As a result, it was found that V_{OC} of the P3HT:fullerene solar cells is independent of the ideality factor n but mainly dependent on the saturation current J_0. From the temperature dependence of J_0, the activation energy E_A and the pre-exponential factor J_{00} are evaluated for J_0. The autohr ascribe the former term to ΔE_{DA} and the latter term to the charge recombination in P3HT:fullerene blends. Interestingly, the latter term is dependent on the absence or presence of the attached groups to the fullerenes. Indeed, J_{00} can be expressed as $J_{00} = qdN_C^2\gamma k_{rec}/k_{dis} = qdN_C^2\gamma_a$ where γ_a is the apparent recombination rate ($\gamma k_{rec}/k_{dis}$). This finding suggests that the recombination in P3HT:fullerene blends is the non-diffusion-limited reaction depending on the electron transfer at the P3HT/fullerene interface. This is consistent with the reduced recombination compared to the Langevin recombination as reported previously. It is concluded that the attached group to the fullerene would reduce both electronic couplings beween fullerene/fullerene H_{AA} and between P3HT/fullerne H_{AB}^{CR}. The samller H_{AA} and H_{AB}^{CR} result in the smaller γ and k_{rec}, respectively, and hence lead to the smaller J_{00} for fullerene derivatives with attached groups. The author therefore propose that a large H_{AB}^{CS} and small H_{AB}^{CR} are the key to improving V_{OC} effectively without loss of the charge generation efficiency in addition to large ΔE_{DA}.

4.5. Experimental

Materials: The following chemicals were used without further purification unless noted: P3HT (regioregular, Aldrich, M_n = 87,000 g mol^{-1}), indene (99%, Sigma–Aldrich), C_{60} (99.5%, Frontier Carbon), C_{70} (99%, Aldrich), PCBM (99.9%, Frontier Carbon), bis-PCBM (99.5%, Sigma–Aldrich), $PC_{84}BM$ (99.8%, Solenne), ThCBM (99%, Sigma–Aldrich), lithium fluoride (99.9%, Sigma–Aldrich), tetrabutylammonium tetrafluoroborate (Wako), acetonitrile (98%, Nacalai tesque), chlorobenzene (99%, Nacalai tesque), *o*-dichlorobenzene (99%, Wako), and 1,2,4-trichlorobenzene (>98%, Tokyo Chemical Industry). Ferrocene (98%, Wako) was purified by recrystallization from dichloromethane three times prior to the measurement.

Synthesis of ICBA: Indene-C_{60}-bisadduct (ICBA) was synthesized according to the procedures reported in a previous report.[34] Fullerene C_{60} (0.856 g, 1.19 mmol) and 1,2,4-trichlorobenzene (50 mL) were placed in a recovery flask and stirred over night at room temperature to dissolve the fullerene homogeneously followed by adding indene (2.07 g, 17.8 mmol) to the flask. The solution was heated to 220 °C and refluxed for 12 h. Subsequently, the cooled solution was poured into 400 mL of methanol to reprecipitate the product. The precipitate was dissolved in 5 mL of chloroform and reprecipitated again in methanol. The crude product was purified by silica gel column chromatography twice using 10% chloroform in hexane (first) and 10% toluene in hexane (second) as eluents. Finally, the product was recrystallized twice from hexane/chloroform. Finally, 43 mg of ICBA was obtained as pure product.

^{1}H NMR (CD_2Cl_2, 400 MHz): δ (ppm) (a) 7.8 – 7.2 (m, 8H), (b) 1.26 (s, 4H), (c) 0.882 (t, 4H, J = 6.8 Hz). Peak (c) was coupled with peak (b), which is confirmed by a decoupling measurement (see the Appendix). APCI–MS: calcd for $C_{78}H_{16}$ 953.0; found 953.1.

Device Fabrication: Indium/tin oxide (ITO)-coated glass substrates (10 Ω per square) were washed by ultrasonication in toluene, acetone, and ethanol for 15 min, dried with N_2, and then cleaned with a UV–O_3 cleaner (Nippon Laser & Electronics NL-UV253S) for 30 min. A thin layer (~40 nm) of poly(3,4-ethylenedioxythiophene):poly(4-styrenesulfonate) (PEDOT:PSS; H. C. Starck PH500) was spin-coated onto the cleaned substrates at a spin rate of 3000 rpm, and the layer was dried at 140 °C for 10 min in air. The solution of PEDOT:PSS was filtered using a 0.45 μm PTFE syringe filter prior to the spin coating. A blend layer of P3HT:fullerene (~100 nm except for $PC_{84}BM$, 80 nm for $PC_{84}BM$) was spin-coated from a chlorobenzene (except for C_{60} and C_{70}) or *o*-dichlorobenzene (C_{60} and C_{70}) solution on the PEDOT:PSS film. Finally, Al (70 nm) (except for ICBA) or LiF (0.5 nm)/Al (70 nm) (for ICBA) was thermally deposited on top of the active layer at 2.5×10^{-4} Pa. Note that LiF was used to ensure the Ohmic contact between fullerene and the electrode. Finally, the devices were thermally annealed at 150 °C in an N_2-filled glovebox for 5 min ($PC_{84}BM$), 10 min (ThCBM), 15 min (C_{70}), 30 min (C_{60}, PCBM, bis-PCBM), and 40 min (ICBA), respectively.

Measurements: The electrochemical measurements were performed using a potentiostat/galvanostat (Princeton Applied Research, model 273A) in an Ar-bubbled *o*-dichlorobenzene/acetonitrile = 4 : 1 (v/v) solution containing 0.1 M of tetrabutylammonium hexafluorophosphate as a supporting electrolyte with an Ag/AgCl wire in a saturated KCl solution as a reference electrode and a Pt wire as a counter electrode. The scan rate was set to 50 mV s^{-1}. The ionization potential of P3HT was measured with a photoelectron yield spectrometer (Riken Keiki, AC-3). The P3HT film was fabricated by spin-coating from chlorobenzene onto an ITO substrate washed by the same procedure as mentioned above. The threshold energy for the photoelectron emission was estimated on the basis of the cubic root of the photoelectron yield plotted

against the incident photon energy as reported previously.[65,66] The *J*–*V* characteristics were measured in an N_2 atmosphere with a direct current/voltage and a current source/monitor (Advantest, model R6243) in the dark and under illumination with AM1.5G simulated solar light at 100 mW cm^{-2}. The light intensity was corrected with a calibrated silicon photodiode reference cell (Bunkoh-Keiki, BS-520). The active area of the device was 0.07 cm^2. The temperature dependence of the dark *J*–*V* characteristics was measured in a liquid-N_2-cooled cryostat (Oxford, Optistat DN-V) at a pressure of $<10^{-3}$ Pa. The temperature was monitored by a platinum resistance thermometer and controlled with a temperature controller (Oxford, ITC503) at a stability of <0.1 K.

4.6. Appendix

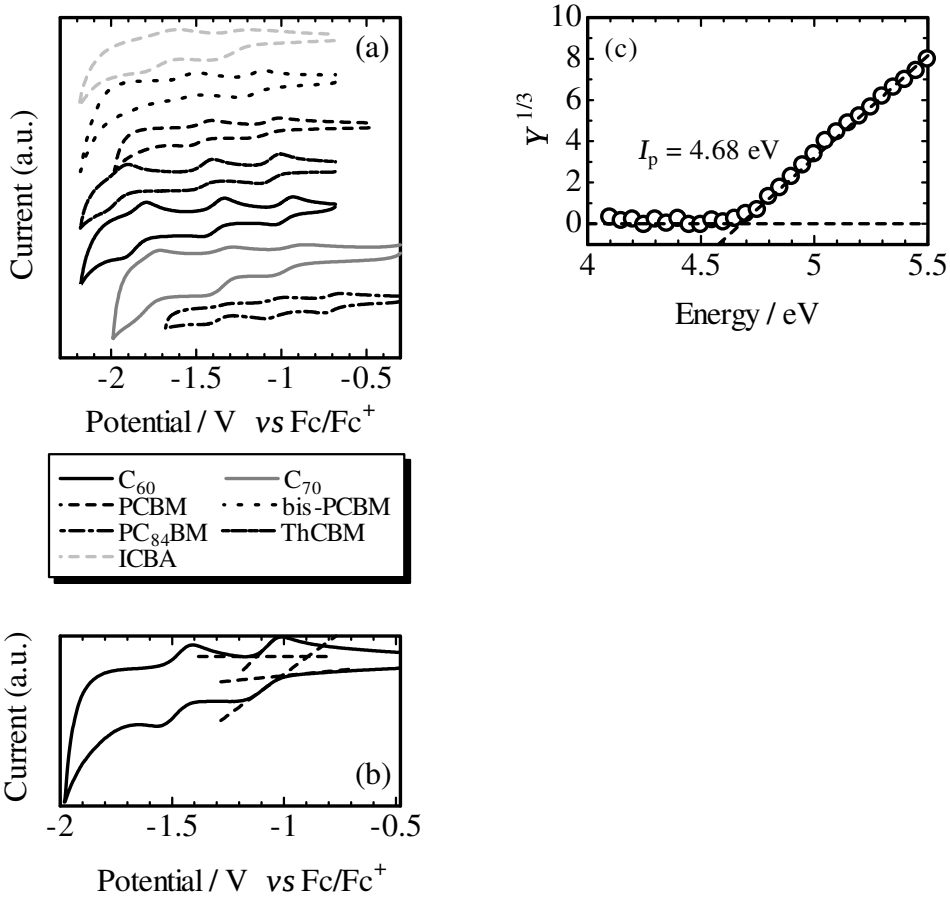

Figure 4-A1. a) Cyclic voltammograms of each fullerene derivative in acetonitrile/*o*-dichlorobenzene = 1 : 4 (v/v) solutions containing 0.1 M of Bu_4NPF_6. The scan rate is 50 mV s^{-1}. b) Estimation procedure of redox potential by voltamogram for PCBM. The LUMO levels were estimated from their first peaks of voltamograms. The potentials were obtained by the average of cut-off position of oxdative and reductive wave, and the LUMO energy were calculated based on the potential of Fc/Fc^+ =4.8 eV *vs* vacuum level[A1-A3]. c) Photoemission yield spectrum of a P3HT pristine film. The cut-off energy was estimated by the threshold of the cubic root of the photoelectron yield.

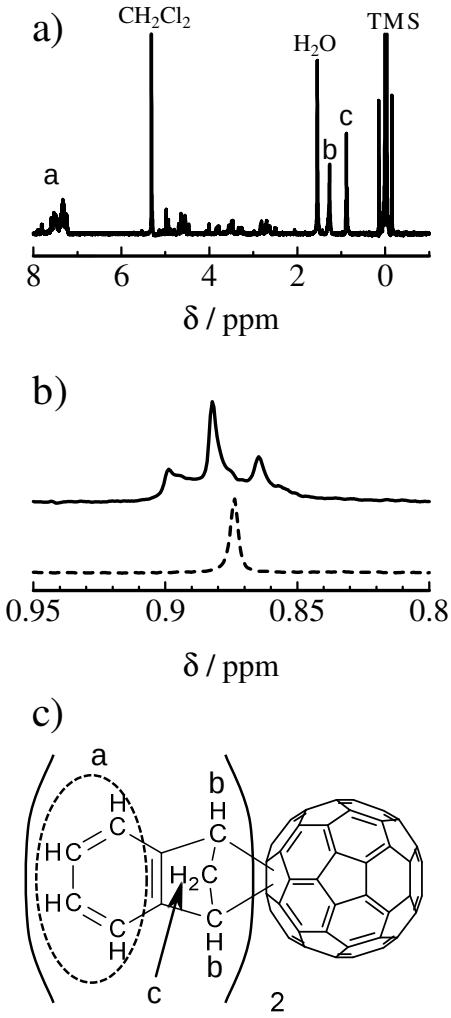

Figure 4-A2. 400 MHz ^{1}H-NMR spectrum of ICBA in CD_2Cl_2 solution. a) The peak signals are observed as follows: a) δ = 7.8 – 7.2 (m, 8H), b) 1.26 (s, 4H), c) 0.882 (t, 4H, *J* = 6.8 Hz). b) The non-decoupled (solid line) and decoupled (broken line) signals at peak-c of ICBA in CD_2Cl_2 solution. The decoupling is performed at 1.26 ppm. c) The assignments of the peaks from a to c observed in ^{1}H-NMR spectra.

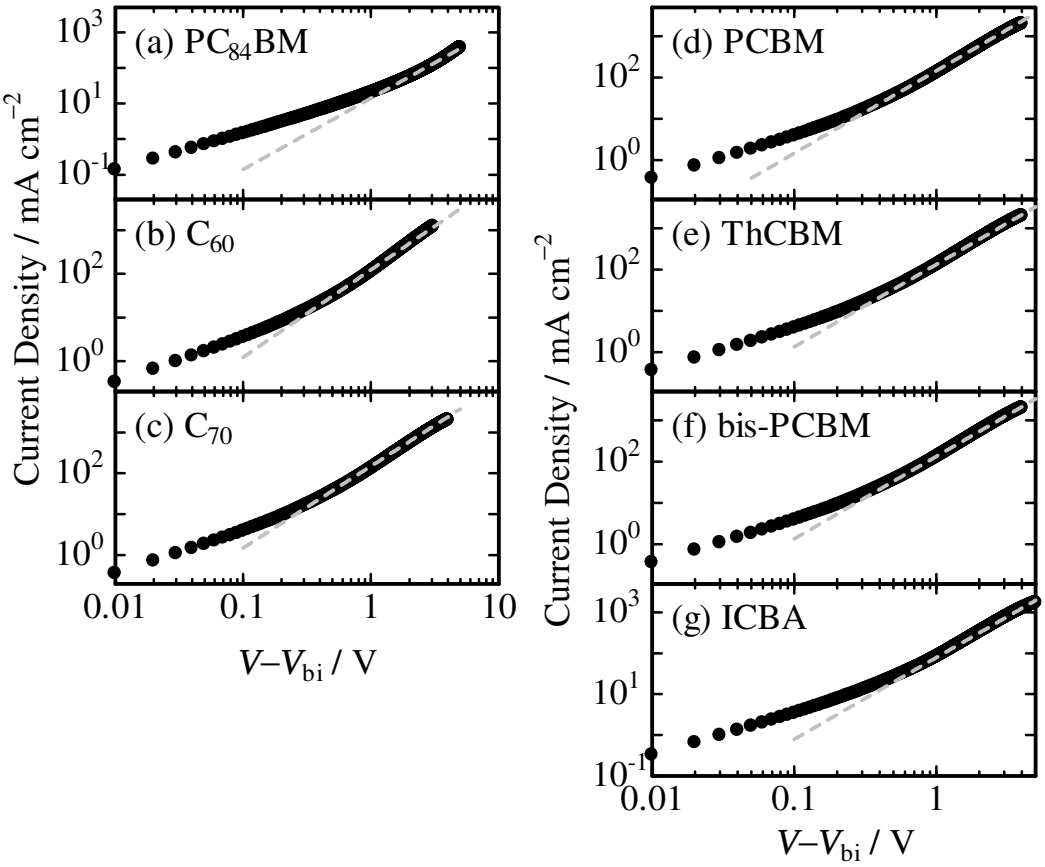

Figure 4-A3. *J–V* characteristics of ITO/PEDOT:PSS/P3HT:fullerene/Au devices. The gray solid lines represent the fitting line by $J = 9/8\ \varepsilon_0\varepsilon_r\mu_h\,(V - V_{bi})^2/d^3$ where ε_0 and ε_r are the permittivity of vacuum and media, μ_h is the hole mobility, V_{bi} is the built-in potential in device, and d is the thickness of the active layer in the device. The built-in potential of these devices is negligible because the work function of Au is almost the same as that of ITO.

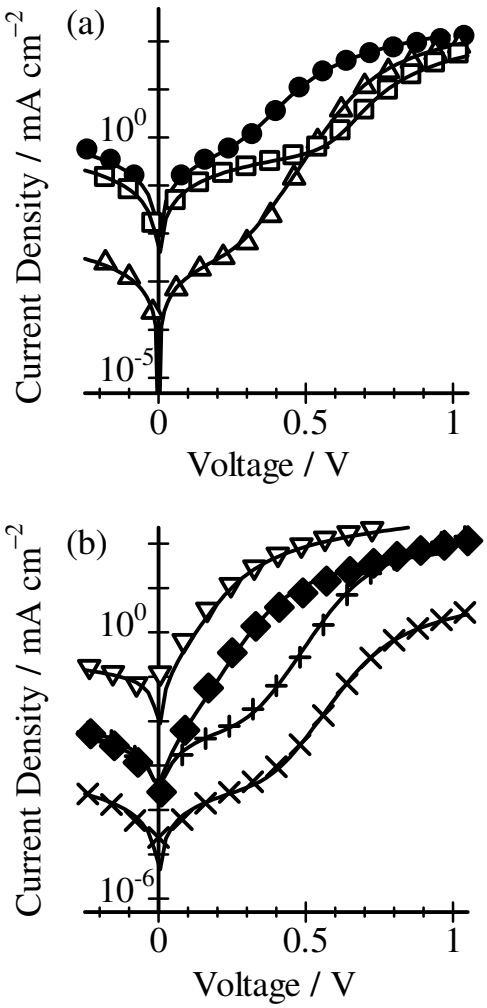

Figure 4-A4. Log plots of the dark current density against applied voltage. The symbols are the same as those in Figure 4-2. The solid lines are fitting curves by Equation 4-3.

4.7. References and Notes

[1] M. A. Green, K. Emery, Y. Hishikawa, W. Warta, *Prog. Photovolt. Res. Appl.* **2011**, *19*, 84–92.

[2] R. F. Service, *Science* **2011**, *332*, 293.

[3] M. M.Wienk, J. M. Kroon, W. J. H. Verhees, J. Knol, J. C. Hummelen, P. A. van Hal, R. A. J.

Janssen, *Angew. Chem. Int. Ed.* **2003**, *42*, 3371–3375.

[4] E. Bundgaard, F. C. Krebs, *Sol. Energy Mater. Sol. Cells* **2007**, *91*, 954–985.

[5] Y. Liang, L. Yu, *Polym. Rev.* **2010**, *50*, 454–473.

[6] J. Peet, J. Y. Kim, N. E. Coates, W. L. Ma, D. Moses, A. J. Heeger, G. C. Bazan, *Nat. Mater.* **2007**, *6*, 497–500.

[7] S. Honda, T. Nogami, H. Ohkita, H. Benten, S. Ito, *ACS Appl. Mater. Interfaces* **2009**, *1*, 804–810.

[8] S. Honda, H. Ohkita, H. Benten, S. Ito, *Chem. Commun.* **2010**, *46*, 6596–6598.

[9] S. Honda, H. Ohkita, H. Benten, S. Ito, *Adv. Energy Mater.* **2011**, *1*, 588–598.

[10] S. Honda, S. Yokoya, H. Ohkita, H. Benten, S. Ito, *J. Phys. Chem. C* **2011**, *115*, 11306–11317.

[11] C. J. Brabec, A. Cravino, D. Meissner, N. S. Sariciftci, T. Fromherz, M. T. Rispens, L. Sanchez, J. C. Hummelen, *Adv. Funct. Mater.* **2001**, *11*, 374–380.

[12] M. C. Scharber, D. Mühlbacher, M. Koppe, P. Denk, C. Waldauf, A. J. Heeger, C. J. Brabec, *Adv. Mater.* **2006**, *18*, 789–794.

[13] D. Veldman, S. C. J. Meskers, R. A. J. Janssen, *Adv. Funct. Mater.* **2009**, *19*, 1939–1948.

[14] K. Vandewal, A. Gadisa, W. D. Oosterbaan, S. Bertho, F. Banishoeib, I. V. Severen, L. Lutsen, T. J. Cleij, D. Vanderzande, J. V. Manca, *Adv. Funct. Mater.* **2008**, *18*, 2064–2070.

[15] H. -Y. Chen, J. Hou, S. Zhang, Y. Liang, G. Yang, Y. Yang, L. Yu, Y. Wu, G. Li, *Nat. Photon.* **2009**, *3*, 649–653.

[16] Y. Liang, Z. Xu, J. Xia, S.-T. Tsai, Y. Wu, G. Li, C. Ray, L. Yu, *Adv. Mater.* **2010**, *22*, E135–E138.

[17] L. J. A. Koster, V. D. Mihailetchi, R. Ramaker, P. W. M. Blom, *Appl. Phys. Lett.* **2005**, *86*, 123509.

[18] L. J. A. Koster, E. C. P. Smits, V. D. Mihailetchi, P. W. M. Blom, *Phys. Rev. B* **2005**, *72*, 085205.

[19] S. R. Cowan, A. Roy, A. J. Heeger, *Phys. Rev. B* **2010**, *81*, 245207.

[20] C. G. Shuttle, B. O'Regan, A. M. Ballantyne, J. Nelson, D. D. C. Bradley, J. R. Durrant, *Phys. Rev. B* **2008**, *78*, 113201.

[21] A. Maurano, R. Hamilton, C. G. Shuttle, A. M. Ballantyne, J. Nelson, B. O'Regan, W. Zhang, I. McCulloch, H. Azimi, M. Morana, C. J. Brabec, J. R. Durrant, *Adv. Mater.* **2010**, *22*, 4987–4992.

[22] M. D. Perez, C. Borek, S. R. Forrest, M. E. Thompson, *J. Am. Chem. Soc.* **2009**, *131*, 9281–9286.

[23] P. Erwin, M. E. Thompson, *Appl. Phys. Lett.* **2011**, *98*, 223305.

[24] W. J. Potscavage, Jr., A. Sharma, B. Kippelen, *Acc. Chem. Res.* **2009**, *42*, 1758–1767.

[25] K. Tvingstedt, K. Vandewal, A. Gadisa, F. Zhang, J. Manca, O. Inganäs, *J. Am. Chem. Soc.* **2009**, *131*,11819–11824.

[26] K. Vandewal, K. Tvingstedt, A. Gadisa, O. Inganäs, J. V. Manca, *Nat. Mater.* **2009**, *8*, 904–909.

[27] K. Vandewal, K. Tvingstedt, A. Gadisa, O. Inganäs, J. V. Manca, *Phys. Rev. B* **2010**, *81*, 125204.

[28] C.-T. Sah, R. N. Noyce, W. Shockley, *Proc. IRE* **1957**, *45*, 1228–1243.

[29] S. M. Sze, *Physics of Semiconductor Devices* 2nd ed., Wiley, New York **1981**.

[30] C. Waldauf, M. C. Scharber, Pavel Schilinsky, J. A. Hauch, C. J. Brabec, *J. Appl. Phys.* **2006**, *99*, 104503.

[31] J. H. Lee, S. Cho, A. Roy, H. –Y. Jung, A. J. Heeger, *Appl. Phys. Lett.* **2010**, *96*, 163303.

[32] T. Kirchartz, B. E. Pieters, J. Kirkpatrick, U. Rau, J. Nelson, *Phys. Rev. B* **2011**, *83*, 115209.

[33] M. Lenes, G.-J. A. H. Wetzelaer, F. B. Kooistra1, S. C. Veenstra, J. C. Hummelen, P. W. M. Blom, *Adv. Mater.* **2008**, *20*, 2116–2119.

[34] M. Lenes, S. W. Shelton, A. B. Sieval, D. F. Kronholm, J. C. (Kees) Hummelen, P. W. M. Blom, *Adv. Funct. Mater.* **2009**, *19*, 3002–3007.

[35] F. B. Kooistra, V. D. Mihailetchi, L. M. Popescu, D. Kronholm, P. W. M. Blom, J. C. Hummelen, *Chem. Mater.* **2006**, *18*, 3068–3073.

[36] L. M. Popescu, P. van't Hof, A. B. Sieval, H. T. Jonkman, J. C. Hummelen, *Appl. Phys. Lett.* **2006**, *89*, 213507.

[37] Y. He, H.-Y. Chen, J. Hou, Y. Li, *J. Am. Chem. Soc.* **2010**, *132*, 1377–1382.

[38] K. Kim, J. Liu, D. L. Carroll, *Appl. Phys. Lett.* **2006**, *88*, 181911.

[39] H. Tang, G. Lu, X. Yang, *IEEE J. Sel. Top. Quant.* **2010**, *16*, 1725–1731.

[37] J. Pommerehne, H. Vestweber, W. Guss, R. F. Mahrt, H. Bässler, M. Porsch, J. Daub, *Adv. Mater.* **1995**, *7*, 551–554.

[38] A. Orimo, K. Masuda, S. Honda, H. Benten, S. Ito, H. Ohkita, H. Tsuji, *Appl. Phys. Lett.* **2010**, *96*, 043305.

[40] S. R. Cowan, W. L. Leong, N. Banerji, G. Dennler, A. J. Heeger, *Adv. Funct. Mater.* **2011**, DOI: 10.1002/adfm.201100514.

[41] J. Guo, H. Ohkita, S. Yokoya, H. Benten, S. Ito, *J. Am. Chem. Soc.* **2010**, *132*, 9631–9637.

[42] Z. Xu, L.-M. Chen, M.-H. Chen, G. Li, Y. Yang, *Appl. Phys. Lett.* **2009**, *95*, 013301.

[43] A. Pivrikas, M. Ullah, Th. B. Singh, C. Simbrunner, G. Matt, H. Sitter, N. S. Sariciftci, *Org. Electron.* **2011**, *12*, 161–168.

[44] S. M. Tuladhar, D. Poplavskyy, S. A. Choulis, J. R. Durrant, D. D. C. Bradley, J. Nelson, *Adv. Funct. Mater.* **2005**, *15*, 1171–1182.

[45] T. D. Anthopoulos, F. B. Kooistra, H. J. Wondergem, D. Kronholm, J. C. Hummelen, D. M. de Leeuw, *Adv. Funct. Mater.* **2006**, *18*, 1679–1684.

[46] A. M. Ballantyne, L. Chen, J. Dane, T. Hammant, F. M. Braun, M. Heeney, W. Duffy, I. McCulloch, D. D. C. Bradley, J. Nelson, *Adv. Funct. Mater.* **2008**, *18*, 2373–2380.

[47] L. J. A. Koster, V. D. Mihailetchi, P. W. M. Blom, *Appl. Phys. Lett.* **2006**, *88*, 052104.

[48] In Ref 47, it has been proposed that the recombination rate in bulk heterojunction devices is limited by the slowest mobility in the blend, and demonstrated that V_{OC} can be well explained by $\gamma_{min} = q \min(\mu_e, \mu_h)/\varepsilon$. As shown in Table 4-1, μ_h of P3HT is as low as ~10^{-4} cm^2 V^{-1} s^{-1} in P3HT:fullerene blend films. This is much smaller than μ_e of pristine fullerenes and fullerene derivatives with attached groups. In other words, the recombination rate in P3HT:fullerene blend films is given by $\gamma_{min} = q\mu_h/\varepsilon$, which is independent of fullerene derivatives, and hence cannot explain the difference in J_{00} at all. In either case, the difference in J_{00} by two orders of magnitude cannot be explained only in terms of the charge mobility.

[49] J. Guo, H. Ohkita, H. Benten, S. Ito, *J. Am. Chem. Soc.* **2010**, *132*, 6154–6164.

[50] C. J. Brabec, G. Zerza, G. Cerullo, S. de Silvestri, S. Luzzati, J. C. Hummelen, S. Sariciftci, *Chem. Phys. Lett.* **2001**, *340*, 232–236.

[51] I. A. Howard, R. Mauer, M. Meister, F. Laquai, *J. Am. Chem. Soc.* **2010**, *132*, 14866–14876.

[52] F. Etzold, I. A. Howard, R. Mauer, M. Meister, T.- D. Kim, K.- S. Lee, N. S. Baek, F. Laquai, *J. Am. Chem. Soc.* **2011**, *133*, 9469–9479.

[53] R. A. Marsh, J. M. Hodgkiss, S. Albert-Seifried, R. H. Friend, *Nano Lett.* **2010**, *10*, 923–930.

[54] R. A. Marcus, *Angew. Chem. Int. Ed.* **1993**, *32*, 1111–1222.

[55] L. B. Schein, A. R. McGhie, *Phys. Rev. B* **1979**, *20*, 1631.

[56] W.-Q. Deng, Q. A. Goddard III, *J. Phys. Chem. B* **2004**, *108*, 8614–8621.

[57] If the recombination rate is limited by the slowest mobility in the blend, the difference in J_{00} should be due to k_{rec} alone because γ is independent of the presence or absence of attached groups to fullerenes. In this case, H_{AB}^2 between P3HT and pristine fullerenes is about 100 times larger than that between P3HT and fullerene derivatives with attached groups.

[58] J. N. Clifford, E. Palomares, M. K. Nazeeruddin, M. Grätzel, J. Nelson, X. Li, N. J. Long, J. R. Durrant, *J. Am. Chem. Soc.* **2004**, *126*, 5225–5233.

[59] D. Kitazawa, N. Watanabe, S. Yamamoto, J. Tsukamoto, *Appl. Phys. Lett.* **2009**, *95*, 053701.

[60] S. H. Park, A. Roy, S. Beaupré, S. Cho, N. Coates, J. S. Moon, D. Moses, M. Laclerc, K. Lee, A. J. Heeger, *Nat. Photon.* **2009**, *3*, 297–303.

[61] T. Liu, A. Troisi, *J. Phys. Chem. C* **2011**, *115*, 2406–2415.

[62] H. Rensmo, S. Lunell, H. Siegbahn, *J. Photochem. Photobiol. A* **1998**, *114*, 117–124.

[63] A. Hagfeldt, M. Grätzel, *Acc. Chem. Res.* **2000**, *33*, 269–277.

[64] Y. Kanai, J. C. Grossman, *Nano Lett.* **2007**, *7*, 1967–1972.

[65] M. Kochi, Y. Harada, T. Hirooka, H. Inokuchi, *Bull. Chem. Soc. Jpn.* **1970**, *43*, 2690.

[66] K. Seki, K. Kanai, *Mol. Cryst. Liq. Cryst.* **2006**, *455*, 145–181.

[A1] J. Pommerehne, H. Vestweber, W. Guss, R. F. Mahrt, H. Bässler, M. Porsch, J. Daub, *Adv. Mater.* **1995**, *7*, 551–554.

[A2] Y. Yang, F. Arias, L. Echegoyen, L. P. F. Chibante, S. Flanagan, A. Robertson, L. J. Wilson, *J. Am. Chem. Soc.* **1995**, *117*, 7801–7804.

[A3] V. H.-M. Koepp, H. Wendt, H. Strehlow, *Z. Electrochem.* **1960**, *64*, 483–491.

Chapter 5

Charge Dissociation and Recombination through Interfacial Charge Transfer State in Low-Bandgap Polymer Solar Cells

5.1. Introduction

Currently, power conversion efficiency (PCE) of polymer/fullerene solar cells is approaching to 10%.[1,2] One of the key materials to the remarkable progress is low-bandgap polymers, which can absorb more photons in the near-IR region than conventional conjugated polymers such as regioregular poly(3-hexylthiophene) (RR-P3HT) and therefore can increase the short-circuit current density (J_{SC}) effectively. Most of low-bandgap polymers have electron donor and acceptor units arranged alternatively in the main chain. The donor/acceptor linkage induces an intramolecular donor–acceptor interaction resulting in the reduction of the bandgap energy. Poly[2,6-(4,4-bis-(2-ethylhexyl)-4*H*-cyclopenta[2,1-b;3,4-b']dithiophene)-*alt*-4,7-(2,1,3-benzothiadiazole)] (PCPDTBT) is a typical low-bandgap polymer, which consists of the cyclopentadithiophene donor unit and the benzothiadiazole acceptor unit in the main chain as shown in Figure 5-1a. Because of the donor–acceptor interaction, this polymer has a red-shifted absorption up to ~800 nm. The PCPDTBT-based polymer solar cell was firstly reported in 2006,[3] and exhibited the improved PCE in excess of 5% by using an additive with high boiling point.[4] In particular, J_{SC} exceeds 15 mA cm^{-2}, which cannot be obtained by conventional polymers studied so far. However, this is still far below a maximum J_{SC} of 23.8 mA cm^{-2} for the 100% light harvesting up to 800 nm.[5] This is because external quantum efficiency (EQE) is as low as 50% for the PCPDTBT-based

polymer solar cell.[3,4,6–8] In other words, the potential PCE would exceed 8% if EQE could be improved up to 80% as is the case for RR-P3HT/PCBM solar cells. For further improvement in the device performance, the origin of low EQE should be understood.

Herein the author studies the charge generation and recombination dynamics in PCPDTBT/PCBM blend films by transient absorption spectroscopy. On a time scale of picoseconds, transient absorption of PCPDTBT singlet exciton and polaron are observed to discuss the charge generation dynamics in PCPDTBT/PCBM blends. Subsequently, the geminate recombination dynamics is observed on a time scale of sub-nanoseconds to discuss the charge dissociation mechanism. On a time scale of nano- to microseconds, the bimolecular recombination of PCPDTBT dissociated polarons is observed to evaluate the charge carrier lifetime in PCPDTBT/PCBM blends. In comparison with RR-P3HT/PCBM solar cells, the origin of the limited EQE of PCPDTBT/PCBM solar cells is discussed in terms of the charge dissociation and recombination mechanism in PCPDTBT/PCBM blends.

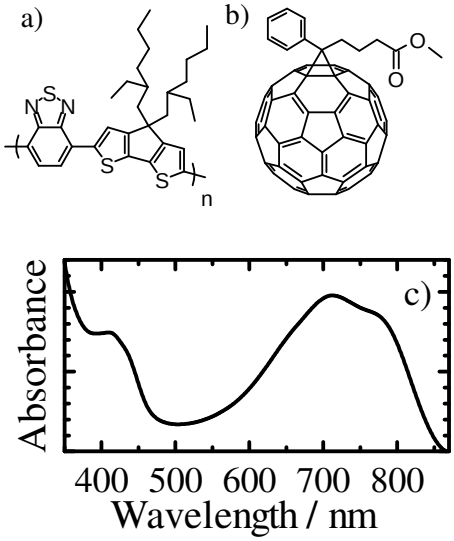

Figure 5-1. Chemical structures of materials employed in this study: a) PCPDTBT and b) PCBM. c) Absorption spectra of PCPDTBT/PCBM blend films (50:50 w/w) fabricated with DIO.

5.2. Results

Figure 5-1c shows the absorption spectra of PCPDTBT/PCBM (50 : 50 w/w) blend films fabricated with 1,8-diiodooctane (DIO) as additive. A large absorption band observed at around 700 nm is ascribed to the intramolecular donor–acceptor interaction band as reported previously.[9,10] In addition, an absorption shoulder observed at around 800 nm is ascribed to the ordering of PCPDTBT as reported previously.[4,11,12] On the other hand, no fluorescence was observed for the blend films. In other words, the exciton quenching efficiency is almost 100% for PCPDTBT/PCBM blend films.

Figures 5-2a shows the transient absorption spectra of PCPDTBT neat films at 0 ps after the laser excitation at 800 nm under various excitation intensities. At low excitation intensities, the absorption peak was found at around 1500 nm. This absorption band is ascribed to PCPDTBT singlet exciton because the decay constant is consistent with the fluorescence lifetime. At high excitation intensities, an additional absorption shoulder was observed at around 1200–1300 nm. This absorption is ascribed to PCPDTBT polaron as described below. Figure 5-2b shows the initial absorbance of PCPDTBT singlet exciton and polaron under various excitation intensities. Below a fluence of 16 μJ cm^{-2}, the slope for the initial absorbance of PCPDTBT singlet exciton was unity, suggesting that bimolecular processes are negligible. Above the fluence of 16 μJ cm^{-2}, the slope reduced to 0.5, suggesting bimolecular quenching of PCPDTBT singlet exciton. On the other hand, the slope for the initial absorbance of PCPDTBT polaron was 2 above the fluence of 16 μJ cm^{-2}, suggesting that polarons are generated via a bimolecular reaction. Thus, it is concluded that PCPDTBT polarons are generated at 0 ps via the singlet–singlet exciton annihilation without exciton diffusion (or two-photon absorption). From the threshold intensity of 16 μJ cm^{-2} (= 1.6×10^{18} cm^{-3}), the interaction radius of PCPDTBT singlet exciton is estimated to be r_{ex} = 4.2 nm at 0 ps after the excitation at 800 nm.

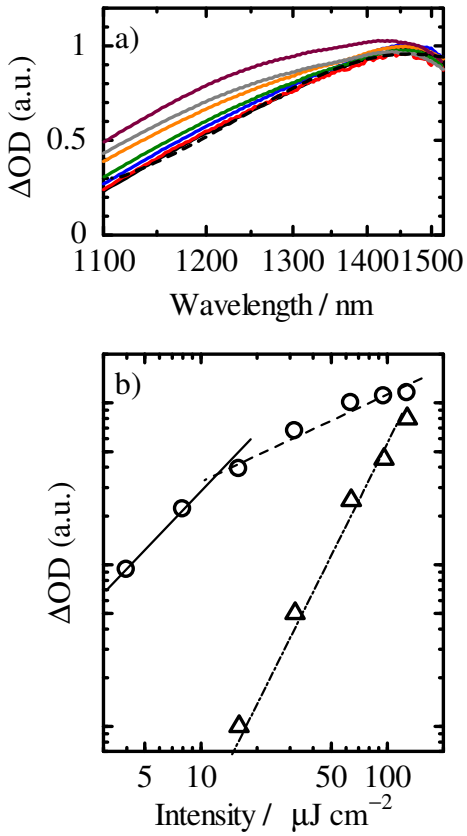

Figure 5-2. a) Transient absorption spectra of a PCPDTBT neat film at 0 ps after the laser excitation at 800 nm with fluences of 4, 8, 16, 32, 64, 96, 128 μJ cm^{-2} from bottom to top in the panel. The broken line shows a fitting line by a Gaussian function for the spectrum at 4 μJ cm^{-2} b) Log–log plots of the initial transient signals of a PCPDTBT neat film of PCPDTBT singlet (open circles) and PCPDTBT polaron (open triangles). The solid, broken, and dashed–dotted lines show the slope of 1, 0.5, and 2, respectively.

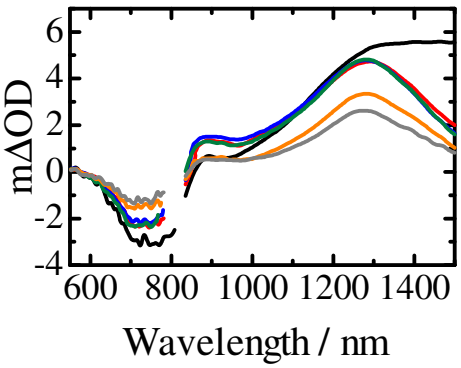

Figure 5-3. Transient absorption spectra of a PCPDTBT/PCBM blend film fabricated with DIO at 0 (black), 2 (red), 10 (blue), 100 (green), 1000 (orange), and 3000 ps (gray) after the laser excitation at 800 nm with a fluence of 4 μJ cm^{-2}.

Figures 5-3 shows the transient absorption spectra of a PCPDTBT/PCBM blend film from 0 to 3 ns after the laser excitation at 800 nm. As shown in Figure 5-3, a broad absorption up to 1500 nm was observed immediately after the laser excitation, the absorption at around 1500 nm disappeared rapidly, and instead the absorption band at around 1300 nm was pronounced in a few picoseconds, and then the absorption band at 1300 nm decayed in a few nanoseconds. The absorption band at 1500 nm is ascribed to PCPDTBT singlet exciton as mentioned above. The absorption band at 1300 nm is ascribed to PCPDTBT polarons because it was still observed on a time scale of microseconds (see the Appendix). In summary, PCPDTBT singlet excitons rapidly disappear and instead PCPDTBT polarons are rapidly generated in a few picoseconds. This is consistent with the efficient fluorescence quenching.

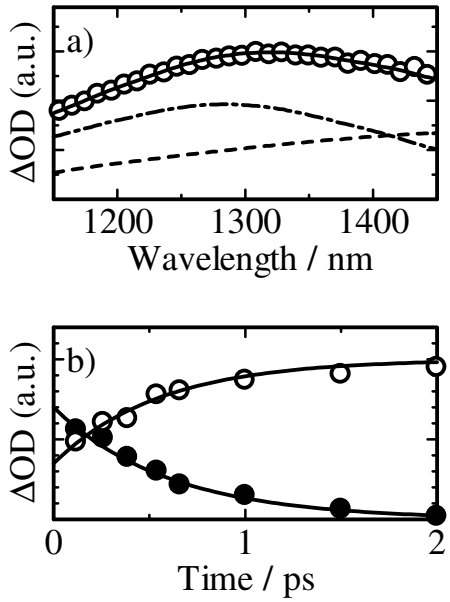

Figure 5-4. a) Transient absorption spectrum at 0.2 ps of the PCPDTBT/PCBM blend film fabricated with DIO (open circles). The solid line shows the spectrum simulated by the sum of the absorption spectra of PCPDTBT singlet exciton (broken line) and PCPDTBT polaron (dashed–dotted line). b) The time evolution of PCPDTBT singlet exciton (closed circles) and PCPDTBT polaron (open circles) in the PCPDTBT/PCBM blend film. The solid lines show the fitting lines by exponential functions: A $\exp(-t/\tau_d)$ for the decay and A$[1 - \exp(-t/\tau_r)]$ + B for the rise kinetics with $\tau_d = \tau_r = 0.6$ ps and A : B = 65 : 35.

To analyze the charge generation dynamics in details, the author resolved the transient absorption spectra into PCPDTBT singlet exciton and polaron by spectral simulation as shown in Figure 5-4a. The absorption spectrum at 0 ps of the PCPDTBT neat film can be used as that of PCPDTBT singlet exciton. The absorption spectrum at 2 ps of the PCPDTBT/PCBM blend film can be used as that of PCPDTBT polaron because the spectral change is finished before 2 ps. As a result, the time evolution of PCPDTBT

singlet exciton and polaron generated in PCPDTBT/PCBM blend films excited at 800 nm were obtained. As shown in Figure 5-4b, PCPDTBT singlet exciton decayed and PCPDTBT polaron was generated with the same time constant. This suggests that PCPDTBT polaron is directly generated from PCPDTBT singlet exciton. The charge generation time constant is evaluated to be 0.6 ps for the PCPDTBT/PCBM blend. Furthermore, 35% of PCPDTBT polarons were promptly generated within the laser pulse width (~0.1 ps).

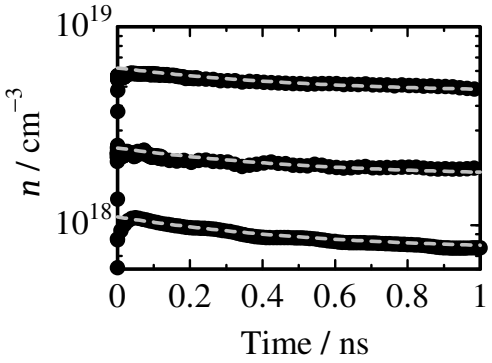

Figure 5-5. Transient decay at 1240 nm of PCPDTBT polaron in PCPDTBT/PCBM blend film excited at 800 nm with fluences of 1, 5, and 10 μJ cm^{-2}. The gray broken lines show the fitting curve by an exponential function: A exp($-t/\tau_m$) + B with τ_m = 480 ps and A : B = 30 : 70.

Figure 5-5 shows the transient decay of PCPDTBT polaron monitored at 1240 nm from 0 to 1 ns after the laser excitation at 800 nm under various excitation conditions. The charge carrier density was evaluated from the molar absorption coefficient of PCPDTBT polaron (ε = 40000 M^{-1} cm^{-1} at 1240 nm) previously reported.[13] The decay dynamics is independent of the excitation intensity and can be well fitted by a single exponential function with a constant fraction: ΔOD = A exp($-t/\tau_m$) + B. It is noted that

the photobleaching at 750 nm recovered with the same time constant. Therefore, the decay dynamics is monomolecular recombination to the ground state. From the fitting, the decay constant and the constant fraction are evaluated to be τ_m = 480 ps and 70%, respectively.

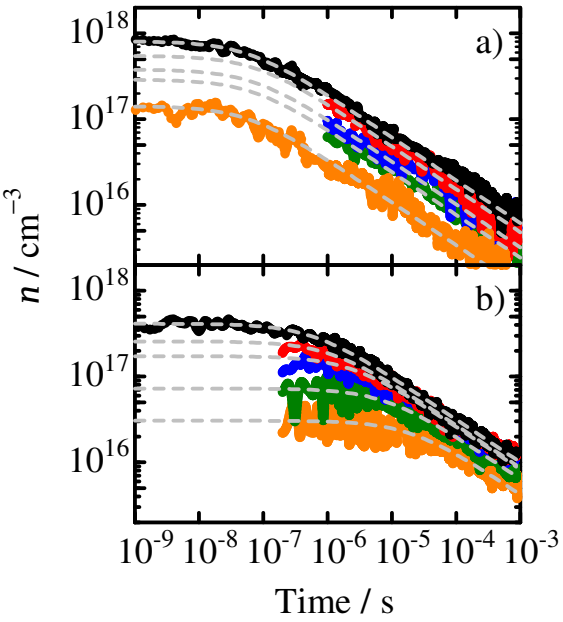

Figure 5-6. Transient decay of polymer polarons with fluences of 1, 2, 5, 10 and 20 μJ cm^{-2} from bottom to top: a) PCPDTBT polaron (1240 nm) in PCPDTBT/PCBM blends excited at 800 nm and b) P3HT polaron (1000 nm) in RR-P3HT/PCBM blends excited at 400 nm. The gray broken lines show the fitting curves by a power-law function: $n(t) = n_0(1 + at)^{-\alpha}$ with $\alpha = 0.5$.

Figure 5-6 shows the transient decay of PCPDTBT polaron monitored at 1240 nm from 1 ns to 1 ms after the laser excitation at 800 nm under various excitation conditions. The charge carrier density was estimated as described in the Appendix. For comparison,

the transient decay of P3HT polaron monitored at 1000 nm in RR-P3HT/PCBM is also shown in Figure 5-6b. In contrast to Figure 5-5, the decay dynamics is dependent on the excitation intensity, suggesting that bimolecular recombination is the dominant decay pathway. All the decay dynamics can be well fitted by an empirical power-law equation

$$n(t) = n_0(1 + at)^{-\alpha} \quad (5\text{-}1)$$

where $n(t)$ is the carrier density at a delay time t, n_0 is the carrier density at $t = 0$, and α and a are parameters. The exponent α represents the slope of the decay in the log–log plots. The inverse of the parameter a is indicative of the time for the carrier density to start decreasing. As shown in the figure, the exponent is constant $\alpha = 0.5$ for PCPDTBT/PCBM and RR-P3HT/PCBM, which is independent of the excitation intensity. The power-law kinetics with $\alpha < 1$ is characteristic of trap-limited bimolecular recombination.[14] On the other hand, the parameter a of PCPDTBT/PCBM is almost independent of the excitation intensity while the parameter a of RR-P3HT/PCBM decreases with increasing excitation intensity. The charge lifetime will be discussed later on the basis of the parameter a.

5.3. Discussion

First, the author focuses on the charge generation dynamics in PCPDTBT/PCBM blends. As mentioned before, PCPDTBT polarons are rapidly generated in a picosecond. This is much faster than that observed for RR-P3HT/PCBM crystalline blends, but similar to that observed for RRa-P3HT/PCBM amorphous blends.[15] More precisely, the charge generation time is slightly slower in PCPDTBT/PCBM (0.6 ps) than RRa-P3HT/PCBM blends (0.2 ps). As reported previously,[4,16–18] PCPDTBT/PCBM blends are not crystalline but rather amorphous films. In such amorphous blend films, PCBM molecules are likely to be homogeneously dispersed, and therefore polymer singlet excitons should be

quenched promptly by neighboring PCBM molecules without exciton diffusion. Indeed, the exciton diffusion is typically negligible in a picosecond. However, if PCBM molecules were completely dispersed homogeneously in amorphous films, the charge generation dynamics would be the same. Thus, the slight difference in the charge generation time suggests that PCBM molecules still form phase separation though they are likely to be homogeneously dispersed in amorphous films. As reported previously, the additive can selectively extract PCBM from PCPDTBT/PCBM blends and is therefore considered to induce PCBM aggregation in the blend.[19] Such aggregation would reduce the effective concentration of PCBM in the blend, which cause the larger separation distance between polymer singlet exciton and PCBM resulting in the slightly slower charge generation. Indeed, the author found larger phase separation for blend films fabricated with DIO as reported previously.[13] Alternatively, it is noted that PCPDTBT singlet exciton (1.67 eV) is more stable than RRa-P3HT singlet exciton (2.34 eV) because of the lower bandgap as shown in Figure 5-1c. In other words, the driving force for the charge separation is smaller in PCPDTBT/PCBM than in RRa-P3HT/PCBM blends. This would have impact on the charge generation dynamics. In any case, the charge generation is much more rapid than the lifetime of the singlet exciton. It can be safely concluded that the exciton diffusion efficiency η_{ED} to and the charge transfer efficiency η_{CT} at a donor/acceptor interface are 100% in PCPDTBT/PCBM blend films. This is the same as those for RRa-P3HT/PCBM amorphous blends but larger than those for RR-P3HT/PCBM crystalline blends.

Next, the author moves onto the monomolecular recombination dynamics on a time scale of sub-nanoseconds. As mentioned before, the decay dynamics of PCPDTBT polaron is in good agreement with the recovery dynamics of the photobleaching and independent of the excitation intensity, suggesting the geminate recombination to the

ground state. Furthermore, this decay constant τ_m = 480 ps is in good agreement with the lifetime of the CT state emission at 1100 nm observed for PCPDTBT/PCBM blend films (480 ps).[20] Therefore the author ascribe the polaron band at around 1250 nm to the CT state at the heterojunction, which is coulombically bound pair of PCPDTBT polaron and PCBM radical anion. From the fitting parameters, the charge dissociation efficiency η_{CD} is estimated to be 70% and the charge dissociation and recombination rates are estimated to be $k_{dis} = 1 \times 10^9$ s^{-1} and $k_{rec} = 6 \times 10^8$ s^{-1}, respectively. This charge dissociation efficiency (η_{CD} = 70%) is larger than that for RRa-P3HT/PCBM (31%) but lower than that for P3HT/PCBM blend films (91%). The difference in η_{CD} is primarily due to the different phase separation. In addition, as reported previously, the singlet exciton size would have impact on the charge dissociation.[21] As mention above, the interaction radius of PCPDTBT singlet exciton is r_{ex} = 4.2 nm. This is larger than that of RRa-P3HT singlet exciton (r_{ex} = 3.2 nm) and smaller than that of RR-P3HT singlet exciton (r_{ex} = 4.3–6.7 nm). In a recent paper, Durrant *et al.* pointed out that the effective Coulomb capture radius would be reduced to ~4 nm at a typical donor/acceptor heterojunction by considering the change in entropy associated with changing from a single exciton to two separated charges.[22] This is consistent with the estimations of the interaction radius of singlet excitons. The author therefore proposes that the larger singlet exciton is likely to provide the larger η_{CD}.

Finally the author discusses the bimolecular recombination dynamics on a time scale of nano- to microseconds. As described above, all the decay dynamics on a time scale of this regime can be well fitted by eq 5-1 with α = 0.5, which is indicative of trap-limited bimolecular recombination. In the bimolecular charge recombination, the charge carrier density $n(t)$ is given by

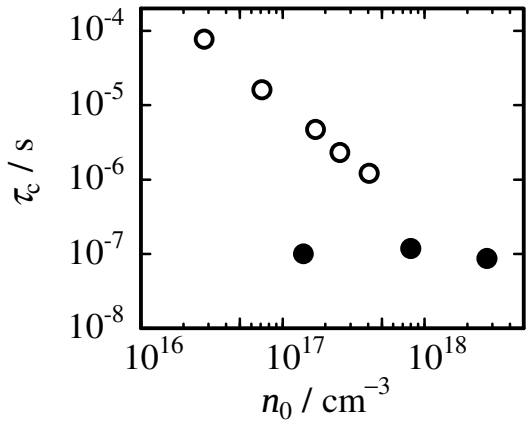

Figure 5-7. Charge carrier lifetime τ_c defined by Equation 5-4 plotted against the initial charge carrier density n_0: PCPDTBT polaron in PCPDTBT/PCBM blends (closed circles) and P3HT polaron in RR-P3HT/PCBM blend films (open circles).

$$dn(t)/dt = -\gamma(t)n^2(t) \tag{5-2}$$

where $\gamma(t)$ is the bimolecular recombination rate at a delay time t. By inserting Equation 5-1 into Equation 5-2, the time-dependent bimolecular recombination rate can be obtained:

$$\gamma(t) = a\alpha n_0^{-1}(1 + at)^{(\alpha-1)} \tag{5-3}$$

Here, the charge carrier lifetime τ_c is defined by

$$\tau_c = [\gamma(0)\, n_0]^{-1} = (a\alpha)^{-1} \tag{5-4}$$

As shown in Figure 5-7, the charge carrier lifetime τ_c is of the order of ~10^{-7} s for PCPDTBT/PCBM blends. On the other hand, the charge collection time at the short circuit can be roughly estimated to be $t_{CC}^{SC} = 2 \times 10^{-7}$ s as a transit time $dd_C/(V\mu)$ where d is the thickness of the active layer (100 nm), d_C is the average collection length (= $d/2$), V is the internal bias (0.6 V), and μ is the charge mobility (4×10^{-4} cm^2 V^{-1} s^{-1}). The charge collection time at the open circuit can be roughly estimated to be $t_{CC}^{OC} = 1 \times 10^{-6}$ s as a diffusion time $d_C^2/(2D) = qd^2/(8k_BT\mu)$ where D is the diffusion constant of charge

Scheme 5-1. Kinetic scheme for the bimolecular recombination via the CT state.

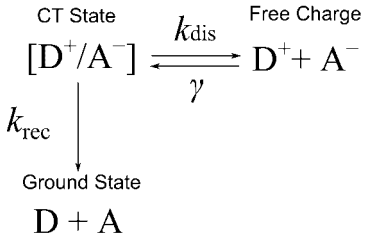

γ_L: the Langevin recombination rate, k_{rec}: the geminate recombination rate of the CT state, k_{dis}: the charge dissociation rate into free carriers from the CT state

carriers (= $k_B T\mu/q$), k_B is the Boltzmann constant, T is temperature, and q is the elementary charge. Thus, the charge carrier lifetime τ_C in PCPDTBT/PCBM blends is comparable to t_{CC}^{SC} but shorter than t_{CC}^{OC}. This is different from that in RR-P3HT/PCBM blends where τ_c is as long as ~10^{-5} – 10^{-4} s even under the open-circuit condition ($n \approx 10^{16}$ – 10^{17} cm^{-3}). Such long lifetime of charge carriers is ascribed to the reduced bimolecular recombination in RR-P3HT/PCBM blends. As reported in many studies, the bimolecular recombination rate in RR-P3HT/PCBM blends is at least two orders magnitude slower than the Langevin recombination rate γ_L.[23,24,25] The author recently proposed that the reduced bimolecular recombination is due to the non-diffusion-limited recombination. In the case of the non-diffusion-limited recombination, the recombination kinetics can be summarized as shown in Scheme 5-1. Under the steady state condition, the apparent recombination rate is given by $k_{rec}/(k_{rec} + k_{dis})\gamma_L$ (see the Appendix). For RR-P3HT/PCBM blends, as reported previously, the apparent recombination rate is reduced by at least more than two orders of magnitude compared to γ_L because k_{dis} is much larger than k_{rec}.[26–29] On the other hand, k_{dis} is comparable to k_{rec} for PCPDTBT/PCBM blends as described above. As a result, the apparent recombination rate would be reduced only by a factor of 1/3. Indeed, the bimolecular recombination rate in PCPDTBT/PCBM blends is evaluated by Equation 5-3 at $n \approx 10^{16}$ – 10^{17} cm^{-3} to be of the order of ~10^{-10} cm^3 s^{-1}, which is comparable to the

Langevin recombination rate $\gamma_L = 8 \times 10^{-10}$ cm^3 s^{-1}. It is therefore concluded that the charge collection is one of the limiting factors to the device performance of PCPDTBT/PCBM solar cells because of the faster bimolecular recombination.

5.4. Conclusions

The charge generation and recombination dynamics in PCPDTBT/PCBM blend films were studied by transient absorption spectroscopy. In PCPDTBT neat films, only PCPDTBT singlet exciton is generated under low excitation conditions, but PCPDTBT polaron is additionally generated under high excitation conditions because of the singlet–singlet exciton annihilation. The interaction radius of PCPDTBT singlet exciton is estimated to be r_{ex} = 4.2 nm. In PCPDTBT/PCBM blend films, PCPDTBT polaron is promptly generated from PCPDTBT singlet exciton in a picosecond. In other words, the efficiency of the exciton diffusion to a donor/acceptor interface η_{ED} and the charge transfer at the interface η_{CT} is 100%. This is because PCBM molecules are likely to be homogeneously dispersed in amorphous blend films. Such 100% efficiency in η_{ED} and η_{CT} is found in other amorphous polymer blends such as RRa-P3HT/PCBM and N-P7/PCBM. On a time scale of nanoseconds, 70% of PCPDTBT polarons are dissociated into free charge carriers and the rest of them recombine geminately to the ground state. The dissociation efficiency η_{CD} = 70% is higher than that of RRa-P3HT/PCBM but lower than that of RR-P3HT/PCBM. The difference is partly due to the difference in the blend morphology. Alternatively, the author proposes that the larger singlet exciton would cause the larger η_{CD} in polymer/PCBM blends: the dissociation efficiency and the interaction radius of singlet excitons are η_{CD} = 30% and r_{ex} = 3.2 nm for RRa-P3HT, 70% and 4.2 nm for PCPDTBT, and >90% and 4.3–6.7 nm for RR-P3HT. Subsequently, PCPDTBT dissociated polarons recombine bimolecularly with

the power-law kinetics from a time scale of tens nanoseconds, while P3HT polarons decay bimolecularly from a time scale of microseconds. Thus, the charge carrier lifetime in PCPDTBT/PCBM blends is estimated to be as short as ~10^{-7} s, which is comparable to the charge collection time at the short circuit but shorter than the charge collection time at the open circuit. Such short lifetime of PCPDTBT dissociated polarons would cause lower charge collection efficiency especially as the applied voltage is approaching to V_{OC}. It is therefore concluded that the limited EQE of PCPDTBT/PCBM solar cells are ascribed mainly to the lower charge dissociation and the shorter charge lifetime. In contrast, the long lifetime of P3HT dissociated polarons is due to the reduced bimolecular recombination. Such slow bimolecular recombination results from non-diffusion-limited recombination due to the high dissociation efficiency in RR-P3HT/PCBM. In other words, the high dissociation efficiency would be the origin of the reduced bimolecular recombination in RR-P3HT/PCBM. On the other hand, the faster recombination in PCPDTBT/PCBM results from the low dissociation efficiency, which is due to the formation of the CT state at the interface because the dissociation from the CT state is limited by the competitive geminate recombination. Such interfacial CT state would be formed from the smaller singlet exciton because of the larger Coulomb interaction. It is therefore concluded that the larger singlet exciton is the key to the higher dissociation efficiency and the reduced recombination, which are essential for highly efficient polymer solar cells.

5.5. Experimental

Materials: The following chemicals were used without further purification: PCBM (99.9%, Frontier Carbon), 1,8-diodooctane (Wako), and chlorobenzene (Wako). The low-bandgap polymer PCPDTBT was synthesized as described elsewhere.[13]

Sample Fabrication: Polymer/fullerene blend films were prepared on glass substrates by spin-coating from a chlorobenzene solution of polymers and PCBM with 2 vol% of 1,8-diiodooctane at a spin rate of 1000 rpm after the spin rate of 400 rpm (10 s) under ambient conditions. The film thickness was typically 300 nm. The weight fraction of PCBM was set at 50 wt%. The blend solution was stirred at 40 °C overnight to be dissolved homogeneously. Before the spin-coating, the glass substrates were cleaned by ultrasonic treatment in toluene, acetone, and ethanol sequentially for 15 min each, and then with a UV–ozone cleaner (Nippon Laser & Electronics Lab., UV253) for 1 h.

Measurements: Transient absorption data were collected in a nitrogen-purged quartz cuvette with three different spectrometers as described below. The femtosecond transient absorption data were collected with a pump and probe transient absorption spectroscopy system (Ultrafast Systems, Helios). The pump light was second harmonic pulses (400 or 800 nm, fwhm 100 fs, 1 kHz) from a regeneratively amplified Ti-sapphire laser (Spectra-Physics, Hurricane). The probe beam was detected with a CMOS linear sensor (Ultrafast Systems, SPEC-VIS) for the visible wavelength range from 400 to 900 nm and with an InGaAs linear diode array sensor (Ultrafast Systems, SPEC-NIR) for the near-IR wavelength range from 850 to 1600 nm. The typical noise level of this system is lower than 2×10^{-4}. The nanosecond transient absorption data were collected with a pump and probe transient absorption spectroscopy system (Ultrafast Systems, EOS). The excitation source was the same as that employed in the femtosecond system. The continuum probe pulse (380 to 1700 nm, 0.5 ns pulse width, 20 kHz repetition rate) was generated by focusing a Nd:YAG laser pulse into a photonic crystal fiber. The probe pulses were synchronized with the femtosecond amplifier, and the delay time was controlled by a digital delay generator electrically (CNT-90, Pendulum Instruments). For the microsecond transient absorption measurement, the sample was excited with a light pulse

(400 nm, 4 Hz) from a dye laser (Photon Technology International, GL-301) that was pumped with a nitrogen laser (Photon Technology International, GL-3300), and probed with a monochromatic light from a 50-W quartz tungsten halogen lamp (Thermo–ORIEL, Model 66997) with a light intensity controller (Thermo–ORIEL, Model 66950), which was equipped with appropriate optical cut-filters and two monochromators (Ritsu, MC-10N) before and after the sample to reduce stray light, scattered light, and emission from the sample. The probe light was detected with a pre-amplified Si photodiode (Costronics Electronics) for the visible wavelength range from 700 to 1100 nm, and pre-amplified InGaAs photodiode (Newport 1811s) for the near-infrared wavelength range from 900 to 1500 nm. The detected signal was sent to the main amplification system with an electronic band-pass filter (Costronics Electronics) to improve the signal-too-noise ratio. The amplified signal was collected with a 200-MHz digital oscilloscope (Tektronix, TDS2022), which was synchronized with a trigger signal of the laser pulse from a photodiode (Thorlabs, DET10A). The detectable absorbance change ΔOD is as small as ~10^{-5} – 10^{-6} depending on the measuring time domain.

5.6. Appendix

5.6.1. Hole Carrier Density on a Time Scale of Microseconds

The density of all hole charge carriers is estimated by eq. 5-A1.

$$n(t) = \Delta OD(t)\, N_A\, (1000\, \varepsilon(t)\, l\,)^{-1} \qquad (5\text{-A1})$$

where $\Delta OD(t)$ is the transient absorption signal measured at a delay time t, N_A is the Avogadro's constant (6.02×10^{23} mol^{-1}), $\varepsilon(t)$ is the molar absorption coefficient of hole carriers, and l is the thickness of blend films. As reported previously, there is hole injection from PCPDTBT to PCBM domains on a time scale of microseconds: the hole injection time constant is τ_{inj} = 2 μs and the equilibrium fraction is $PCPDTBT^+$: $PCBM^+$ =

70 : 30. Therefore, the charge carrier density is estimated on time-dependent molar absorption coefficients $\varepsilon(t)$ defined as follows:

$$\varepsilon(t) = \varepsilon_{\mathrm{PCPDTBT}^+} \exp(-t/\tau_{\mathrm{inj}}) \tag{5-A2}$$

where $\varepsilon_{\mathrm{PCPDTBT}^+}$ is the molar absorption coefficient of PCPDTBT polaron ($\varepsilon_{\mathrm{PCPDTBT}^+}$ = 40000 $\mathrm{M^{-1}\ cm^{-1}}$).

5.6.2. Non-Diffusion-Limited Bimolecular Recombination

The apparent bimolecular recombination rate constant under steady state is derived as follows. The concentration of free charge n_{free} and CT state n_{CT} are given by

$$\frac{\mathrm{d}n_{\mathrm{free}}}{\mathrm{d}t} = -\gamma_{\mathrm{L}} n_{\mathrm{free}}^2 + k_{\mathrm{dis}} n_{\mathrm{CT}} \tag{5-A3}$$

$$\frac{\mathrm{d}n_{\mathrm{CT}}}{\mathrm{d}t} = \gamma n_{\mathrm{free}}^2 - (k_{\mathrm{dis}} + k_{\mathrm{rec}}) n_{\mathrm{CT}} \tag{5-A4}$$

Under steady-state approximation, $\mathrm{d}n_{\mathrm{CT}}/\mathrm{d}t = 0$ can be assumed and hence obtain

$$\frac{\mathrm{d}n_{\mathrm{free}}}{\mathrm{d}t} = -\frac{k_{\mathrm{rec}}}{k_{\mathrm{dis}} + k_{\mathrm{rec}}} \gamma_{\mathrm{L}} n_{\mathrm{free}}^2 \tag{5-A5}$$

Therefore, the apparent bimolecular recombination constant is reduced by $k_{\mathrm{rec}}/(k_{\mathrm{rec}} + k_{\mathrm{dis}})$ compared to the Langevin recombination constant γ_{L}.

5.6.3. Transient Absorption Spectrum on a Time Scale of Microseconds

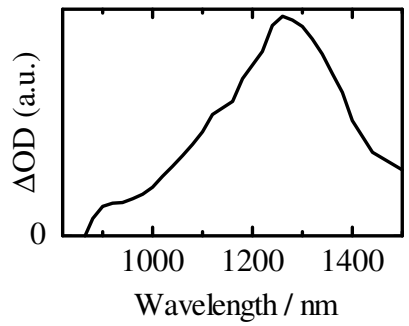

Figure 5-A1 Transient absorption spectrum of PCPDTBT/PCBM blend film (50:50 w/w) fabricated with DIO at 0.5 μs after the laser excitation at 400 nm.

5.6.4. Mobility Estimated by SCLC Method

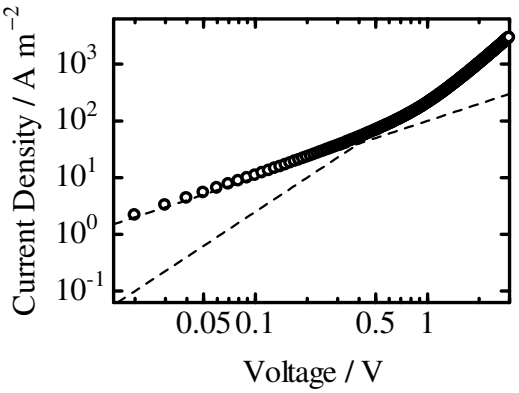

Figure 5-A2. *J–V* characteristics of a hole only device with a layer structure of ITO|PCPDTBT:PCBM|Au. The broken lines show the fitting curves to the symbols. The hole mobility is estimated to be 3.63×10^{-4} cm^2 V^{-1} s^{-1}.

5.7. References and Notes

[1] M. A. Green, K. Emery, Y. Hishikawa, W. Warta, *Prog. Photovolt. Res. Appl.* **2011**, *19*, 84–92.

[2] R. F. Service, *Science* **2011**, *332*, 293.

[3] D. Mühlbacher, M. Scharber, M. Morana, Z. Zhu, D. Waller, R. Gaudiana, C. Brabec, *Adv. Mater.* **2006**, *18*, 2884–2889.

[4] J. Peet, J. Y. Kim, N. E. Coates, W. L. Ma, D. Moses, A. J. Heeger, G. C. Bazan, *Nat. Mater.* **2007**, *6*, 497–500.

[5] E. Bundgaard, F. C. Krebs, *Sol. Energy Mater. Sol. Cells* **2007**, *91*, 954–985.

[6] D. J. D. Moet, M. Lenes, M. Morana, H. Azimi, C. J. Brabec, P. W. M. Blom, *Appl. Phys. Lett.* **2010**, *96*, 213506.

[7] J. C. Bijleveld, M. Shahid, J. Gilot, M. M. Wienk, R. A. J. Janssen, *Adv. Funct. Mater.* **2009**,

19, 3262–3276.

[8] T. J. K. Brenner, Z. Li, C. R. McNeil, *J. Phys. Chem. C* **2011**, *115*, 22075–22083.

[9] E. E. Havinga, W. Hoeve, H. Wynberg, *Polym. Bull.* **1992**, *29*, 119–126.

[10] H. Ohkita, S. Ito, *Polymer* **2011**, *52*, 4397–4417.

[11] T. Agostinelli, T. A. M. Ferenczi, E. Pires, S. Foster, A. Maurano, C. Müller, A. Ballantyne, M. Hampton, S. Lilliu, M. Campoy-Quiles, H. Azimi, M. Morana, D. D. C. Bradley, J. Durrant, J. E. Macdonald, N. Stingelin, J. Nelson, *J. Polym. Sci. B: Polym. Phys.* **2011**, *49*, 717–724.

[12] M. Morana, H. Azimi, G. Dennler, H.-J. Egelhaaf, M. Scharber, K. Forberich, J. Hauch, R. Gaudiana, D. Waller, Z. Zhu, K. Hingerl, S. S. van Bavel, J. Loos, C. J. Brabec, *Adv. Funct. Mater.* **2010**, *20*, 1180–1188.

[13] see the Capter 3.

[14] J. Nelson, *Phys. Rev. B* **2003**, *67*, 155209.

[15] J. Guo, H. Ohkita, H. Benten, S. Ito, *J. Am. Chem. Soc.* **2010**, *132*, 6154–6164.

[16] H-Y. Chen, J. Hou, A. M. Hayden, H. Yang, K. N. Houk, Y. Yang, *Adv. Mater.* **2009**, *21*, 371–375.

[17] J. T. Rogers, K. Schmidt, M. F. Toney, E. J. Kramer, G. C. Bazan, *Adv. Mater.* **2011**, *23*, 2284–2288.

[18] M. Morana, M. Wegscheider, A. Bonanni, N. Kopidakis, S. Shaheen, M. Scharber, Z. Zhu, D. Waller, R. Gaudiana, C. Brabec, *Adv. Funct. Mater.* **2008**, *8*, 1757–1766.

[19] J. K. Lee, W. L. Ma, C. J. Brabec, J. Yuen, J. S. Moon, J. Y. Kim, K. Lee, G. C. Bazan, A. J. Heeger, *J. Am. Chem. Soc.* **2008** *130*, 3619–3623.

[20] D. Jarzab, F. Cordella, J. Gao, M. Scharber, H.-J. Egelhaaf, M. A. Loi, *Adv. Energy Mater.* **2011**, *1*, 604–609.

[21] C. Deibel, T. Strobel, V. Dyakonov, *Phys. Rev. Lett.* **2009**, *103*, 036402.

[22] T. M. Clarke, J. R. Durrant, *Chem. Rev.* **2010**, *110*, 6736–6767.

[23] A. Pivrikas, G. Juška, A. J. Mozer, M. Scharber, K. Arlauskas, N. S. Sariciftci, H. Stubb, R. Österbacka, *Phys. Rev. Lett.* **2005**, *94*, 176806.

[24] J. Guo, H. Ohkita, S. Yokoya, H. Benten, S. Ito, *J. Am. Chem. Soc.* **2010**, *132*, 9631–9637.

[25] A. Baumann, J. Lorrmann, C. Deibel, V. Dyakonov, *Appl. Phys. Lett.* **2008**, *93*, 252104.

[26] C. J. Brabec, G. Zerza, G. Cerullo, S. de Silvestri, S. Luzzati, J. C. Hummelen, S. Sariciftci, *Chem. Phys. Lett.* **2001**, *340*, 232–236.

[27] I. A. Howard, R. Mauer, M. Meister, F. Laquai, *J. Am. Chem. Soc.* **2010**, *132*, 14866–14876.

[28] F. Etzold, I. A. Howard, R. Mauer, M. Meister, T.- D. Kim, K.- S. Lee, N. S. Baek, F. Laquai, *J. Am. Chem. Soc.* **2011**, *133*, 9469–9479.

[29] R. A. Marsh, J. M. Hodgkiss, S. Albert-Seifried, R. H. Friend, *Nano Lett.* **2010**, *10*, 923–930.

Chapter 6

Charge Generation and Recombination in Fluorene-based Polymer Solar Cells

6.1. Introduction

Polymer/fullerene solar cells have made remarkable progress in recent years. Currently, power conversion efficiency (PCE) of them is approaching to 10%.[1,2] This is due largely to intensive developments in various conjugated polymers. There are two synthetic strategies of conjugated polymers for improving the device performance of polymer solar cells. One is to reduce the bandgap energy in order to increase the short-circuit current density (J_{SC}).[3–5] The other is to increase the ionization potential in order to obtain larger open-circuit voltage (V_{OC}).[6–8] As such, various fluorene-based copolymers have been intensively developed because their optoelectronic properties can be finely tuned by chemical modifications and copolymerization with various units.[9–12] Some fluorene-based copolymers have ionization potentials larger than a benchmark polymer of poly(3-hexylthiohene) (P3HT) that exhibits a modest V_{OC} of ~0.6 V. For example, a polymer solar cell based on a blend of a fluorene-based copolymer poly[2,7-(9,9-dioctylfluorene)-*alt*-5,5-(5',8'-di-2-thienyl-2',3'-diphenylquinoxaline)] (N-P7) and a C_{70} fullerene derivative ([70]PCBM) has shown a large V_{OC} of 0.99 V and hence a high PCE of 5.5%.[13,14] Interestingly, the device performance, in particular J_{SC}, is strongly dependent on the spin-coating solvent. This finding suggests that the device performance is dependent on the phase-separated structures.

Herein, the charge generation and recombination dynamics in N-P7/PCBM blends fabricated with different spin-coating solvents by transient absorption spectroscopy were studied. By analyzing the transient decay dynamics, the author evaluate the efficiency of the exciton diffusion to a donor/acceptor interface, the efficiency of the the charge transfer at the interface, and the efficiency of the charge dissociation into free carriers at the interface. In addition, the efficiency of the charge collection to the electrode is evaluated from the saturation current at a reverse bias voltage. As a result, it was found that the device performance is primarily limited by the charge dissociation and collection efficiency. These two processes are dependent on the blend morphology. Furthermore, the author discusses the origin of such limitation in N-P7/PCBM solar cells by comparing the efficiency of each fundamental process mentioned above with P3HT/PCBM solar cells.

6.2. Results

6.2.1 Photovoltaic Properties

Figure 6-1a shows the aborption spectra of N-P7/PCBM solar cells. The large absorption band at 550 nm is ascribed to N-P7. The spectra suggest that the photon absorption is due mainly to N-P7 because PCBM has no distinct absorption band in the visible region. From the absorbance, the thickness of the active layer was estimated to be 220 nm for the device fabricated from chlorobenzene and 270 nm for the device fabricated from chloroform. Note that the thickness is not optimized but rather adjusted to that of P3HT/PCBM solar cells for comparison.[15] The photon absorption efficiency η_A can be roughly estimated from twice the absorbance of the film assuming the 100% reflection at the metal electrode and the 4% reflection loss at the air/glass interface. As shown in Figure 6-1b, the photon absorption efficiency η_A of the solar cell was ~0.8 for the device fabricated from chlorobenzene and ~0.9 for the device fabricated from chloroform.

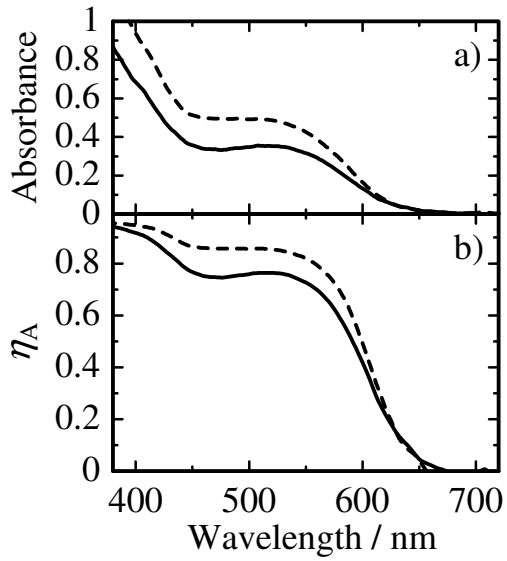

Figure 6-1. a) Absorption spectra of N-P7/PCBM blend films fabricated from chlorobenzene (solid line) and chloroform (broken line). b) Photon absorption efficiency η_A calculated from twice the absorbance in the panel (a) assuming the 100% reflection at the metal electrode and the 4% reflection loss.

Table 6-1. The device parameters of N-P7/PCBM solar cells.

	J_{SC} / mA cm^{-2}	V_{OC} / V	FF	PCE / %
Chlorobenzene	9.15	0.92	0.41	3.45
Chloroform	7.64	0.92	0.40	2.83

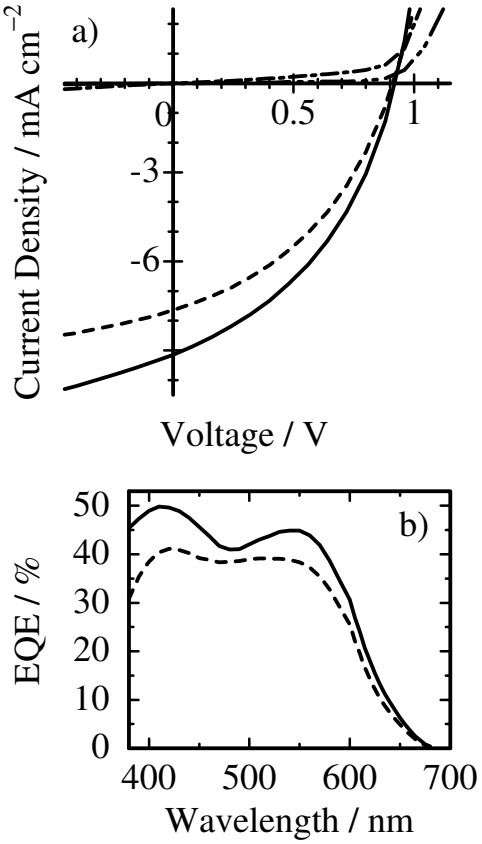

Figure 6-2. a) *J–V* characteristics of N-P7/PCBM solar cells fabricated from chlorobenzene (solid line) and chloroform (broken line) under AM1.5G simulated solar illumination at 100 mW cm^{-2}. The *J–V* characteristics in dark are also shown by dashed-dotted and dashed double-dotted line for solar cell fabricated from chlorobenzene and chloroform, respectively. b) EQE spectra of N-P7/PCBM solar cells fabricated from chlorobenzene (solid line) and chloroform (broken line).

Figure 6-2a shows the *J–V* characteristics of N-P7/PCBM solar cells in the dark and under the simulated solar illumination at 100 mW cm^{-2}. The short-circuit current density (J_{SC}) was ~9 mA cm^{-2} for the device fabricated from chlorobenzene and ~8 mA cm^{-2} for the device fabricated from chloroform. No distinct difference was found in V_{OC}

and fill factor. The device parameters are summarized in Table 6-1. This device performance is slightly lower but comparable to that of N-P7/[70]PCBM solar cells reported previously.[13,14] Figure 6-2b shows the EQE spectra of the N-P7/PCBM solar cells. The EQE around 500 – 550 nm was ~45% for the device fabricated from chlorobenzene and ~40% for the device fabricated from chloroform.

6.2.2 Transient Absorption

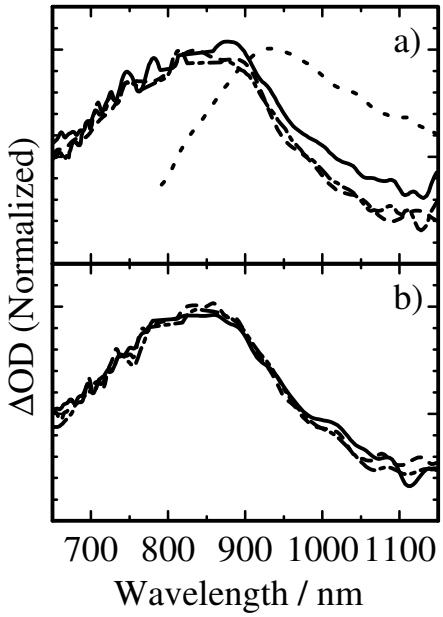

Figure 6-3. Transient absorption spectra of N-P7/PCBM blend films fabricated from a) chlorobenzene and b) chloroform. The excitation fluence was set at 8 μJ cm^{-2} at 400 nm. The delay times are 0 (solid lines), 2 (broken lines), and 100 ps (dashed-dotted lines). The dotted line in the panel (a) shows the spectra of N-P7 neat film at 0 ps.

Figure 6-3 shows the normalized transient absorption spectra of N-P7/PCBM blend films. For N-P7/PCBM blend films fabricated from chlorobenzene, as shown in

Figure 6-3a, a large absorption band was observed at around 850 nm but the absorption spectrum at 0 ps was different from the other spectra a few picoseconds after the laser excitation: there was a spectral difference over 900 to 1200 nm. On the other hand, as shown in Figure 6-3b, a large absorption band was observed at around 850 nm for N-P7/PCBM blend films fabricated from chloroform. This band did not change at all with time. For N-P7 neat films, as shown by the dotted line in Figure 6-3a, an absorption band was observed at around 920 nm. This band is ascribed to N-P7 singlet exciton. Therefore the small absorption observed over 900 to 1200 nm at 0 ps was ascribed to N-P7 singlet exciton. On the other hand, the large absorption band at around 850 nm decayed in a few nanoseconds and was still observed on a time scale of microseconds even in an oxygen atmosphere. Therefore the large absorption at around 850 nm was ascribed to N-P7 polarons. This is consistent with the previous report: N-P7 polaron exhibits an absorption peak with a molar absorption coefficient of $\varepsilon_{N\text{-}P7}{}^{+} = 40000\ M^{-1}\ cm^{-1}$ at 850 nm. Indeed, the transient absorption spectrum at 0 ps in Figure 6-3a can be well reproduced by the sum of the absorption spectrum at 10 ps (N-P7 polaron and PCBM radical anion) and the absorption spectrum of N-P7 singlet exciton. The rapid generation of N-P7 polarons is consistent with the efficient fluorescence quenching.

To analyze the charge generation dynamics, the transient absorption spectra were resolved into N-P7 singlet exciton and charged species (N-P7 polaron and PCBM radical anion) by spectral simulation as mentioned above. Figure 6-4 shows the time evolution of N-P7 singlet exciton and polaron in N-P7/PCBM blend films fabricated from chlorobenzene. The N-P7 singlet exciton decayed exponentially with a time constant of 0.8 ps and N-P7 polarons were generated with the same time constant as the singlet decay. Note that 80% of N-P7 polarons were promptly generated at 0 ps. As summarized in Table 6-2, N-P7 polarons are generated in a few picoseconds in N-P7/PCBM blend films.

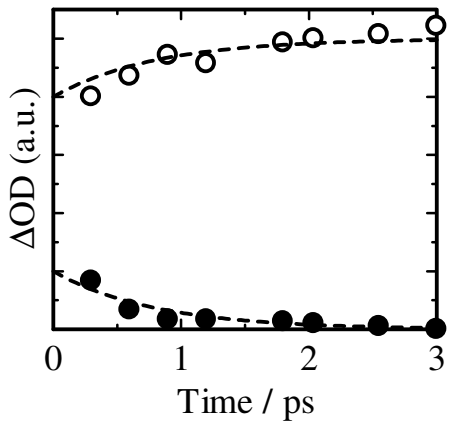

Figure 6-4. Time evolution of N-P7 singlet exciton (closed circles) and N-P7 polaron (open cirlcues) in N-P7/PCBM blend films fabricated from chlorobenzene. The broken lines show the fitting curves by exponential functions: $\Delta OD = A \exp(-t/\tau_d)$ for the decay and $A[1 - \exp(-t/\tau_r)] + B$ for the rise kinetics with $\tau_d = \tau_r = 0.8$ ps.

Such a rapid charge generation has been observed for amorphous blend films.[16] As reported previously, fluorene-based copolymers forms amorphous films.[17,18] In amorphous film, PCBM molecules are likely to be homogeneously dispersed. Thus, polymer singlet excitons should be quenched promptly by neighboring PCBM molecules in a few picoseconds when the exciton diffusion is generally negligible. The slight difference in the charge generation dynamics observed for the two blend films indicates that there are some differences in phase-separated structures of PCBM even in amorphous films. In any case, N-P7 polarons are rapidly generated in a few picoseconds, which is much shorter than the lifetime of N-P7 singlet exciton (1.9 ns). Thus, the efficiency of the exciton diffusion η_{ED} and the charge transfer η_{CT} is estimated to be unity. After a few picoseconds, the absorption spectra remained the same up to nanoseconds and were independent of the spin-coating solvent and the PCBM fraction. These spectra suggest

that similar charge separated states are formed in these blends on a time scale of picoseconds.

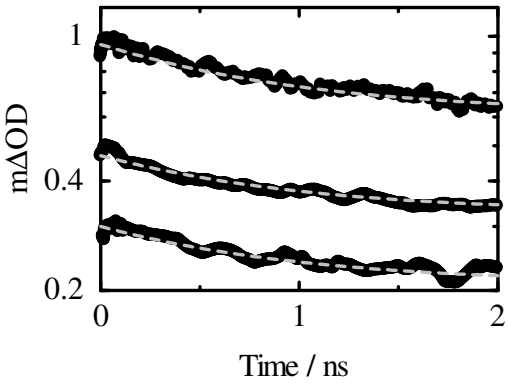

Figure 6-5. Time evolution of transient signals of N-P7 polaron in a N-P7/PCBM blend film fabricated from chlorobenzene probed at 900 nm. The laser fluence is 1 to 4 μJ cm^{-2} at 400 nm. The broken lines show the fitting by an exponential function with a constant fraction: $\Delta OD = A \exp(-t/\tau_g) + B$ with τ_g = 900 ps and A : B = 30 : 70.

Table 6-2. Kinetic parameters for the geminate recombination in N-P7/PCBM blends.

	τ_m / ns	B / %	k_{dis} / s^{-1}	k_{rec} / s^{-1}
Chlorobenzene	0.9	70	8×10^8	3×10^8
Chloroform	1.2	65	5×10^8	3×10^8

k_{dis}: dissociation rate constant of CT state, k_{rec}: recombination rate constant of CT state.

Next the author focuses on the recombination dynamics on a time scale of nanoseconds. Figure 6-5 shows the time evolution of transient signals at 900 nm (N-P7 polaron) observed for N-P7/PCBM blend films fabricated from chlorobenzene. As shown in the figure, the decay dynamics was independent of the excitation intensity. This

suggests monomolecular recombination. Note that the polaron decay was in good agreement with the photobleaching recovery (see the Appendix). This shows that the recombination to the ground state. As shown in the figure, the polaron decay was well fitted by an exponential function with a constant fraction: $\Delta OD = A \exp(-t/\tau_m) + B$. As summarized in Table 6-2, the lifetime of polarons is about ~1 ns for both blends. This is in good agreement with the lifetime of the CT emission observed for blend films of fluorene-based copolymer and PCBM.[19–22] Therefore polaron band at around 850 nm is ascribed to the CT state, which is coulombically bound pair of N-P7 polaron and PCBM radical anion at the heterojunction. On the basis of these assignments, the rate constants of CT state dissociation k_{dis} and CT state recombination k_{rec} and the charge dissociation efficiency η_{CD} are estimated by the following equations with the kinetic parameters obtained.

$$k_{rec} + k_{dis} = \tau_m^{-1} \quad (6\text{-}1)$$

$$\eta_{CD} = k_{dis}/(k_{rec} + k_{dis}) = k_{dis}\,\tau_m = B/(A + B) \quad (6\text{-}2)$$

As summarized in Table 6-2, k_{rec} is 3×10^8 s^{-1} for both blends while k_{dis} is 8×10^8 s^{-1} (chlorobenzene) and 5×10^8 s^{-1} (chloroform), and η_{CD} is 0.7 (chlorobenzene) and 0.65 (chloroform). This finding suggests that the charge dissociation efficiency η_{CD} is primarily dependent on k_{dis} rather than k_{rec}. As discussed later, this is probably because k_{dis} is dependent on the blend morphology while k_{rec} is dependent on the CT state at the donor/acceptor interface.

The author moves onto the bimolecular recombination of free charges on a time scale of microseconds. Figure 6-6 shows the decay dynamics of N-P7 polarons in N-P7/PCBM blends under various excitation conditions. The charge carrier density $n(t)$ was estimated as described in the Appendix. All the decay dynamics was well fitted by

an empirical power-law equation: $n(t) = n_0(1+at)^{-\alpha}$ with $\alpha = 0.42$ for blend films fabricated from chlorobenzene and $\alpha = 0.23$ for blend films fabricated from chloroform.

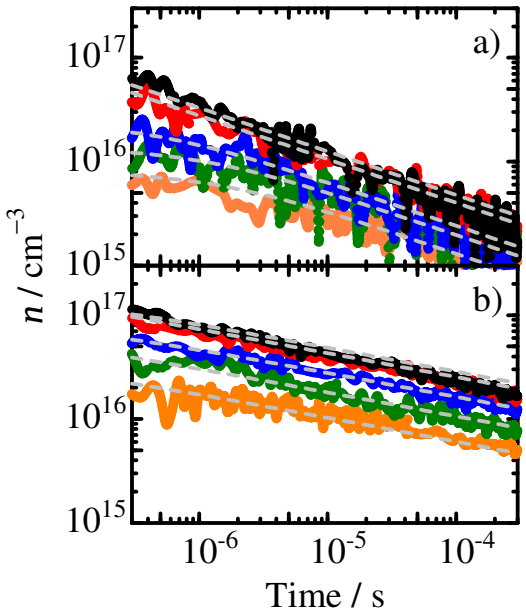

Figure 6-6. Time evolution of the charge carrier density in N-P7/PCBM blend films fabricated from a) chlorobenzene and b) chloroform. The fluence is varied from 0.6, 1, 3, 6, and 60 μJ cm^{-2} from bottom to top. The gray broken lines show the fitting curves by a power-law function: $n(t) = n_0(1 + at)^{-\alpha}$ with α = a) 0.42 and b) 0.23.

The power-law kinetics with $\alpha < 1$ is characteristic of trap-limited bimolecular recombination.[23] From the fitting of these dynamics, the bimolecular recombination rate $\gamma(n)$ and the charge carrier lifetime τ_c are obtained by

$$\gamma(n) = a\alpha n_0^{-1/\alpha} n^{(1/\alpha)-1} \quad (6\text{-}3)$$

$$\tau_c = [\gamma(n_0)n_0]^{-1} = (a\alpha)^{-1} \quad (6\text{-}4)$$

As shown in Figure 6-7, the charge carrier lifetime is of the order of ~10^{-6} s for the device fabricated from chlorobenzene and <10^{-7} s for the device fabricated from chloroform at a

charge density of ~10^{16} – 10^{17} cm^{-3}. Note that τ_c is the upper limit for blend films fabricated from chloroform because no inflection point was observed in the time range measured. Details will be discussed in the following section.

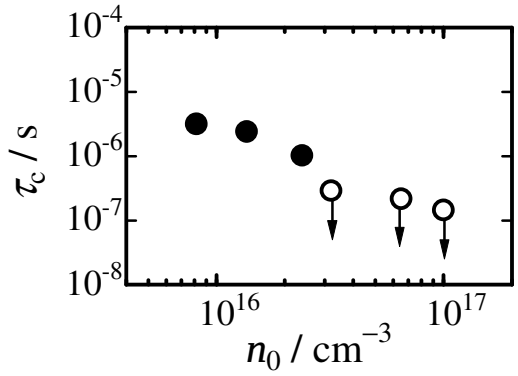

Figure 6-7. Charge carrier lifetime τ_c in N-P7/PCBM blend films fabricated from chlorobenzene (closed circles) and chloroform (opened circles) plotted against the initial carrier density n_0. Note that the τ_c for chloroform is the upper limit.

6.3. Discussion

To address the origin of the difference in the solvent-dependent device performance of N-P7/PCBM solar cells, the author discusses here the efficiency of each photovoltaic conversion process after the photon absorption: the efficiency of the exciton diffusion to a donor/acceptor interface η_{ED}, the efficiency of the charge transfer at the donor/acceptor interface η_{CT}, the efficiency of the charge dissociation into free carriers at the donor/acceptor interface η_{CD}, and the efficiency of the charge collection to each electrode η_{CC}. As mentioned before, no difference is found in η_{ED} or η_{CT} for N-P7/PCBM solar cells, both of which are almost unity independently of the spin-coating solvent. This is because PCBM molecules are homogeneously dispersed in amorphous blend films. Thus, the author focuses on the charge dissociation and collection efficiency.

The charge dissociation efficiency η_{CD} is dependent on the spin-coating solvent: η_{CD} = 0.7 (chlorobenzene) is larger by 7% than η_{CD} = 0.65 (chloroform). This is because k_{dis} is 1.6 times larger for chlorobenzene than for chloroform while k_{rec} is almost independent of the spin-coating solvent. The larger k_{dis} is due to the formation of larger PCBM aggregates in blend films fabricated by chlorobenzene rather than chloroform. Such large PCBM aggregates are consistent with the relatively slow exciton quenching in blend films fabricated by chlorobenzene. Janssen *et al.* have reported for another fluorene-based solar cell that the formation of PCBM nanocrystals would promote the charge dissociation because of the higher local electron mobility.[22] The same would be true for N-P7/PCBM solar cells. On the other hand, the solvent-independent k_{rec} is indicative of a similar CT state at the donor/acceptor interface. This is consistent with the solvent-independent transient absorption spectra of the CT state as shown in Figure 6-3. Thus, it is concluded that the charge dissociation efficiency η_{CD} is primarily dependent on the blend morphology rather than the CT state at the donor/acceptor interface.

To evaluate the charge collection efficiency η_{CC}, the author focuses on the *J*–*V* characteristics of N-P7/PCBM solar cells in the dark and under the illumination. As shown in Figure 6-2, the photocurrent profile is different from the darkcurrent diode profile. This finding suggests that the photoinduced current $J_{ph}(V)$ is dependent on the applied voltage V as follows:

$$J(V) = J_d(V) - J_{ph}(V) = J_d(V) - qGd\,\eta_{CC}(V) \quad (6\text{-}5)$$

to qGd because $\eta_{CC}(V_{sat}) = 1$. Thus, $\eta_{CC}(V)$ can be obtained by

$$\eta_{CC}(V) = [J_d(V) - J(V)]/[J(V_{sat}) - J_d(V_{sat})] \quad (6\text{-}6)$$

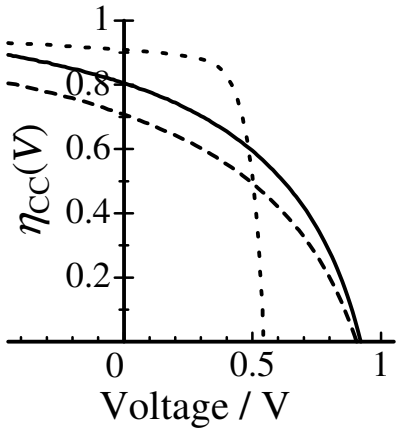

Figure 6-8. Charge collection efficiency $\eta_{CC}(V)$ of N-P7/PCBM solar cells fabricated from chlorobenzene (solid line) and chloroform (broken line) plotted against applied voltage. The dotted line shows the charge collection efficiency $\eta_{CC}(V)$ of P3HT/PCBM solar cells, which is taken from Ref 15.

Figure 6-8 shows $\eta_{CC}(V)$ of N-P7/PCBM solar cells fabricated from chlorobenzene and from chloroform and in addition $\eta_{CC}(V)$ of P3HT/PCBM solar cells for comparison. For N-P7/PCBM solar cells fabricated from chlorobenzene, as shown in the figure, the charge collection efficiency is η_{CC} = 0.8 under the short circuit condition, decreases with increasing voltage, and drops down to 0.57 at the maximum power voltage. Similarly, the charge collection efficiency of N-P7/PCBM solar cells fabricated from chloroform is η_{CC} = 0.7 under the short circuit condition and drops to 0.47 at the maximum power voltage. In contrast, as shown by the dotted line in Figure 6-8, the charge collection efficiency of P3HT/PCBM solar cells is as high as η_{CC} = 0.9 under the short circuit condition and still more than 0.8 at the maximum power voltage. This is a clear difference between N-P7/PCBM and P3HT/PCBM solar cells, which is discussed later in details. As summarized in Table 6-3, the product of all the efficiency $\Pi\eta_i$ is 0.45 for blend films

fabricated from chlorobenzene and 0.4 for blend films fabricated from chloroform. These are consistent with the observed EQE as shown in Figure 6-2. This suggests that all the efficiency evaluated from the transient study is closely related to the device performance.

Table 6-3. The photovoltaic conversion efficiency in N-P7/PCBM blends.

	η_A	η_{ED}	η_{CT}	η_{CD}	η_{CC}	$\Pi\eta_i$ [a]
Chlorobenzene	~0.8	1	1	0.7	0.8	0.45
Chloroform	~0.9	1	1	0.65	0.7	0.4

[a] $\Pi\eta_i = \eta_A\,\eta_{ED}\,\eta_{CT}\,\eta_{CD}\,\eta_{CC}$

To discuss the solvent-dependent η_{CC}, the author focuses η_{CC} (V = 0 V) under the short circuit condition where η_{CC} is larger for the N-P7/PCBM solar cell fabricated from chlorobenzene than that from chloroform. The charge collection time at a voltage of 0 V can be roughly estimated to be $t_{CC}^{SC} = 5 \times 10^{-7}$ s (chlorobenzene) and $t_{CC}^{SC} = 4 \times 10^{-6}$ s (chloroform) as a transit time $dd_C/(V_b\mu)$ where d is the thickness of the active layer, d_C is the average collection length (= d/2), V_b is the internal bias voltage at the short circuit (~ V_{OC}), and μ is the charge mobility. The difference in t_{CC}^{SC} is due to the difference in the charge mobility and the thickness: $\mu_h = 5 \times 10^{-4}$ cm^2 V^{-1} s^{-1}, d = 220 nm (chlorobenzene); $\mu_h = 1 \times 10^{-4}$ cm^2 V^{-1} s^{-1}, d = 270 nm (chloroform). For the device fabricated from chlorobenzene, the charge carrier lifetime τ_c of N-P7 polarons is longer than the collection time t_{CC}^{SC} even at a charge density of ~10^{16} cm^{-3} as shown in Figure 6-7. At the short circuit, the charge carrier lifetime τ_c should be much longer because of the lower charge density. In other words, η_{CC} should be dependent on the charge collection time rather than the charge carrier lifetime. For the device fabricated from chloroform, on the other hand, the charge carrier lifetime τ_c of N-P7 polarons is shorter than the collection time

t_{CC}^{SC}. Thus, η_{CC} should be limited by the charge carrier lifetime rather than the charge collection time. In summary, the lower η_{CC} for the device fabricated from chloroform is ascribed to the longer charge collection time and the shorter charge carrier lifetime.

Finally, the difference in the device performance between N-P7/PCBM with P3HT/PCBM solar cells is discussed. Here, the author focuses on N-P7/PCBM solar cells fabricated with chlorobenzene and P3HT/PCBM solar cells. As mentioned before, the voltage-dependence $\eta_{CC}(V)$ is different between them especially at around V_{OC}. Under the open circuit condition, the charge collection time at around V_{OC} can be roughly estimated to be $t_{CC}^{OC} = 5 \times 10^{-6}$ s as a diffusion time $d_C^2/(2D) = qd^2/(8k_BT\mu)$ where D is the diffusion constant of charge carriers (= $\mu k_BT/q$), k_B is the Boltzmann constant, and T is temperature. As shown in Figure 6-7, the charge carrier lifetime τ_c of N-P7 polarons is comparable to the collection time t_{CC}^{OC} at a charge density of ~10^{16} cm^{-3}, which is a typical density under the open circuit condition. In other words, most of charge carriers would recombine before the charge collection at around V_{OC}. In contrast, the charge lifetime in P3HT/PCBM solar cells has been reported to be still longer than the charge collection time even at around V_{OC}.[24,25] As a result, P3HT/PCBM solar cells exhibit a relatively high fill factor even with a thickness of ~200 nm. Such long lifetime of charge carriers results from the reduced recombination in P3HT/PCBM: the bimolecular recombination rate γ is at least two orders of magnitude slower than the Langevin recombination rate γ_L, which is given by $q(\mu_e + \mu_h)/\varepsilon\varepsilon_0$ where μ_e and μ_h are the electron and hole mobility, respectively, and ε is the dielectric constant of the charge transport material, and ε_0 is the vacuum permittivity.[26] Recently, the author proposed that the reduced recombination is due to non-diffusion-limited recombination where the apparent recombination rate γ_a is given by $k_{rec}/(k_{rec} + k_{dis})\gamma_L$ under the steady state condition. In P3HT/PCBM solar cells, most of free charge carriers are promptly generated at the

donor/acceptor interface on a time scale of <0.1 ps ($k_{dis} > 10^{13}$ s^{-1}). At disordered interface, some polarons recombine geminately with a rate constant of $k_{rec} \approx 10^{9}$ s^{-1}. Thus, γ_a would be reduced by $k_{rec}/(k_{rec} + k_{dis}) \approx 10^{-4}$ relative to γ_L. On the other hand, $k_{rec}/(k_{rec} + k_{dis})$ is as large as ~0.3 for N-P7/PCBM solar cells fabricated from chlorobenzene. Indeed, the bimolecular recombination rate γ is evaluated to be $\gamma \approx 4 \times 10^{-11}$ cm^3 s^{-1}, which is reduced by a factor of 0.25 relative to $\gamma_L = 2 \times 10^{-10}$ cm^3 s^{-1}.[27] The small reduction is due to the comparable k_{rec} and k_{dis} of the CT state at the interface. The small reduction in γ is due to the short lifetime of the CT state at the interface: krec is as large as kdis. Such large krec has been reported for many compact donor-acceptor dyad systems with small separation distance because of the large electronic coupling.[28,29] We therefore propose that the formation of the CT state at the interface cause the faster bimolecular recombination in N-P7/PCBM than in P3HT/PCBM blends.

6.4. Conclusion

The charge generation and recombination dynamics were studied by transient absorption spectroscopy for N-P7/PCBM blend films fabricated spin-coating from difference solvents such as chlorobenzene and chloroform. Upon the photoexcitation, N-P7 singlet excitons rapidly decay and N-P7 polarons are promptly generated with 100% efficiency in a few picoseconds for both blend films. Thus, the exciton diffusion and charge transfer efficiency is estimated to be $\eta_{ED} = 1$ and $\eta_{CT} = 1$. In a nanosecond, the N-P7 polarons are ascribed to the CT state at the heterojunction because the monomolecular decay constant is consistent with the lifetime of the CT emission reported previously. The majority of N-P7 polarons in the CT state are dissociated into free carriers and the rest of them recombine to the ground state. The dissociation efficiency is estimated to be $\eta_{CD} = 0.7$ for the device fabricated from chlorobenzene and $\eta_{CD} = 0.65$ for

the device fabricated from chloroform. The higher η_{CD} is due to the larger dissociation rate k_{dis}. The recombination rate k_{rec} is rather independent of the spincoating solvent. This is probably because the CT state is dependent on the donor/acceptor materials but less dependent of the blend morpholgy. This is consistent with the solvent-independent transient absorption spectra of the CT state. On the other hand, the larger dissociation rate k_{dis} is due to larger PCBM aggregates in the device fabricated from chlorobenzene. This would be promoted by the higher local electron mobility and the improved separation of CT states at the donor/acceptor interface as reported previously. The charge collection efficiency η_{CC} is evaluated from the saturated current at a reversed bias voltate of the devices. As a result, it is estimated to be η_{CC} = 0.8 for the device fabricated from chlorobenzene and η_{CD} = 0.7 for the device fabricated from chloroform. The difference in η_{CD} is due to the difference in the charge collection time and the charge lifetime. In summary, η_{ED} of N-P7/PCBM solar cells is higher than that of P3HT/PCBM solar cells. This is because PCBM molecules are likely to be homogeneously dispersed in amorphous N-P7/PCBM blends. On the other hand, η_{CD} and η_{CC} of N-P7/PCBM solar cells are lower than those of P3HT/PCBM solar cells. This is due to the formation of the CT state at the donor/acceptor interface in N-P7/PCBM blends. Thus, the dissociation from the CT state is limited by the competitive recombination to the ground state. The relatively low dissociation efficiecy is less beneficial for the reduced bimolecular recombination. This is in contrast to that observed in P3HT/PCBM with high dissociation efficiecy. The author propose that high dissociation efficiency is the key to highly effcient performance especially for polymer solar cells with thick active layer.

6.5. Experimental

For the device fabrication, indium/tin oxide (ITO)-coated glass substrates (10 Ω per square) were washed by ultrasonication in toluene, acetone, and ethanol for 15 min, dried with N_2, and then cleaned with a UV–O_3 cleaner (Nippon Laser & Electronics NL-UV253S) for 30 min. A thin layer (~40 nm) of poly(3,4-ethylenedioxythiophene):poly(4-styrenesulfonate) (PEDOT:PSS; H. C. Starck, PH500) was spin-coated onto the cleaned substrates at a spin rate of 3000 rpm, and the layer was dried at 140 °C for 10 min in air. The solution of PEDOT:PSS was filtered using a 0.45-μm PTFE syringe filter prior to the spin coating. A blend layer of N-P7/PCBM (~200 nm) was spin-coated from a chlorobenzene or chloroform solution. Finally, LiF (1 nm)/Al (80 nm) was thermally deposited on top of the active layer at 2.5×10^{-4} Pa.

Blend films of N-P7 and [6,6]-phenyl-C_{61}-butyric acid methyl ester (PCBM) were fabricated by spin-coating on a glass substrate from chloroform or chlorobenzene solution. The glass substrates were washed as mentioned above. The N-P7 polymer was supplied from Toray Industries, Inc and PCBM (99.9%) was purchased from Frontier Carbon, both of which were used without further purification. The transient absorption measurements were performed for these sample films over the time range from picosecond to microsecond in nitrogen atmosphere. The apparatus employed here has been described in the Capter 3.

6.6. Appendix

6.6.1. Transient Photobleaching Decay Dynamics

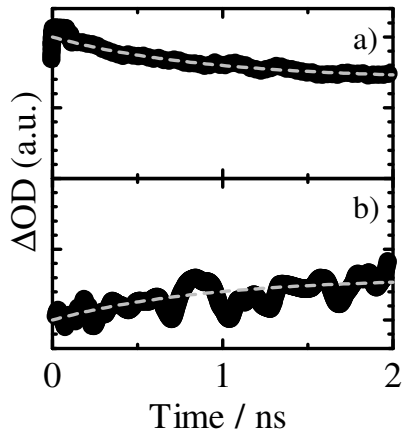

Figure 6-A1. Time evolution of transient signals of N-P7/PCBM blend films fabricated from chlorobenzene: a) N-P7 polaron at 900 nm, b) photobleaching at 530 nm. The fluence is 2 μJ cm^{-2} at 400 nm.

6.6.2. Charge Carrier Density Estimation

The density of charge carrier density is estimated by the Equation 6-A1.

$$n(t) = \Delta OD(t)\, N_A\, (1000\, \varepsilon(t)\, l\,)^{-1} \qquad (6\text{-A1})$$

where $\Delta OD(t)$ is the transient absorption signal measured at a delay time t, N_A is the Avogadro's constant (6.02×10^{23} mol^{-1}), $\varepsilon(t)$ is the extinction coefficient of positive carriers, and l is the thickness of blend films. Note that in time regime, positive carrier composition changed exponentially with time constant of τ_{inj} = 15 ns toward $N\text{-}P7^{+}$:$PCBM^{+}$ = 40:60 by hole injection process (see the Chapter 3); therefore, the charge carrier density is estimated on a time-dependent extinction coefficients $\varepsilon(t)$ defined as following equation:

$$\varepsilon(t) = \exp(-t/\tau_{inj})\, \varepsilon_{PCBM}{}^{+} + [1- \exp(-t/\tau_{inj})]\, \varepsilon_{PCBM}{}^{+} \qquad (6\text{-A2})$$

where $\varepsilon_{N\text{-}P7}^{+}$ and ε_{PCBM}^{+} are the extinction coefficient of N-P7 cation and PCBM cation($\varepsilon_{N\text{-}P7}^{+}$ = 35000 M^{-1} cm^{-1} and ε_{PCBM}^{+} = 9000 M^{-1} cm^{-1}).

6.6.3. Hole Mobility of N-P7/PCBM Blend Films

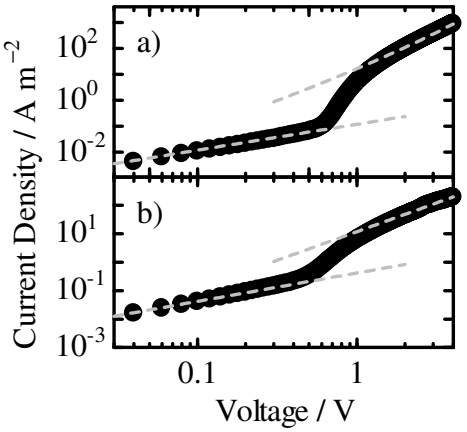

Figure 6-A2. *J–V* characteristics of a hole only device with a layer structure of ITO|N-P7:PCBM|Au fabricated from (a)chlorobenzene and (b)chloroform. The broken lines show the fitting curves to the symbols. The hole mobilities are estimated to be 4.7 × 10^{-4} and 9.4 × 10^{-5} cm^2 V^{-1} s^{-1} for chlorobenzene-film and chloroform-film, respectively.

6.7. References and Notes

[1] M. A. Green, K. Emery, Y. Hishikawa, W. Warta, *Prog. Photovolt. Res. Appl.* **2011**, *19*, 84–92.

[2] R. F. Service, *Science* **2011**, *332*, 293.

[3] J. Peet, J. Y. Kim, N. E. Coates, W. L. Ma, D. Moses, A. J. Heeger, G. C. Bazan, *Nat. Mater.* **2007**, *6*, 497–500.

[4] E. Bundgaard, F. C. Krebs, *Sol. Energy Mater. Sol. Cells* **2007**, *91*, 954–985.

[5] Y. Liang, L. Yu, *Polym. Rev.* **2010**, *50*, 454–473.

[6] C. J. Brabec, A. Cravino, D. Meissner, N. S. Sariciftci, T. Fromherz, M. T. Rispens, L. Sanchez, J. C. Hummelen, *Adv. Funct. Mater.* **2001**, *11*, 374.

[7] M. C. Scharber, D. Mühlbacher, M. Koppe, P. Denk, C. Waldauf, A. J. Heeger, C. J. Brabec, *Adv. Mater.* **2006**, *18*, 789–794.

[8] K. Vandewal, A. Gadisa, W. D. Oosterbaan, S. Bertho, F. Banishoeib, I. V. Severen, L. Lutsen, T. J. Cleij, D. Vanderzande, J. V. Manca, *Adv. Funct. Mater.* **2008**, *18*, 2064–2070.

[9] M. Svensson, F. Zhang, S. C. Veenstra, W. J. H. Verhees, J. C. Hummelen, J. M. Kroon, O. Inganäs, M. R. Andersson, *Adv. Mater.* **2003**, *15*, 988–991.

[10] O. Inganäs, F. Zhang, M. R. Andersson, *Acc. Chem. Res.* **2009**, *42*, 1731–1739.

[11] J. Chen, Y. Cao, *Acc. Chem. Res.* **2009**, *42*, 1709–1718.

[12] E. Zhou, J. Cong, K. Tajima, K. Hashimoto, *Chem. Mater.* **2010**, *22*, 4890–4895.

[13] D. Kitazawa, N. Watanabe, S. Yamamoto, J. Tsukamoto, *J. Photopolym. Sci. Technol.* **2010**, *23*, 293–296.

[14] D. Kitazawa, N. Watanabe, S. Yamamoto, J. Tsukamoto, *Appl. Phys. Lett.* **2009**, *95*, 053701.

[15] S. Honda, H. Ohkita, H. Benten, S. Ito, *Adv. Energy Mater.* **2011**, *1*, 588–598.

[16] J. Guo, H. Ohkita, H. Benten, S. Ito, *J. Am. Chem. Soc.* **2010**, *132*, 6154–6164.

[17] Y. Li, J. Ding, M. Day, Y. Tao, J. Lu, M. D'iorio, *Chem. Mater.* **2004**, *16*, 2165–2173.

[18] P. E. Keivanidis, I. A. Howard, R. H. Friend, *Adv. Funct. Mater.* **2008**, *18*, 3189–3202.

[19] M. A. Loi, S. Toffanin, M. Muccini, M. Forster, U. Scherf, M. Scharber, *Adv. Funct. Mater.* **2007**, *17*, 2111–2116.

[20] D. Veldman, S. C. J. Meskers, R. A. J. Janssen, *Adv. Funct. Mater.* **2009**, *19*, 1939–1948.

[21] K. Tvingstedt, K. Vandewal, A. Gadisa, F. Zhang, J. Manca, O. Inganäs, *J. Am. Chem. Soc.* **2009**, *131*,11819–11824.

[22] D. Veldman, Ö. İpek, S. C. J. Meskers, J. Sweelssen, M. M. Koetse, S. C. Veenstra, J. M. Kroon, S. S. van Bavel, J. Loos, R. A. J. Janssen, *J. Am. Chem. Soc.* **2008**, *130*, 7721–7735.

[23] J. Nelson, *Phys. Rev. B* **2003**, *67*, 155209.

[24] J. Guo, H. Ohkita, S. Yokoya, H. Benten, S. Ito, *J. Am. Chem. Soc.* **2010**, *132*, 9631–9637.

[25] C. G. Shuttle, B. O'regan, A. M. Ballantyne, J. Nelson, D. D. Bradley, *Appl. Phys. Lett.* **2008**,

92, 093311.

[26] A. Pivrikas, G. Juška, A. J. Mozer, M. Scharber, K. Arlauskas, N. S. Sariciftci, H. Stubb, R. Österbacka, *Phys. Rev. Lett.* **2005**, *94*, 176806.

[27] Assuming $\mu_e = 10^{-4}$ cm^2 V^{-1} s^{-1} and $\varepsilon_r = 3.8$, γ_L is estimated to be 4×10^{-10} cm^3 s^{-1} for the chlorobenzene-film.

[28] M. R. Wasielewski, *Chem. Rev.* **1992**, *92*, 435–461.

[29] J. W. Verhoeven, *J. Photochem. Photobiol. C: Photochem. Rev.* **2006**, *7*, 40–60.

Summary

The author investigated photovoltaic conversion mechanism in polymer/fullerene solar cells. On the basis of photophysical and device physical studies, the photovoltaic conversion was discussed in terms of each elemental process.

In Chapter 2, photogenerated charge carriers in blend films of poly[2-methoxy-5-(3,7-dimethyloctyloxy)-1,4-phenylenevinylene] (MDMO-PPV) and [6,6]-phenyl-C_{61}-butyric acid methyl ester (PCBM) were investigated by transient absorption spectroscopy. The blend film with a low PCBM fraction (<10 wt%) exhibited wide absorption ranging from 900 to 1000 nm, which is characteristic of the MDMO-PPV hole polaron and PCBM radical anion. On the other hand, the blend film with a higher PCBM fraction (>30 wt%) exhibited a major absorption band at ~900 nm, which is characteristic of the PCBM radical cation. For identification of charge carriers, the absorption spectrum and molar absorption coefficient of each charged species were evaluated separately using various combinations of electron donor and acceptor materials. Consequently, the MDMO-PPV hole polaron was found to have a broad absorption at ~950 nm and the PCBM radical anion and cation showed a distinct absorption at 1020 and at 890 nm, respectively. On the basis of these absorption spectra, the transient spectra observed for the blend films were simulated. The spectrum for a low PCBM fraction was well reproduced by a superposition of the absorption spectra of MDMO-PPV hole polaron and PCBM radical anion. On the other hand, the spectrum for a high PCBM fraction was well reproduced by superposition of the absorption of the MDMO-PPV hole polaron, PCBM radical anion, and PCBM radical cation, indicating that the PCBM radical cation is formed in the blend films with PCBM at a high concentration of PCBM.

In Chapter 3, the charge carrier dynamics in blend films of PCBM and conjugated polymers with different ionization potentials was measured by transient absorption spectroscopy in order to study the formation mechanism of the PCBM radical cation, which described in Chapter 2. On a time scale of nanoseconds after the photoexcitation, the polymer hole polaron and PCBM radical anion were observed but no PCBM radical cation was found in the blends. Subsequently, the fraction of polymer hole polaron decreased and instead that of PCBM radical cation increased with time. Finally, the fraction of PCBM radical cation became constant on a time scale of microseconds. The final fraction of PCBM radical cation was dependent on the ionization potential of polymers but independent of the excitation wavelength. These findings show that the formation of PCBM radical cation is due to hole injection from polymer to PCBM domains. Furthermore, the energetic conditions for such hole injection in polymer/PCBM blend films are discussed on the basis of the Monte Carlo analysis for hole hopping in a disordered donor/acceptor heterojunction with varying energetic parameters.

In Chapter 4, the origin of the open-circuit voltage (V_{OC}) was studied for polymer solar cells based on a blend of regioregular poly(3-hexythiphene) (RR-P3HT) and seven fullerene derivatives with different LUMO energy levels and side chains. The temperature dependence of J–V characteristics was analyzed by an equivalent circuit model. As a result, V_{OC} increased with the decrease in the saturation current density J_0 of the device. Furthermore, J_0 was dependent on the activation energy E_A for J_0, which is related to the HOMO–LUMO energy gap between P3HT and fullerene. Interestingly, the pre-exponential term J_{00} for J_0 was larger for pristine fullerenes than for substituted fullerene derivatives, suggesting that the electronic coupling between molecules also has substantial impact on V_{OC}. This is probably because the recombination is a non-diffusion-limited reaction depending on electron transfer at the RR-P3HT/fullerene

interface. In summary, the origin of V_{OC} is ascribed not only to the relative HOMO–LUMO energy gap but also to the electronic couplings between fullerene/fullerene and polymer/fullerene.

In Chapter 5, the charge carrier dynamics in blend films of poly[2,6-(4,4-bis-(2-ethylhexyl)-4*H*-cyclopenta[2,1-b;3,4-b']dithiophene)-*alt*-4,7-(2,1,3-benzothiadiazole)] (PCPDTBT) and PCBM were studied by transient absorption spectroscopy in order to address the origin of limited external quantum efficiency (EQE) of this solar cell compared to that of a benchmark solar cell of RR-P3HT and PCBM. Upon the photoexcitation, PCPDTBT polarons are promptly generated from the PCPDTBT singlet exciton with almost 100% efficiency in a picosecond. In other words, the exciton diffusion efficiency η_{ED} and charge transfer efficiency η_{CT} are 100% in this blend, which is higher than and comparable to those of the RR-P3HT/PCBM solar cell, respectively. On a time scale of nanoseconds, 70% of PCPDTBT polarons are dissociated into free charge carriers and the others recombine geminately to the ground state through the interfacial charge transfer (CT) state. The charge dissociation efficiency η_{CD} = 70% is lower than that of RR-P3HT/PCBM solar cell. The dissociated PCPDTBT polarons recombine bimolecularly on a time scale of nano- to microseconds with a charge lifetime of ~10^{-7} s, which is shorter than that observed for RR-P3HT/PCBM blends. In summary, the lower charge dissociation efficiency and shorter charge lifetime are the limiting factors for the photovoltaic performance of PCPDTBT/PCBM solar cells. Furthermore, the origin of such limitation is also discussed in terms of the charge dissociation and recombination through the interfacial CT state in PCPDTBT/PCBM blends.

In Chapter 6, the charge generation and recombination dynamics in blend films of poly[2,7-(9,9-dioctylfluorene)-*alt*-5,5-(5',8'-di-2-thienyl-2',3'-diphenylquinoxaline)] (N-P7) and PCBM was studied by transient absorption spectroscopy in order to address the

limiting process of the photovoltaic conversion. Upon photoexcitation, N-P7 singlet excitons are promptly converted to the interfacial charge transfer (CT) state, which is a coulombically bound pair of the N-P7 polaron and PCBM radical anion, with 100% efficiency in a few picoseconds. More than half of the N-P7 polarons in the CT state are dissociated into free carriers and the rest of them recombine to the ground state in a nanosecond. The dissociation efficiency is estimated to be ~0.7 for the device fabricated from chlorobenzene and ~0.65 for the device fabricated from chloroform, suggesting that it is primarily dependent on the blend morphology. From the saturated current at a sufficiently reverse bias voltage, the charge collection efficiency is estimated to be ~0.8 for the device fabricated from chlorobenzene and ~0.7 for the device fabricated from chloroform. In summary, the charge dissociation and collection are the processes limiting the photovoltaic performance of N-P7/PCBM solar cells. The origin of the limitation in N-P7/PCBM solar cells is also discussed in terms of the charge collection time and the charge lifetime.

List of Publications

Chapter 2.

"Formation of Methanofullerene Cation in Bulk Heterojunction Polymer Solar Cells Studied by Transient Absorption Spectroscopy"

Shunsuke Yamamoto, Jiamo Guo, Hideo Ohkita, Shinzaburo Ito

Adv. Funct. Mater. **2008**, *18*, 2555–2562.

Chapter 3.

"Formation Mechanism of Fullerene Cation in Bulk Heterojunction Polymer Solar Cells"

Shunsuke Yamamoto, Hideo Ohkita, Hiroaki Benten, Shinzaburo Ito

Submitted to *Adv. Funct. Mater.*

Chapter 4.

"Molecular Understanding of the Open-Circuit Voltage of Polymer:Fullerene Solar Cells"

Shunsuke Yamamoto, Akiko Orimo, Hideo Ohkita, Hiroaki Benten,

Shinzaburo Ito

Adv. Energy. Mater. in press. doi:10.1002/aenm.201100549.

Chapter 5.

"Charge Dissociation and Recombination through Interfacial Charge Transfer State in Low-Bandgap Polymer Solar Cells"

Shunsuke Yamamoto, Hideo Ohkita, Hiroaki Benten, Shinzaburo Ito

to be submitted

Chapter 6.

"Charge Generation and Recombination in Fluorene-Based Polymer Solar Cells"

Shunsuke Yamamoto, Hideo Ohkita, Hiroaki Benten, Shinzaburo Ito,

Shuhei Yamamoto, Daisuke Kitazawa, Jun Tsukamoto

to be submitted

Acknowledgment

The present thesis is based on the studies that the author and his co-workers have carried out at Department of Polymer Chemistry, Graduate School of Engineering, Kyoto University, Japan, from 2006 to 2012, under the guidance of Professor Shinzaburo Ito. The author sincerely expresses his gratitude to Professor Shinzaburo Ito for his kind guidance, pointed advices and continuous encouragement throughout this work.

The author is heartily grateful to Associate Professor Hideo Ohkita for his great deal of continuous supports, and valuable suggestions throughout this work. Many ideas in this thesis were created from these fulfilling discussions. The author is also indebted to Associate Professor Hiroyuki Aoki and Assistant Professor Hiroaki Benten for their valuable suggestions and discussions. The author would like to give special thanks to Dr. Jiamo Guo for the great guides to transient absorption techniques. The author thank to Ms. Akiko Orimo for her path-breaking works of equivalent circuit model analysis, to Mr. Takaaki Wada for the first guide to synthetic technique, and to Mr. Daisuke Mori and Ms. Izumi Okada for great support on device fabrication. The author would like to express his gratitude for Toray Industries, Inc. for providing the N-P7 polymer and great support. The author is in acknowledgment of the JSPS Fellowship for Young Scientists, and the Global COE program (International Center for Integrated Research and Advanced Education in Materials Science) from the Ministry of Education, Culture, Sports, Science, and Technology, Japan.

The author wishes to express his thanks to all members of Ito Lab., in particular, Dr. Li-Ting Lee, Dr. Ryojun Sekine, Dr. Kohji Masuda, Dr. Michihiro Ogawa, Dr. Toru Ube, Dr. Satoshi Honda, Mr. Yoshifumi Ikeda, Mr. Jun-ichi Kakuta and Mr. Toshiaki Takahashi, Mr. Tianhua Ouyang, Mr. Yasunari Tamai, Ms. Huajun Xu, Mr. Seiichirou

Yokoya, Mr. Junya Kosaka, Mr. Kazuki Mori, Mr. Yongyoon Cho, Mr. Shunji Ohara, Mr. Yuu Matsuura, Mr. Toshiaki Hirata, Mr. Yuta Izumiya, Mr. Hiroaki Yasuda, Mr. Junya Fujita, Ms. Han Jin, Ms. Shuang Ji, Ms. Kaoru Ogawa, Ms. Miki Osaka, and Mr. Kazuki Tsuda for their attentive advices, helpful discussions, and for having a good time in Lab. The author is much obliged to Ms. Aki Yamasaki, Ms. Kayo Kawamura, and Ms. Yuki Munemoto for their assistance during the author's school life. The author also thanks to all member of Idobata Science Lab and Student's Conference on Organic Device for exciting events and fruitful discussions from various viewpoints.

Finally, the author expresses his heartfelt thanks to his parents, Mr. Yoshihiko Yamamoto and Ms. Masayo Yamamoto, his brother, Mr. Kenta Yamamoto, his grandparents, Mr. Rishichi Yamamoto, Ms. Kayono Yamamoto, Mr. Tatsuo Nakai, and Ms. Nobuko Nakai for their continuous support, hearty assistance and encouragement.

March 2012

Shunsuke YAMAMOTO